Duncan, R. A., Backman, J., Peterson, L. C., et al., 1990
Proceedings of the Ocean Drilling Program, Scientific Results, Vol. 115

29. PLIOCENE-PLEISTOCENE ARAGONITE CYCLIC VARIATIONS IN HOLES 714A AND 716B (THE MALDIVES) COMPARED WITH HOLE 633A (THE BAHAMAS): RECORDS OF CLIMATE-INDUCED $CaCO_3$ PRESERVATION AT INTERMEDIATE WATER DEPTHS[1]

André W. Droxler,[2] Geoffrey A. Haddad,[2] David A. Mucciarone,[2] and James L. Cullen[3]

ABSTRACT

Ocean Drilling Program (ODP) Leg 115 post-cruise research was focused on two Maldives sites, more precisely on the top 108 m of Hole 716B (water depth, 540 m), equivalent to the past 3.5 m.y., and the top 19.5 m of Hole 714A (water depth, 2195 m), equivalent to the past 0.55 m.y. These sediments consist of mostly unaltered and undisturbed, turbidite-free, periplatform ooze. Results of our research are compared with existing data on Hole 633A (water depth, 1681 m), drilled in the Bahamas during ODP Leg 101, using age/depth models built on the basis of oxygen isotope, nannofossil, and magnetic stratigraphies.

Climate-induced, long-term (roughly 0.5 m.y.) aragonite cycles, superposed on short-term (roughly 0.04 and 0.1 m.y.) aragonite cycles, have been established at least during the past 2.0 m.y., in the Maldives and the Bahamas. Our most interesting result is the clear correlation among the aragonite long-term cycles in the Maldives and the Bahamas and the carbonate-preservation, long-term cycles from the open Pacific, Indian, and North Atlantic oceans. The mid-Brunhes dissolution interval, corresponding to the youngest preservation minima of the carbonate-preservation, long-term cycles, is clearly defined by fine aragonite minimum values in the deep periplatform sites, and by maximum fragmentation of pteropod tests in the shallow sites. Aragonite and planktonic $\delta^{18}O$ records, usually in phase during the late Pleistocene, display, further back in time, discreet intervals where the two records do not match with one another. Major mismatches between both records occur synchronously in the Maldives and Bahamas periplatform sites and seem to correspond to extreme events of either carbonate-preservation or dissolution in the deep pelagic carbonate sites of the equatorial Pacific Ocean.

Based on our findings, short- and long-term aragonite cycles can no longer be explained only by variations of aragonite input from the nearby shallow carbonate banks, in response to their alternate flooding and exposure through cyclic sea-level fluctuations. The aragonite long-term cycles in the periplatform environments are interpreted as carbonate-preservation cycles at intermediate-water depths. Their occurrence shows, therefore, that the carbonate chemistry of the entire water column has been influenced by long-term (0.5 m.y.) cyclic variations during the past 2.0 m.y. These major changes of the water-column carbonate chemistry are linked to the climate-induced carbon cycling among the different atmospheric, oceanic, and sedimentary carbon reservoirs.

INTRODUCTION

Deep-sea carbonate sediments play an important role in the global carbon cycle by storing or releasing large volumes of carbon through time. Because of the chemical interactions at the seafloor between sediments and the overlying water masses, deep-sea carbonate sediments have also recorded, at least partially, the carbonate chemistry variations of different water masses. In addition, since the general deep-ocean circulation is modulated and intimately linked to global fluctuations of Quaternary climate, deep-sea sediments contain unique records of the interactions between the atmosphere and the ocean.

Below the calcite lysocline (3500–4000 m), deep-sea sediments have recorded cyclic changes of the ocean carbonate chemistry over the Milankovitch orbital time scale (10^4–10^5 yr) in deep- and bottom-water masses. Above the calcite lysocline, in intermediate-water depths, little or no dissolution is generally observed in planktonic calcitic sediments, which consist mainly of coccolith and foraminifer tests. Aragonite, a less stable carbonate phase and therefore more sensitive to minor chemical changes than calcite, has been used to study the carbonate chemistry variations at intermediate-water depths. Previous studies have used the occurrence and depth distribution of pteropods (planktonic micro-mollusks with aragonitic tests) to define the aragonite lysocline and aragonite compensation depth (ACD) at intermediate-water depths (Chen, 1964; Herman, 1971; Berner, 1977, 1981; Berger, 1978; Berner et al., 1976; Droxler et al., 1988a). Chen (1968) and Herman (1971) are among a few authors who have related the downcore pteropod distribution to late Pleistocene paleoclimatic fluctuations. To our knowledge, however, no studies based on the downcore occurrence and distribution of pteropod tests have demonstrated cyclic changes of the ocean carbonate chemistry within Milankovitch frequencies (10^{th}–100^{th} k.y.) in oceanic intermediate-water masses. These cycles would be analogous to the cyclic carbonate variations well established in the three major oceans that have mainly recorded carbonate chemistry variations of deep- and bottom-water masses.

The late Pleistocene aragonite cycles observed in the periplatform ooze, deposited in the deep surroundings of the carbonate Bahamas Banks, are well established and have been the subject of several studies (Supko, 1963; Kier and Pilkey, 1971; Lynts et al., 1973; Droxler et al., 1983; Boardman et al., 1986; Haddad, 1986; Burns and Neumann, 1987; Slowey et al., 1989). The detailed correlation between the aragonite cycles and the oxygen isotope planktonic record (Droxler et al., 1983; Boardman et al., 1986) shows the clear tie between the aragonite cycles and the late Pleistocene climatic fluctuations. The origin of

---

[1] Duncan, R. A., Backman, J., Peterson, L. C., et al., 1990. *Proc. ODP, Sci. Results,* 115: College Station, TX (Ocean Drilling Program).

[2] Department of Geology and Geophysics, Rice University, P.O. Box 1892, Houston, TX 77251, U.S.A.

[3] Department of Geological Sciences, Salem State College, Salem, MA 01970, U.S.A.

these cycles, however, has remained quite controversial for the past 5 yr (for a summary, see Droxler and Schlager, 1985b; Droxler, 1986; Boardman and Neumann, 1985, 1986).

One way to explain the periplatform aragonite cycles is by simply varying the input of bank-derived aragonite. Variations in input are directly tied to alternate flooding and exposure of the shallow carbonate banks and, therefore, are a direct result of late Pleistocene climate-induced, sea-level fluctuations (Supko, 1963; Kier and Pilkey, 1971; Boardman et al., 1986; Boardman and Neumann, 1985, 1986). Export of bank-derived fine aragonite toward the deep basins is directly modulated by maximum aragonite production during intervals of bank flooding and by minimum aragonite production during intervals of bank exposure. Supko (1963), Kier and Pilkey (1973), Lynts et al. (1973), Boardman (1978), Schlager and Chermark (1979), Hanna and Moore (1979), Mullins et al. (1980), Hine et al. (1981), Mullins (1983), Droxler et al. (1983), Boardman and Neumann (1984), Droxler and Schlager (1985a), and Reymer et al. (1988) have described and summarized this concept as "carbonate high-stand shedding." In this case, therefore, high aragonite content in periplatform sediments corresponds to interglacial stages (sea-level high stand), whereas low aragonite content corresponds to glacial intervals (sea-level low stand).

Carbonate cycles are well established in deep waters of the equatorial Pacific (Arrhenius, 1952; Hays et al., 1969; Berger, 1973; Thompson and Saito, 1974; Pisias et al., 1975; Adelseck, 1977; Volat et al., 1980; Farrell and Prell, 1987, 1989), Indian (Oba, 1969; Volat et al., 1980; Peterson and Prell, 1985; Williams et al., 1985), and Atlantic oceans (Berger, 1973; Gardner, 1975; Volat et al., 1980; Balsam, 1983; Diester-Haas, 1985; Crowley, 1983, 1985). By analogy with these carbonate cycles, a second way to explain the aragonite periplatform cycles is to modify the aragonite input (concept of carbonate high-stand shedding) by varying its degree of preservation through partial or full seafloor dissolution. Carbonate preservation at the seafloor is tied to climate-induced changes in carbonate chemistry of intermediate-water masses, specifically to the shallowing or deepening of the aragonite saturation level. In the latter case, the aragonite cycles become analogous to the carbonate (calcite) cycles well established in the deep oceans and mainly explained by climate-induced fluctuations in planktonic calcite production and preservation on the seafloor. Modification of the aragonite input signal by seafloor dissolution is not always obvious, especially in the late Pleistocene aragonite cycles in the Bahamas, where input and preservation signals appear to be in phase, as usually is the case for carbonate cycles in the deep North Atlantic Ocean (Volat et al., 1980; Crowley, 1983). Interglacial stages, which are characterized by maximum aragonite input, would then correspond to intervals of good carbonate preservation, whereas glacial stages, characterized by low aragonite input, would correspond to intervals of poor preservation

Given the subtle evidence and careful observations, we have favored the interpretation initiated by Lynts et al. (1973) that the aragonite cycles are formed by varying the input of bank-derived aragonite, which is subsequently either fully preserved or partially/totally dissolved by chemical reaction with the overlying water masses at the seafloor (Droxler et al., 1983, 1988b; Droxler, 1985). The major evidence consists of the following:

1. The general asymmetry of the aragonite cycles (sharp glacial-to-interglacial transitions followed by gentle interglacial-to-glacial transitions) cannot be clearly explained by flooding and exposure of the carbonate banks, because of the characteristic flat bank tops and steep bank edges. This typical bank physiography should lead to sudden flooding during an interval of sea-level rise as well as to sudden exposure once sea level falls. The aragonite input function should, therefore, be symmetrical.

2. The close tie between aragonite and oxygen isotope signals is remarkable and occurs not only during interglacial stages, but also during glacial stages when aragonite production, and therefore input, could not have varied much because the shallow banks were exposed. Detailed analyses of the last glacial-to-interglacial transitions also clearly show that the last bank flooding in the Bahamas occurred several thousands of years after the recorded aragonite increase in the basins (Droxler et al., 1983; Droxler, 1985). Direct observations of aragonite dissolution in waters of less than 800 m based on pteropod tests are quite rare. Pteropod fragmentation seems to increase during the past several glacial intervals in a core collected from Northwest Providence Channel in the Bahamas at only 680 m (Haddad, 1986); and pteropod casts, resulting from sea floor dissolution, were observed during the last glacial intervals in cores from Northwest Providence Channel (Burns, 1983).

The cyclic pattern of carbonate preservation in deep waters is not always in phase with interglacial intervals, as is typically the case for the North Atlantic Ocean during the late Pleistocene (Berger, 1973; Gardner, 1975; Volat et al., 1980; Balsam, 1983; Diester-Haas, 1985; Crowley, 1983, 1985). In contrast, the carbonate preservation pattern in the Pacific Ocean is totally out of phase with the Atlantic pattern. In the Pacific Ocean, better preservation roughly corresponds with glacial intervals and dissolution roughly with interglacial intervals (Arrhenius, 1952; Hays et al., 1969; Berger, 1973; Thompson and Saito, 1974; Pisias et al., 1975; Adelseck, 1977; Volat et al., 1980; Farrell and Prell, 1989). In addition to these differences between basins, a global pattern of carbonate preservation common to the three major oceans appears during the late Pleistocene and is characterized by generally good preservation at the glacial-to-interglacial transitions and generally poor preservation at the interglacial-to-glacial transitions (Crowley, 1985).

To investigate the origin of the aragonite cycles further, we expanded our research geographically by establishing research programs in periplatform environments on the Nicaragua Rise (Caribbean Sea), the Maldives (Indian Ocean), and the Queensland Plateau (southwest Pacific Ocean) (Droxler et al., 1989). The Atlantic and Pacific patterns, characteristic of the carbonate (calcite) cycles, seem also to appear at intermediate-water depths in the periplatform aragonite cycles. On the Queensland Plateau (southwest Pacific Ocean), aragonite values are higher during the second half of the last glacial stage and lower during the past 6000 yr and during the previous interglacial stage. In the Maldives, aragonite maxima always occur at the glacial-to-interglacial transitions, whereas aragonite minima occur at the interglacial-to-glacial transitions. A similar pattern in deep-water carbonate records (i.e., good carbonate preservation at the glacial-to-interglacial transition and poor preservation at the interglacial-to-glacial transition) has been demonstrated by Peterson and Prell (1985) from the Ninetyeast Ridge (eastern equatorial Indian Ocean) and by Farrell and Prell (1989) from the equatorial Pacific Ocean.

We also expanded our research further back in time than the late Pleistocene by studying longer periplatform sequences collected in the Bahamas and in the Maldives during Ocean Drilling Program (ODP) Legs 101 and 115. In Hole 633A (the Bahamas), Droxler et al. (1988b) have demonstrated that the aragonite cycles did not always remain in phase with the oxygen isotope record. In several cases, the aragonite increase clearly lags or leads the oxygen isotope depletion characteristic of an interglacial/glacial transition. Because a constant-phase relationship is required by the high-stand hypothesis, we think that the aragonite cycles cannot be solely explained by high-stand shedding. In addition, aragonite supercycles in Hole 633A were revealed by connecting the minimum aragonite values for the successive Pleistocene glacial stages. The timing of these aragonite supercycles, characterized by a periodicity of roughly 0.4–0.5 m.y., is in good agreement with the timing of the long-term carbonate preservation records well established in the Pacific, Indian, and Atlantic oceans (Hays et al., 1969; Adelseck, 1977; Vincent, 1985; Moore et al., 1982; Farrell and Prell, 1987, 1989; Oba, 1969; Peterson and Prell, 1985; Crowley, 1985; Diester-Haas, 1985).

Two long periplatform sequences were drilled during Leg 115 at Site 716 (540 m water depth, 108-m-thick unaltered periplatform sequence corresponding to the past 3.5 m.y.) and at Site 714 (2195 m water depth, 19.5-m-thick unaltered periplatform sequence corresponding to the past 0.55 m.y.) (Backman, Duncan, et al., 1988). This is a unique opportunity to extend the existing late Pleistocene aragonite record in the Indian Ocean (Droxler et al., 1989) back to the Pliocene, and to compare two aragonite records from different water depths (540 and 2195 m) for the past 0.55 m.y. Based on these new records, we can address several new questions.

1. How have the climate-induced aragonite cycles evolved during the early and middle Pleistocene as well as during the late Pliocene? Specifically, how have major climatic events such as the onset of major glaciations in the Northern Hemisphere at 2.4 Ma (Shackleton et al., 1984), or the change from high frequencies/low amplitudes to low frequencies/high amplitudes at the early/middle Pleistocene boundary (0.9 Ma; Prell, 1982) been recorded in the aragonite record?
2. How well does the aragonite record correlate with the oxygen isotope record on planktonic foraminifers? What is the phasing between the aragonite and oxygen records? Can we observe any systematic pattern with the phase changes or the different time lags between the two signals?
3. Do the aragonite supercycles discovered in the Bahamas (Droxler et al., 1988b) also occur in the Maldives? If yes, do these aragonite supercycles in the Maldives correlate with the ones in the Bahamas as well as with the carbonate supercycles well established in the equatorial Pacific and Atlantic oceans.

Because a 2.1-m.y. continuous aragonite record has already been determined in Hole 633A from the Bahamas (Droxler et al., 1988b), a comparative study between the two late Pliocene/Pleistocene aragonite records from the Maldives and from the Bahamas can easily be done. To help the comparison between the two records, we present our data vs. time instead of core depth, given age/depth models built on oxygen isotope, nannofossil, and magnetic stratigraphies.

LOCATION AND SEDIMENT DESCRIPTION

The Maldives Archipelago consists of a double chain of atolls separated by a series of deep internal basins with water depths ranging from 200 to 600 m. The archipelago is located on top of an elevated ridge, 2500 m above the adjacent abyssal plains (Fig. 1). Because of this particular physiographic setting, the sediments deposited in close proximity to the shallow carbonate environments cover a wide range of water depths (200–2500 m). This paper presents the results of a post-cruise research program that focused on two long periplatform records from Holes 714A and 716B, collected by advanced piston coring (APC) in the central part of the Maldives Archipelago during Leg 115.

In Hole 716B, we recovered a single 260-m-thick lithologic unit consisting mainly of foraminifer-bearing nannofossil calcareous ooze without any distinct turbidite layers (Backman, Duncan, et al., 1988). The sedimentary sequence at Site 716 represents a somewhat continuous late Miocene through Pleistocene record. Although the first appearance of chalky levels was shallow (75 mbsf), a complete transformation from ooze to chalk was not evident even at the bottom of Hole 716B. The chalk proportions ranged from 10% to 60% and were highly variable from one core to another in the bottom half of Site 716. We have restricted our detailed studies to the top 108 m (Cores 115-716B-1H to -12H) of Hole 716B to avoid sediment with obvious signs of diagenetic recrystallization. The top eight cores are chalk free, whereas Cores 115-716B-9H to -12H contain a maximum of 5% chalk.

We also analyzed 10–20-cm-spaced samples from the 19.5-m-thick upper unit of Hole 714A corresponding to late/middle Pleistocene age (0.55 Ma). This upper unit overlies the very top of Unit II, a greenish gray nannofossil ooze of late Miocene age (8.0 Ma, NN10 [CN8]; Backman, Duncan, et al., 1988). A 7.5-m.y. hiatus, therefore, separates the bottom of Unit I and the top of Unit II and its presence unfortunately has limited our study of Hole 714A to the late/middle Pleistocene. Lithotypes of this upper unit range from foraminifer-bearing, clay-bearing nannofossil ooze to foraminifer-bearing clayey nannofossil ooze. These sediments, which display cyclic color changes, do not include any chalk. A single turbidite 50 cm above the hiatus at the Unit I/II boundary, was identified in Holes 714A and 714B, suggesting only minor disturbance in Unit I (Backman, Duncan, et al., 1988).

Onshore laboratory analyses, including size fraction separation, carbonate content, carbonate mineralogy, and stable oxygen isotope on planktonic foraminifers, show that these sediments consist of a mixture of pelagic, calcitic ooze and of bank-derived fine aragonite and magnesian calcite, typical for a periplatform ooze (Schlager and James, 1978).

For comparison with the new data generated from Holes 714A and 716B, we have included in this paper results from the top 43.75 m of Hole 633A, which were published in the *Proceedings of the Ocean Drilling Program, Scientific Results,* Volume 101 (Droxler et al., 1988b). Hole 633A was drilled in the southern part of Exuma Sound on the toe-of-slope of the Great Bahama Bank, in 1681 m water depth (Fig. 1). The top 43.75 m corresponds to Unit I, defined in Austin, Schlager, et al. (1986) as a periplatform-ooze sequence with cyclic variations in color and a few scattered 1–10-cm-thick calcareous turbidite layers. Considering the proximal position of Hole 633A, the fine-grained turbidites in Unit I are unusually thin. These characteristics can be explained by the location of the site on a topographic high that rises 20–40 m above the surrounding seafloor and could be caused by progradation of a spur of the gullied slope or by large-scale slumping prior to the deposition of Unit I (Austin, Schlager, et al., 1986). For methods (sediment sampling and analyses, carbonate content in fine fraction, carbonate mineralogy, stratigraphy, and oxygen isotope), we refer the reader to Droxler et al. (1988b, pp. 222–223).

METHODS

Sediment Sampling and Analyses

The top 108 m of Hole 716B were sampled every 20 cm (Appendix A) and the top 19.5 m of Hole 714A every 10 cm (Appendix B). Sampling the periplatform ooze was simplified because both holes are free of turbidite layers with the exception in Hole 714A of one turbidite layer at 19.0 mbsf (Backman, Duncan, et al., 1988). Care was taken to avoid sampling obviously reworked or disturbed features at the top and bottom of the core. Each 10-cm^3 sediment sample was dried in an oven at 60°C, weighed, and suspended in distilled water (pH 8). The coarse fraction of the sediment was separated from the fine fraction through a 63-μm mesh sieve and then dried at 60°C and weighed again. The fine fraction (< 63 μm) was left to stand in distilled water for 1–2 days until the particles were completely

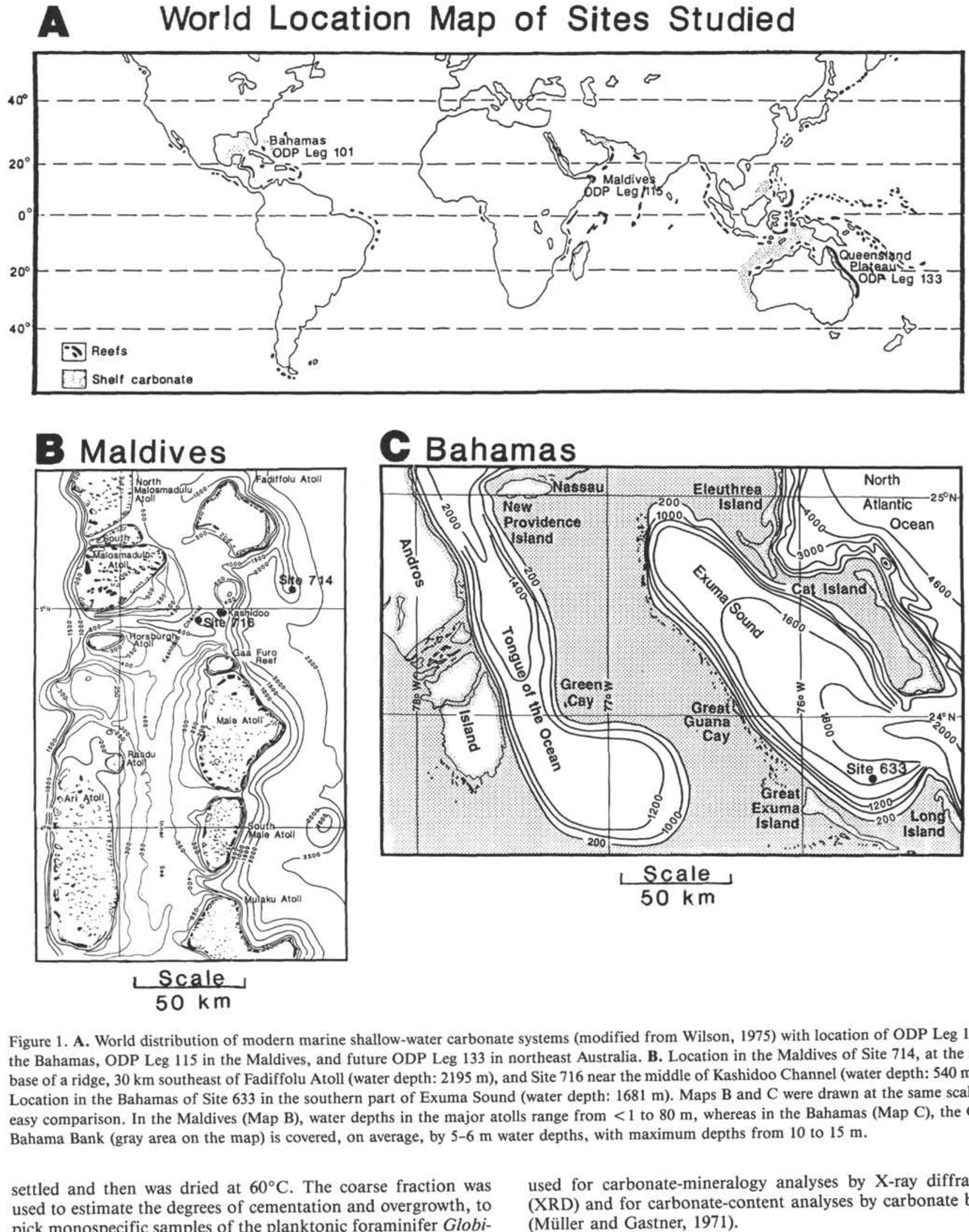

Figure 1. **A.** World distribution of modern marine shallow-water carbonate systems (modified from Wilson, 1975) with location of ODP Leg 101 in the Bahamas, ODP Leg 115 in the Maldives, and future ODP Leg 133 in northeast Australia. **B.** Location in the Maldives of Site 714, at the slope base of a ridge, 30 km southeast of Fadiffolu Atoll (water depth: 2195 m), and Site 716 near the middle of Kashidoo Channel (water depth: 540 m). **C.** Location in the Bahamas of Site 633 in the southern part of Exuma Sound (water depth: 1681 m). Maps B and C were drawn at the same scale for easy comparison. In the Maldives (Map B), water depths in the major atolls range from <1 to 80 m, whereas in the Bahamas (Map C), the Great Bahama Bank (gray area on the map) is covered, on average, by 5–6 m water depths, with maximum depths from 10 to 15 m.

settled and then was dried at 60°C. The coarse fraction was used to estimate the degrees of cementation and overgrowth, to pick monospecific samples of the planktonic foraminifer *Globigerinoides sacculifera* for oxygen isotope analyses, and to evaluate pteropod preservation for the top 17.25 mbsf of Hole 716B (down the cores to Sample 115-716B-3H-4, 40–42 cm) (see Cullen and Droxler, this volume, for details). The fine fraction was used for carbonate-mineralogy analyses by X-ray diffraction (XRD) and for carbonate-content analyses by carbonate bomb (Müller and Gastner, 1971).

Carbonate Content in the Fine Fraction

The carbonate-bomb method was used to determine the total carbonate content of the fine fraction in each sample from the

CO_2 pressure generated by dissolving the carbonate fraction in 50% concentrated HCL (Müller and Gastner, 1971). The pressure of CO_2 released by the fraction of the carbonate with the acid was compared with pressure released by an equal amount of 100% $CaCO_3$ standard. Accuracy of the method for marine sediments remained within ±2% for $CaCO_3$ values ranging from 5% to 95% (Birch, 1979).

Carbonate Mineralogy of the Fine Fraction

Relative proportions of the different carbonate minerals were quantified by XRD analyses. Each sample of fine sediment was dried at 60°C, ground for <1 min by hand in an agate mortar, sieved to obtain an agglomerate of <63-μm particles, and packed with a spatula into an aluminum sample holder. The effects of particle size on the semiquantitative XRD estimate and the effects of mineralogy change by grinding are minimized through these procedures (Milliman, 1974). Each sample was analyzed with a Phillips-Norelco Model 12045 (60 cycles) diffractometer with Dapple Systems Controller Thetaplus® Software. The diffractometer setting used was at 35 kV and 20 mA, and the analysis was conducted through a two-segmented scan from 25.5° to 27.5° for the aragonite primary peak and from 28.5° to 32° for the calcite and dolomite peaks, at a low scanning speed of 0.02°/s for optimal resolution. Areas under the aragonite peak, the dolomite peak (if present), and the calcite peaks (calcite and magnesian calcite) separated by deconvolution were calculated by integration of the counts under the respective peak and above the general noise background. The aragonite portion in each sample was calculated with an accuracy of better than 5% from a calibration curve (Droxler, 1984). Reproducibility of the deconvolution method used to separate calcite from magnesian calcite is within a measured maximum discrepancy of $<5\%$.

Stratigraphies

Oxygen Isotopes

Oxygen isotopes were analyzed on *Globigerinoides sacculifera* at 20-cm intervals down to Sample 115-716B-5H-6, 60–62 cm (36.15 mbsf) in Hole 716B and down to Sample 115-714A-3H-5 (19.48 mbsf) in Hole 714A, using the same samples in Holes 716B and 714A as were used for fine-fraction studies in the mineralogical studies. For each sample, 20–30 foraminifer tests were picked in a narrow size fraction between 300 and 350 μm, cleaned ultrasonically to remove any calcareous mud clinging to the tests, and dried at 60°C. They were reacted at 50°C with excess 100% H_3PO_4, and the CO_2 gas was analyzed in a semiautomated VG Micromass 602E at the Stable Isotope Laboratory of Rice University (R. Dunbar). Results are reported relative to the PDB standard. Analytical precision on standards was better than 0.1‰.

Nannostratigraphy

Nannostratigraphy datums are based on research conducted on board Leg 115 (Backman, Duncan, et al., 1988) and post-cruise research by H. Okada, D. Rio, A. Chepstow-Lusty, and J. Backman published in this volume. We refer the reader to their respective articles published in this volume for more details on their respective methodologies.

RAW DATA

We are calling "raw data" the direct results that come out of the different analyses as applied to the periplatform samples (see "Methods" section, this chapter, for more details). Figures 2, 3, and 4 display the raw data for the top 108 mbsf of Hole 716B, representing the past 3.5 m.y., for the top 19.5 mbsf of Hole 714A, representing the past 0.55 m.y.; and for the top 44 mbsf of Hole 633A, representing the past 2.1 m.y., respectively.

Proportion of the Fine Fraction

Hole 716B

Downcore variations of the fine fraction proportions in Hole 716B display a high-frequency cyclic pattern (Fig. 2A). The 110-m-long periplatform sequence can be divided into three segments according to the average values and amplitudes of the variations. In the upper segment (0–31 mbsf) of Hole 716B, values of fine fraction content average 40%, ranging from 25% to 65%; in the middle segment (31–85 mbsf), they average 50%, ranging from 40% to 75%; and in the lower segment (85–110 mbsf) they average 40%, ranging from 30% to 60%. The average amplitude of the cyclic pattern for each segment thus decreases downcore from 40% to 35%, and finally to 30%. Minimum values, ranging from 10% to 20%, are concentrated within a few meters, centered around 30 mbsf. This particular level corresponds to a distinct event that separates the early Pleistocene from the middle.

Hole 714A

Fine fraction values average 45%, ranging from 25% to 70% in the upper 19.5 m of Hole 714A (Fig. 3A), and are therefore quite similar to the values in the upper segment of Hole 716B.

Hole 633A

Fine fraction values in the top 40 m of Hole 633A (Fig. 4A) always remain higher than the values observed in Holes 714A and 716B. They average 82%, ranging from 70% to 90%, and remain relatively constant in the top 30 m; they average 70%, ranging from 40% to 90%, for the lower 14 m of the section. The lowest fine fraction values occur mainly during the late Pliocene and at the beginning of the early Pleistocene at levels where foraminifer tests display partial overgrowths and where agglomerates of periplatform sediments are common. In other words, the low values of the fine fraction or the high values of the coarse fraction can be explained in these cases by diagenesis through early cementation.

Carbonate Content in the Fine Fraction

Hole 716B

The top 108 m of Hole 716B can be easily separated into two segments (Fig. 2B). The lower segment, from 30 to 108 mbsf, is characterized by high carbonate values and low (5%) amplitude variations; average values vary from 91% at 30 mbsf, 96% at 40 mbsf, and 93% between 50 and 110 mbsf. The upper 30-m-long segment contrasts drastically with the lower segment. The upper segment is characterized by low carbonate values, ranging from 96% to 83%; 10% amplitude cyclic variations; and a systematic decrease of the average carbonate values from 91% at 30 mbsf to 87% mbsf in the surface sediments. As already observed in the fine fraction variations, the 30-mbsf level of Hole 716B, which corresponds to the early/middle Pleistocene boundary, shows a drastic change in the carbonate values within the fine fraction. At that level, irregular low-amplitude cyclic carbonate variations with high carbonate values suddenly change into regular high-amplitude carbonate cycles, with average values gradually decreasing toward the surface sediments.

Hole 714A

Carbonate values in the fine fraction of the top 19.5 m in Hole 714A (Fig. 3B) range between 40% and 80%, and their variations display regular cycles, similar to the ones observed in the top 30 m of Hole 716B, but with higher amplitudes (30% instead of 10%) and lower average carbonate values decreasing systematically from 70% at 20 mbsf to 60% in the surface sediments.

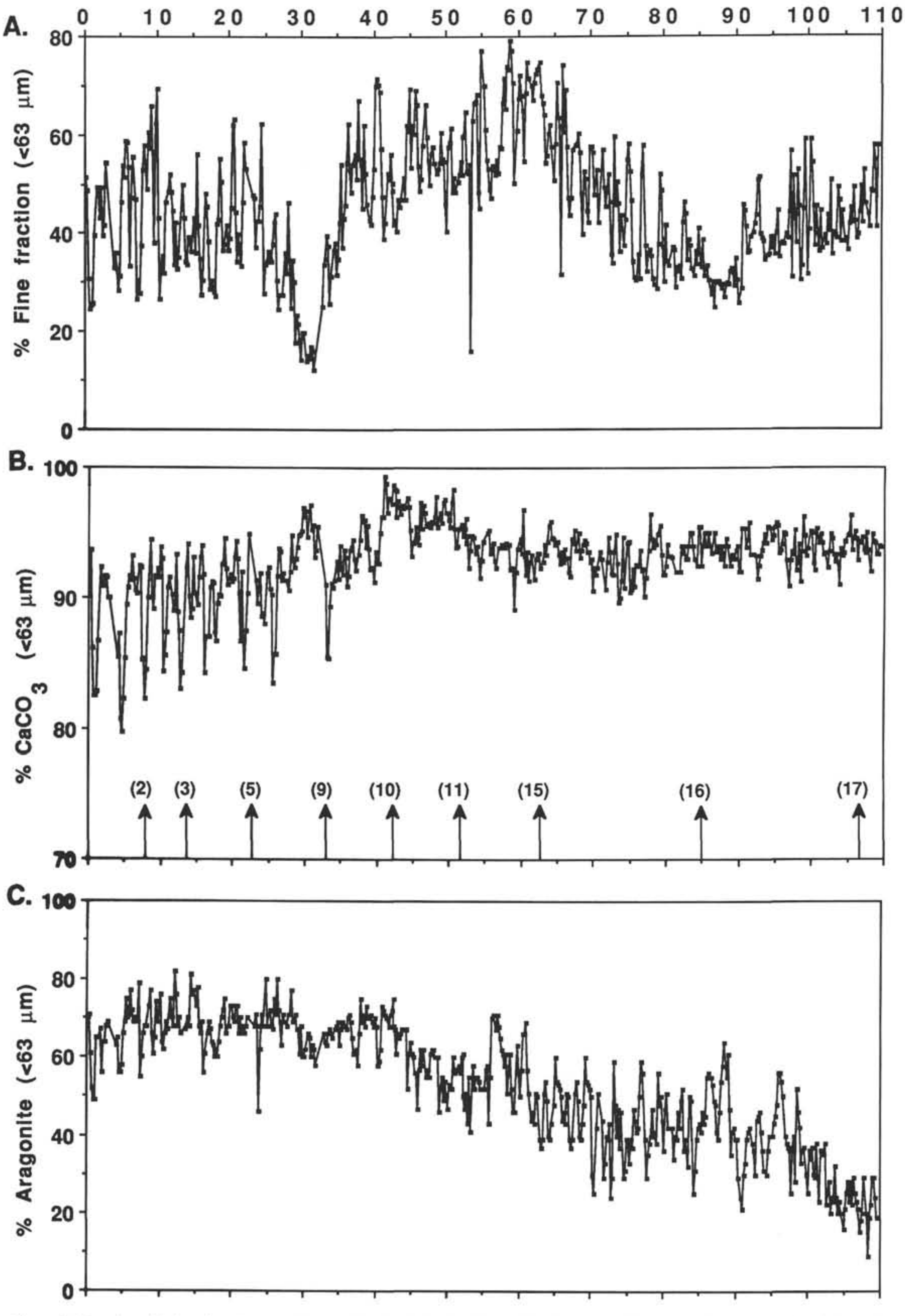

Figure 2. Depth variations for the top 108 m of Hole 716B of (**A**) the fine fraction, (**B**) the $CaCO_3$ content in the fine fraction, (**C**) aragonite and (**D**) magnesian calcite content in the carbonate fraction of the fine fraction, and (**E**) the planktonic $\delta^{18}O$ record of *Globigerinoides sacculifera*. The numbers in parentheses refer to the datum levels based on nannofossil stratigraphy; see Table 2 for corresponding datum levels.

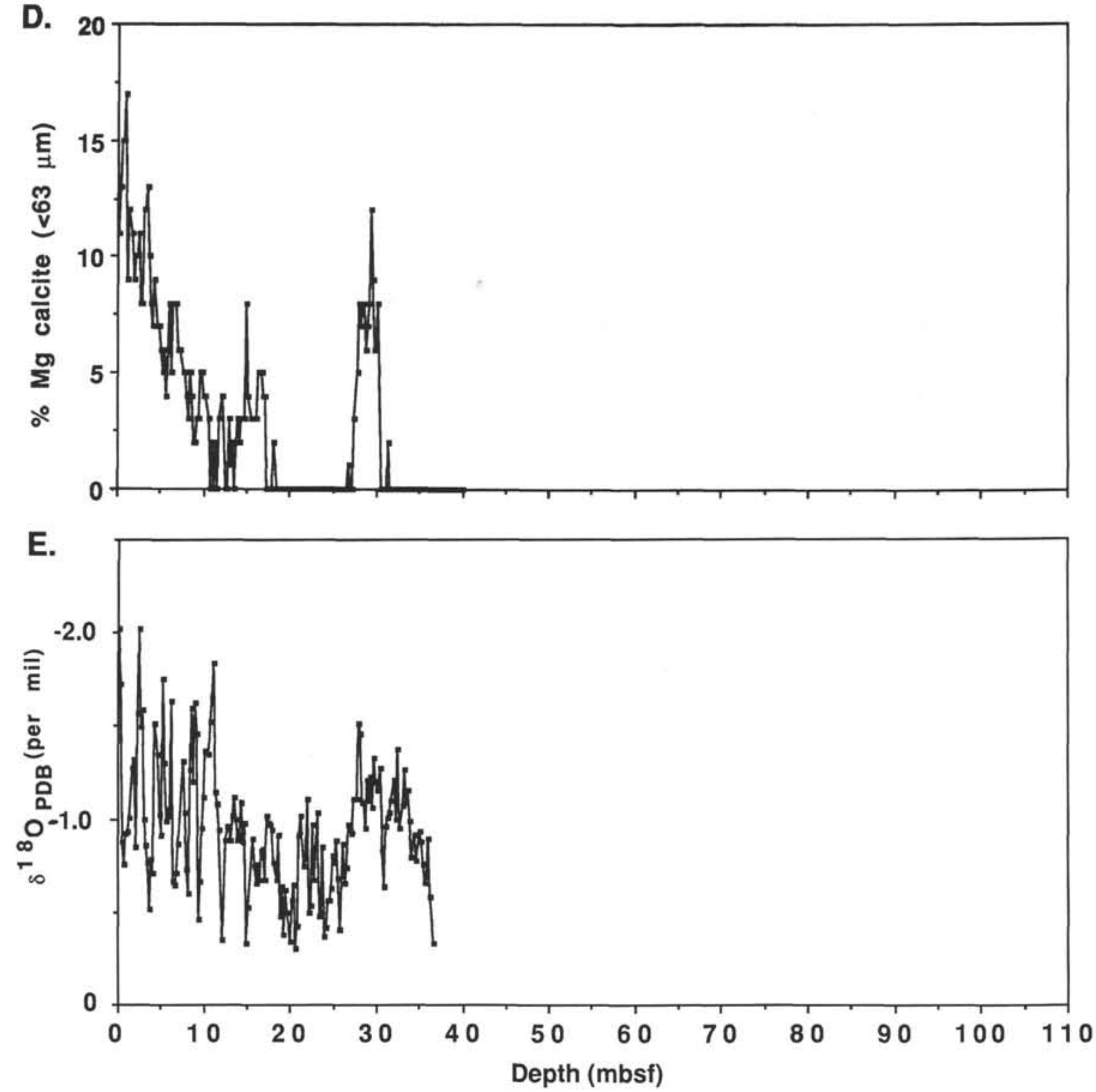

Figure 2 (continued).

Hole 633A

Average carbonate values in the top 44 m of Hole 633A (Fig. 4B) oscillate between 95% and 90%. Values lower than 90% correspond in the upper 20 m of Hole 633A to clay-rich layers that can easily be observed visually by color change on the core surface (Droxler et al., 1988b). Variations of the carbonate values have a cyclic, but quite irregular, character, especially when one compares them with the regular well-defined carbonate cycles in the top 30 m of Hole 716B.

Aragonite Content in the Fine Carbonate Fraction

Hole 716B

Average aragonite values for Hole 716B (Fig. 2C) vary from 60% within the surface sediment to 25% at the bottom (110 mbsf), reaching a maximum of 65% between 10 and 25 mbsf. Absolute aragonite values range from 80% at 10 mbsf to 10% at 110 mbsf. A rough cyclic pattern can be detected within the downcore aragonite variations. Amplitudes of the aragonite cycles vary downcore in Hole 716B, ranging from a few percent to 10%–15%. The largest amplitude of the aragonite cycles occur in the bottom half and in the top 10 m of Hole 716B.

Hole 714A

Aragonite absolute values vary between 0% and 65% in the top 19.5 m of Hole 714A and display a regular cyclic pattern (Fig. 3C). Maximum aragonite values for each cycle decrease downcore, from 65% for the three most recent peaks, to 50% for the previous two peaks, and finally to 40% for the oldest peak recorded in Hole 714A. The amplitudes of the aragonite cycles as well as the length of intervals without aragonite also increase downcore.

Hole 633A

Variations of aragonite content display a regular cyclic pattern within the top 35 m of Hole 633A (Fig. 4C). Amplitudes of these cycles are highly variable, ranging from 20% to 75%. Be-

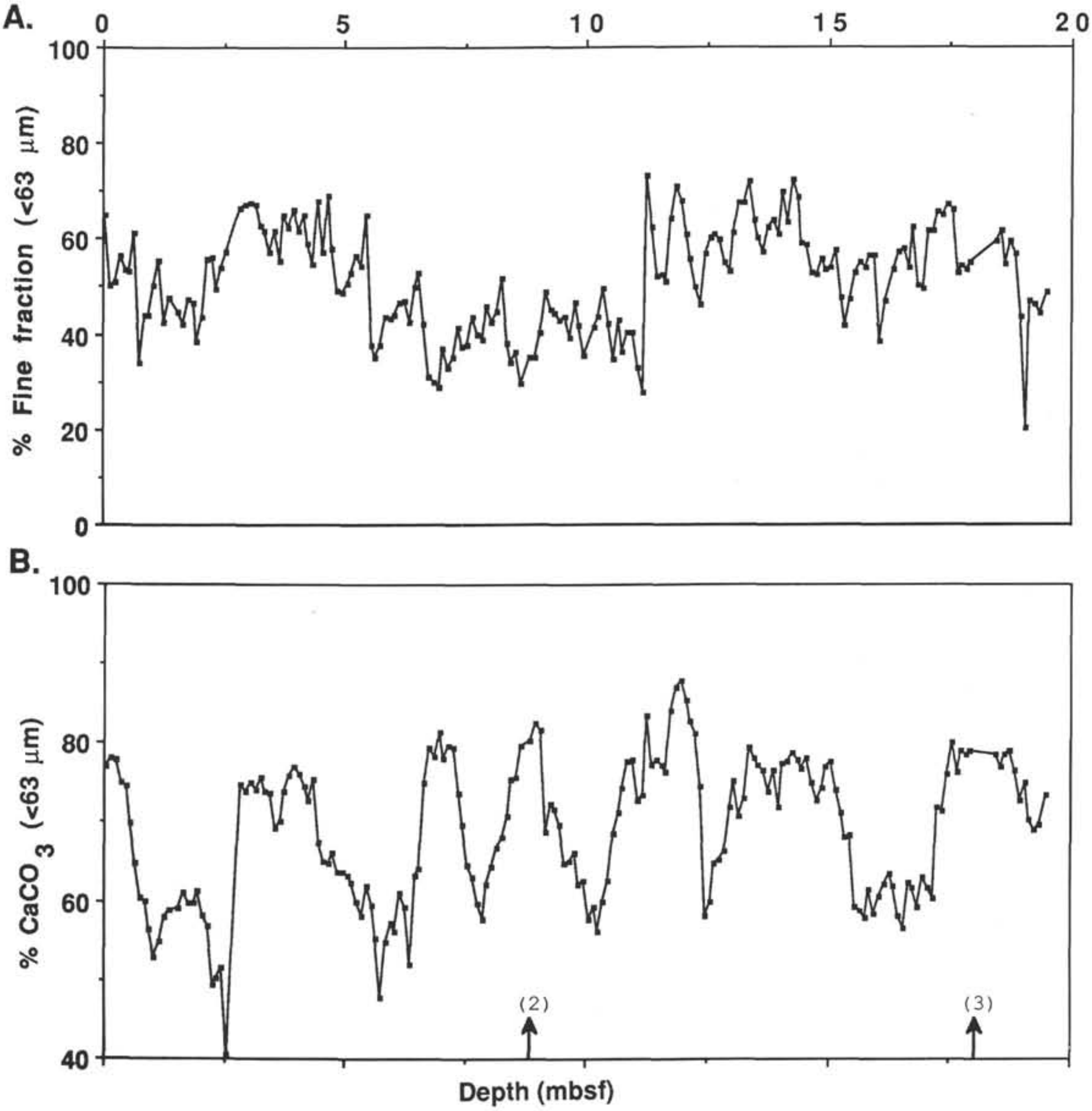

Figure 3. Depth variations for the top 19.5 m of Hole 714A of (**A**) the fine fraction, (**B**) the $CaCO_3$ content in the fine fraction, (**C**) aragonite content in the carbonate fraction of the fine fraction, and (**D**) planktonic $\delta^{18}O$ record of *Globigerinoides sacculifera.* The numbers in parentheses refer to the datum levels based on nannofossil stratigraphy; see Table 2 for corresponding datum levels.

low 35 mbsf, aragonite disappears in several intervals. Aragonite cycles in Hole 633A have been fully described in Droxler et al. (1988b).

Magnesian Calcite in Fine Carbonate Fraction

Hole 716B

Values of magnesian calcite content within the fine carbonate fraction decrease downcore from a maximum of 15% close to the top of Hole 716B to 0% at 11 mbsf (Fig. 2D). Magnesian calcite reappears twice as isolated peaks, the shallowest one centered at 15 mbsf (average magnesian calcite content value of 3%), and the second one centered at 19 mbsf (average magnesian calcite value of 7%).

Hole 714A

Magnesian calcite was not detected in any of the analyzed samples from Hole 714A.

Hole 633A

The resemblance between the downcore variations of magnesian calcite in Hole 633A and Hole 716B is quite striking. In Hole 633A (Fig. 4D), magnesian calcite content is at its maximum (15% close to its top) and then decreases regularly to reappear within two intervals, centered at 13 and 10 mbsf (see Droxler et al., 1988b).

Oxygen Isotope Record

Hole 716B

The oxygen isotope record shows well-developed cycles with high amplitudes (1.3‰–1.5‰) in the top 12 m, and then with fairly low amplitudes (0.75‰) further down the hole. This record mimics both classic $\delta^{18}O$ records and the SPECMAP smoothed stack record. Comments on the oxygen isotopic re-

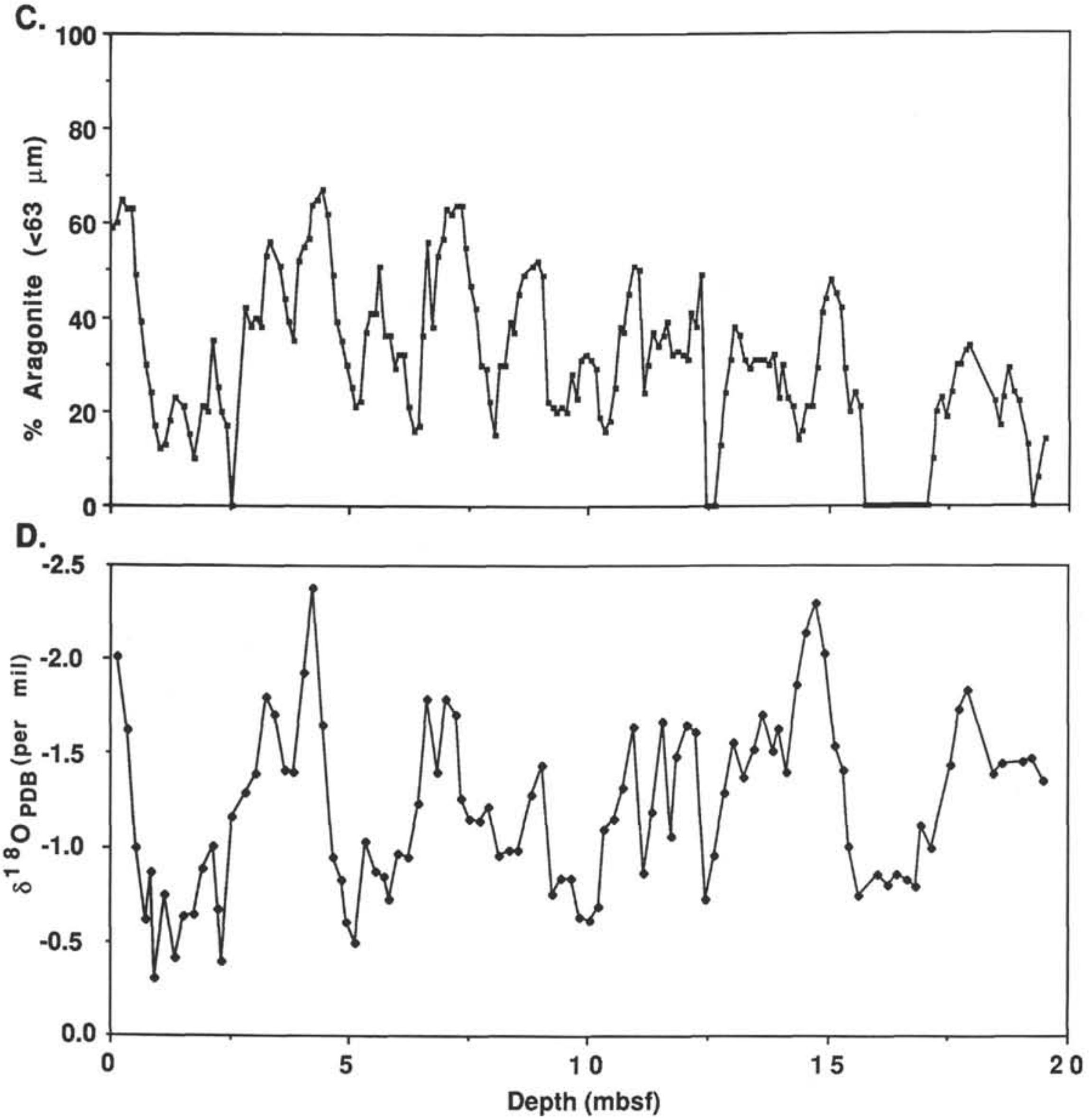

Figure 3 (continued).

cord are expanded in the "Isotope Stratigraphy" section (this chapter).

Hole 714A

In the top 19.5 m of Hole 714A, the $\delta^{18}O$ record shows well-developed cyclic variations, with signal amplitudes ranging from 1.0‰ to 1.7‰, and corresponding to the $\delta^{18}O$ record of the top 17 m in Hole 716B (Fig. 3E).

Hole 633A

The $\delta^{18}O$ record for the top 44 m of Hole 633A (Fig. 4E) is from Droxler et al. (1988a). This record is mainly based on *Globigerinoides sacculifera* with a few analyses performed on *Globigerinoides rubra* in the top 10 m of the hole (see Droxler et al., 1988b, for more detail).

The three $\delta^{18}O$ records from Holes 716B, 714A, and 633A will serve as a basis on which to establish a time scale for the last 1.1 m.y. by comparing them with the SPECMAP $\delta^{18}O$ record of Imbrie et al. (1984) and the composite $\delta^{18}O$ record of Williams et al. (1988).

TIME SCALE IN HOLES 716B, 714A, AND 633A

The chronology developed for the three holes is based on nannofossil stratigraphy (716B, 714A, and 633A), magnetostratigraphy (633A), *Globorotalia menardii* complex stratigraphy (633A), and oxygen isotope stratigraphy in Holes 716B and 633A for the last 1.1 m.y., and in Hole 714A for the last 0.55 m.y.

Late and Middle Pleistocene: 0–1.1 Ma, Holes 716B and 633A, and 0–0.55 Ma, Hole 714A

Our time scale for the last million years (more precisely, from 0 to 1.05 Ma) is based mainly on the identification of the oxygen isotope stages from the planktonic records that we generated for Holes 716B, 714A, and 633A by comparing them with such records as V28-239 (Shackleton and Opdyke, 1976), DSDP Site 502 (Prell, 1982), and DSDP 607 (Ruddiman et al., 1987), and with the smoothed-stack $\delta^{18}O$ record of Imbrie et al. (1984) and the composite $\delta^{18}O$ record of Williams et al. (1988). Sedimentation rates are assumed to be constant for each particular

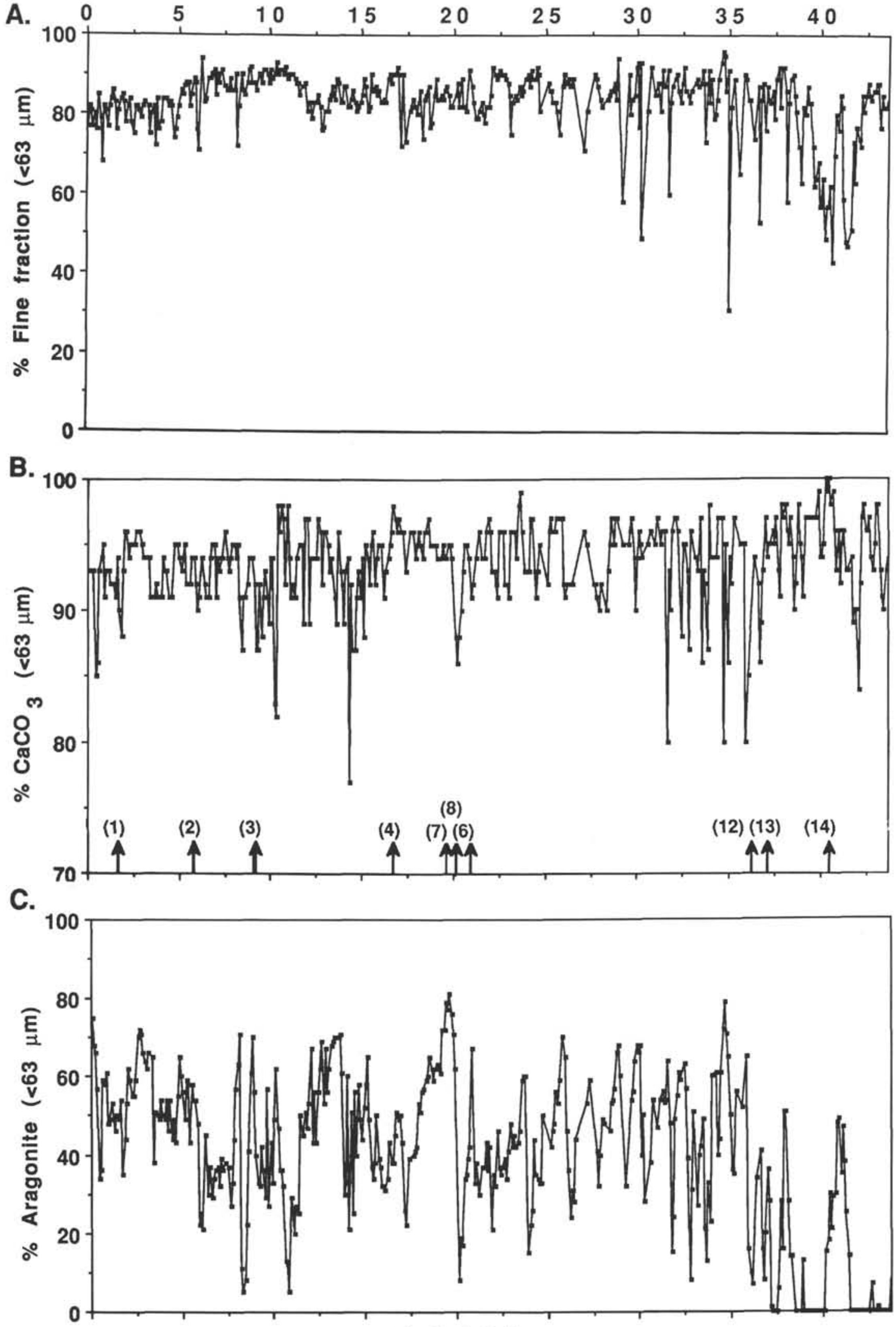

Figure 4. Depth variations for the top 43.5 m of Hole 633A of **(A)** the fine fraction, **(B)** the $CaCO_3$ content in the fine fraction, **(C)** aragonite and **(D)** magnesian calcite content in the carbonate fraction of the fine fraction, and **(E)** the planktonic record based mainly on *Globigerinoides sacculifera,* with some analyses done on *Globigerinoides rubra* in the top 8 m of Hole 633A. The numbers in parentheses refer to the datum levels based on nannofossil and magnetic stratigraphies; see Table 2 for corresponding datum levels.

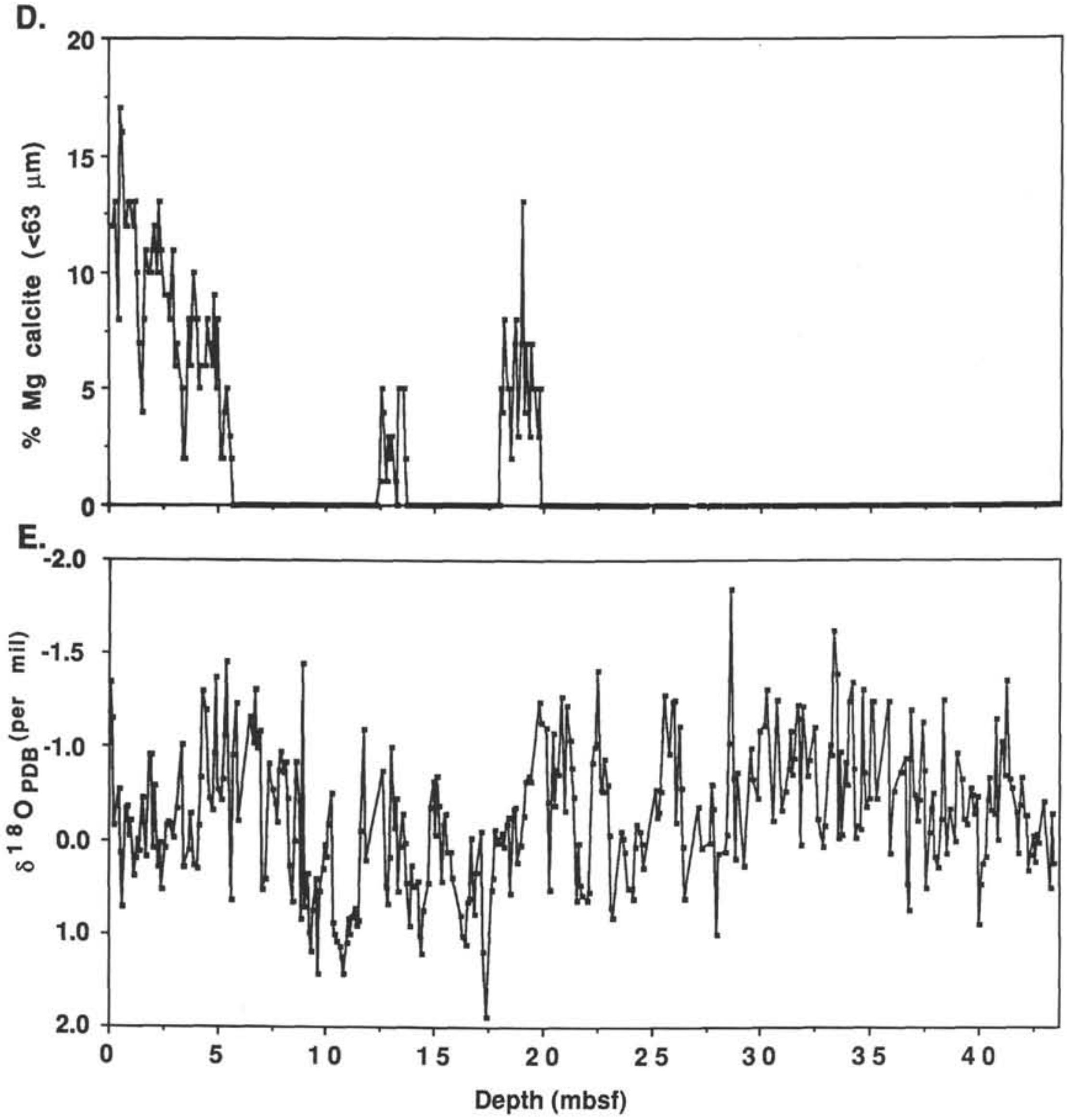

Figure 4 (continued).

isotope stage. The chronology of $\delta^{18}O$ stage boundaries developed by Imbrie et al. (1984) is used for the last 0.8 m.y., corresponding to the Stage 21/22 boundary, and the chronology developed by Williams et al. (1988) for the time interval between 0.8 and 1.1 Ma, applying some modifications of the stage numbers used by Williams et al. (1988). Figure 5 shows $\delta^{18}O$ chronologies based on Imbrie et al. (1984) and Williams et al. (1988). Discrepancies between the two chronologies are quite significant and range between ~37 and 24 k.y. (see Table IX in Williams et al., 1988) within the past 0.8 m.y. The discrepancy between the time scales for the isotope Stage 21/22 boundary is quite small (~0.4 k.y.). Preference was given to Imbrie's chronology for oxygen isotope stage boundaries down to the Stage 21/22 boundary, since the papers to which we refer in our discussion have used the Imbrie et al. (1984) time scale. Further back in time, we have relied on the time scale of Williams et al. (1988). We have, however, maintained the stage numbers published by Shackleton and Opdyke (1976) on V28-239 and by Prell (1982) on DSDP Site 502, where the Stage 23/24 boundary is defined as the upper boundary (0.92 Ma; Harland et al., 1982) of the normal polarity Jaramillo Subchron. In this paper, our Stage 23 includes Stages 23–27 of Williams et al. (1988). Our Stage 24 becomes their Stage 28, and our Stage 26 is equivalent to their Stage 32. In summary, our Stage 23/24, 24/25, and 25/26 boundaries are equivalent to the Stage 27/28, 28/29, and 31/32 boundaries, respectively, of Williams et al. (1988) and their individual ages, therefore, are 0.917, 0.930, and 1.007 Ma (Fig. 5 and Table 1).

Figure 6 shows a comparison of the SPECMAP smoothed-stack $\delta^{18}O$ record with the three $\delta^{18}O$ records of this study plotted vs. time, including the 1.1-Ma $\delta^{18}O$ records for Holes 633A and 716B, and the 0.55-Ma $\delta^{18}O$ record for Hole 714A. In this comparative diagram, the correlation between the different records, although at a few levels somewhat laborious, gives an insight into the quality of the $\delta^{18}O$ stratigraphy that can be applied to the three ODP sites of this study. Figure 7 shows depth vs age in the time scale based on $\delta^{18}O$ stratigraphy for the three sites analyzed in this paper. In Hole 716B (Fig. 7A), the available nannofossil datums (Table 2) plot quite well within the $\delta^{18}O$ time frame: datums 5 and 10 are somewhat off, but they have not been defined globally as have datums 2 and 3 (Thierstein et al., 1977). In Hole 714A (Fig. 7B), datums 2 and 3 (Table 2) fall

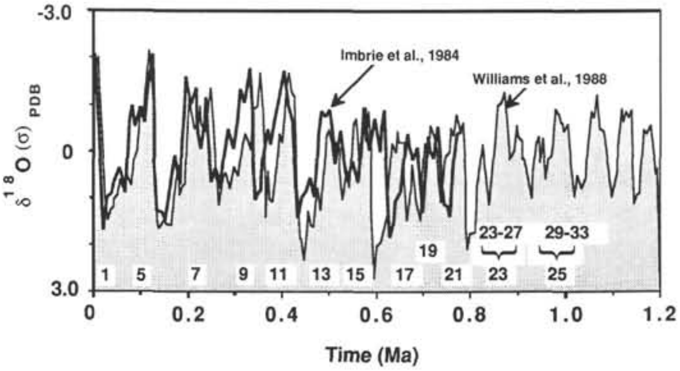

Figure 5. Comparison of mean linear interpolation ages (Williams et al., 1988) and SPECMAP ages (Imbrie et al., 1984) for stage boundaries, including the Stage 21/22 boundary (0.80 Ma). The stage numbers used in this paper are included. Stages 23, 24, and 25, which are identified in this paper, correspond to Stages 23–27, 28, and 29–33, respectively, of Williams et al. (1988).

close to the $\delta^{18}O$ time frame (within 1.5 m). In Hole 633A (Fig. 7C), datums based on nannofossil stratigraphy and magnetostratigraphy are available (Table 2) and show that the $\delta^{18}O$ time frame is correct. On the basis of Figure 7A–7C, general sedimentation rates remain quite constant for the last 1.1 m.y., even though sedimentation rates during interglacial stages are much higher than during glacial stages.

Early Pleistocene–Pliocene: 1.0–3.5 Ma, Hole 716B, and 1.0–2.15 Ma, Hole 633A

Because a $\delta^{18}O$ record is not yet available for Hole 716B and because it is difficult to identify on the $\delta^{18}O$ record in Hole 633A the different stages that Williams et al. (1988) have numbered in their composite record for the early Pleistocene, the time scale for the early Pleistocene and late Pliocene is based on the most accepted nannofossil datums (11, 15, 16, and 17; Table 2) available for Hole 716B, and on magnetostratigraphy (normal polarity Olduvai Subchron upper and lower boundaries 13 and 14) and nannofossil datum 12 (Table 2) available for Hole 633A. Based on Figures 7A and 7C, sedimentation rates drop by almost a factor of 2 during the late Pliocene in Holes 716B and

Table 1. Isotope stage boundaries with corresponding ages and core depths for Holes 714A and 716B (Maldives) and Hole 633A (Bahamas).

Isotope stages	Age (Ma)	Depth (mbsf)		
		Hole 716B	Hole 714A	Hole 633A
1/2	0.012	0.50	0.65	0.40
2/3	0.024	1.00	1.45	0.50
3/4	0.059	2.00	2.20	1.75
4/5	0.710	2.20	2.45	1.95
5/6	0.128	4.10	4.50	3.60
6/7	0.186	5.20	6.20	4.30
7/8	0.245	7.45	9.15	5.90
8/9	0.303	8.45	10.40	6.70
9/10	0.339	10.40	12.35	8.30
10/11	0.362	11.30	12.70	8.90
11/12	0.423	12.75	15.30	9.20
12/13	0.478	13.60	16.50	9.75
13/14	0.524	16.10	19.00	10.30
14/15	0.565	16.75	—	11.55
15/16	0.620	20.00	—	13.75
16/17	0.659	22.05	—	14.80
17/18	0.689	23.80	—	15.80
18/19	0.726	24.45	—	16.70
19/20	0.736	25.60	—	17.20
20/21	0.763	26.35	—	17.80
21/22	0.790	27.30	—	18.50
22/23	0.813	28.20	—	19.05
23/24 (27/28)[a]	0.917	32.75	—	20.15
24/25 (28/29)[a]	0.930	33.90	—	20.40
25/26 (29/30)[a]	1.007	36.40	—	21.50
26/27 (30/31)[a]	1.043	38.60	—	22.20

[a] Williams et al. (1988) equivalent stage boundaries.

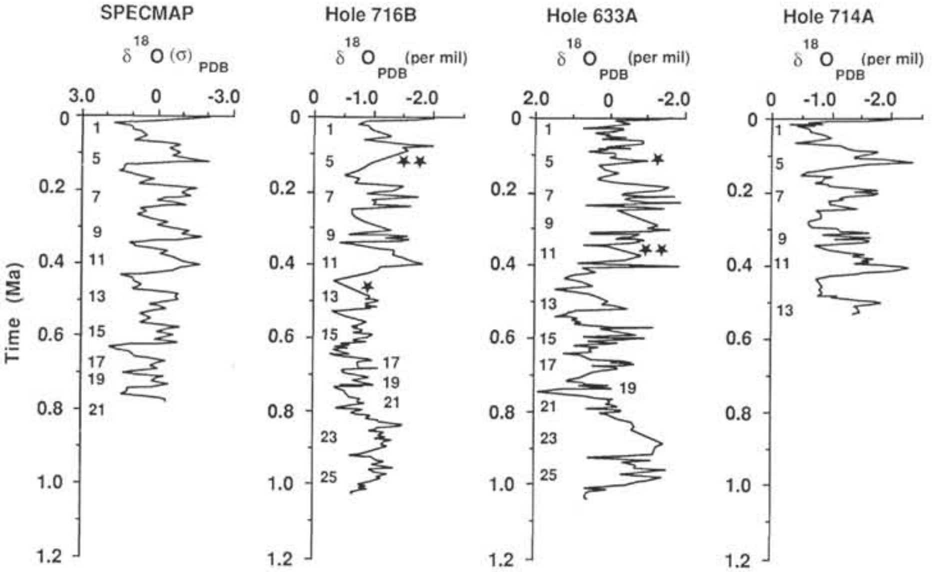

Figure 6. Comparison between SPECMAP smoothed $\delta^{18}O$ record (Imbrie et al., 1984) and the planktonic $\delta^{18}O$ records in Holes 716B, 633A, and 714A. Core-depth conversion to time is based on the identification of the oxygen-isotope stages in comparison with the SPECMAP $\delta^{18}O$ record and the use of ages for stage boundaries down to the 21/22 stage boundary from Imbrie et al. (1984). For earlier stages, boundary ages are from Williams et al. (1988) applied to their modified stage numbers (see text for details; selected ages for stage boundaries are included in Table 1). Sedimentation rates are assumed to be constant for each stage. * = 0.2–0.5-m hiatus; ** = 0.5–1.0-m hiatus.

Table 2. Age controls for Holes 714A and 716B (Maldives) and Hole 633A (Bahamas).

Age (Ma)	Datum levels	Depth (mbsf) Hole 716B	Depth (mbsf) Hole 714A	Depth (mbsf) Hole 633A
0.08	(1) *E. huxleyi* Acme Zone	—	—	2.05
0.27	(2) FO *E. huxleyi*	8.90	8.85	6.00
0.46	(3) LO *P. lacunosa*	14.65	18.00	9.00
0.73	(4) Brunhes/Matuyama boundary	—	—	17.11
0.82	(5) *Reticulofenestra* sp. A (L)	23.90	—	—
0.92	(6) *Gephyrocapsa oceanica* rejuvenation	—	—	21.10
0.92	(7) Matuyama/upper Jaramillo boundary	—	—	19.50
0.97	(8) lower Jaramillo/Matuyama	—	—	20.15
1.10	(9) LO large *G. oceanica*	34.45	—	—
1.29-1.36	(10) FO large *G. oceanica*	43.20	—	—
1.45-1.46	(11) LO *Calcidiscus macintyrei*	52.30	—	—
1.6	(12) FO *G. caribbeanica*		—	36.40
1.67	(13) upper Olduvai boundary	—	—	37.65
1.87	(14) lower Olduvai boundary	—	—	40.65
1.89	(15) LO *D. brouweri*	62.95	—	—
2.35	(16) LO *D. pentaradiatus*	85.25	—	—
3.45	(17) LO *Sphenolithus* sp.	106.00	—	—

Note: FO = first occurrence and LO = last occurrence.

633A. In Hole 716B, sedimentation rates drop from 36 to 19 m/m.y. just before 2.4 Ma, whereas in Hole 633A sedimentation rates drop from 24 to 12 m/m.y. at the Pliocene/Pleistocene boundary (around 1.6 Ma; see also figs. 3 and 4 in Droxler et al., 1988a).

RESULTS

Presentation of Results

Fine Aragonite to Total Sediment

Because of the high and cyclic downcore variations in Holes 714A and 716B (Figs. 2 and 3) of (1) the fine fraction ($<63\ \mu$m) (= $\%$ Fine Fract$_{(\text{tot sed})}$; (2) the carbonate content in the fine fraction ($<63\ \mu$m) (= $\%$ Fine CaCO$_{3(\text{Fine Fract})}$); and (3) the aragonite and magnesian calcite proportions in the carbonate content of the fine fraction itself (= $\%$ Fine Arag$_{(\text{Fine CaCO3})}$) and (= $\%$ Fine MgCalc$_{(\text{Fine CaCO3})}$), respectively, it is important to recalculate the "raw data" values for aragonite and magnesian calcite content relative to the total sediment by the following simple relation:

$$\%\ \text{Fine Arag}_{(\text{tot sed})} = [\%\ \text{Fine Arag}_{(\text{Fine CaCO3})} \times \%\ \text{Fine CaCO}_{3(\text{Fine Fract})} \times \%\ \text{Fine Fract}_{(\text{tot sed})}] \ / \ 10^4 \qquad (1)$$

and

$$\%\ \text{Fine MgCalc}_{(\text{tot sed})} = [\%\ \text{Fine MgCalc}_{(\text{Fine CaCO3})} \times \%\ \text{Fine CaCO}_{3(\text{Fine Fract})} \times \%\ \text{Fine Fract}_{(\text{tot sed})}] \ / \ 10^4. \qquad (2)$$

Even though downcore variations of the fine fraction ($<63\ \mu$m) and the carbonate content in the fine fraction ($<63\ \mu$m) were not as high in Hole 633A (Fig. 4) as in Holes 714A and 716B, the values of the raw data of Hole 633A were also recalculated relative to the total sediment in order to make an easier comparison between holes in the Maldives and in the Bahamas.

Aragonite and Magnesian Calcite vs. Time

Since we were able to develop an age/depth model for the three holes based on oxygen isotope, nannofossil and magnetic stratigraphies (see previous section), we present the mineralogical data relative not only to the total sediment, but vs. "Time" rather than "Core Depth". Results are then displayed in two separate sections. The first section presents a comparison of the fine aragonite and magnesian calcite content (%) to "Total Sediment" with their respective δ^{18}O record for the last 1.1 m.y. in Hole 716B, the last 0.55 m.y. in Hole 714A, and the last 2.0 m.y. in Hole 633A. The second results section presents a comparison between the different aragonite records from the three holes and the published carbonate (calcite) preservation records in deep-waters based on the carbonate content of the sediments (Hays et al., 1969; Farrell and Prell, 1987), and on the foraminifer dissolution (calcite) indexes of Peterson and Prell (1985) and Crowley (1985), as well as the pteropod dissolution (aragonite) index of Haddad (1986).

Comparison between Fine Aragonite and δ^{18}O Records

The comparison between δ^{18}O records and the fine aragonite cyclic variations downcore is quite important in understanding the origin of the aragonite cycles in periplatform sediments. Low-latitude δ^{18}O planktonic records, in addition to their great potential in terms of Pleistocene stratigraphy, can also be used as a proxy sea-level curve (Shackleton and Opdyke, 1973; Shackleton, 1986). If one assumes that the aragonite cycles only reflect the input variations of bank-derived aragonite in relation to flooding and exposure of the shallow banks, then the aragonite cycles will be in phase with the proxy sea-level δ^{18}O curve, which in turn will be roughly equivalent to a flooding curve. In this case, light oxygen isotope values during sea-level high stand will correspond to periods of flooded banks, whereas heavy oxygen isotope values during sea-level low stands will correspond to periods of exposed banks.

Figure 8 displays the comparison between δ^{18}O and aragonite cycles in Holes 633A and 716B for the past 1.0 m.y. and in Hole 714A for the past 0.55 m.y. Figures 9, 10, and 11 are enlarged segments from 0 to 0.4 Ma, from 0.3 to 0.7 Ma, and from 0.65 to 1.05 Ma of the entire record shown in Figure 8 to aid the visual comparison of both records.

The aragonite and δ^{18}O records for the three holes are usually in phase with one another; intervals of high aragonite content parallel intervals characterized by light δ^{18}O values, which are thought to correspond with periods of flooded banks, whereas intervals of low aragonite content parallel intervals characterized by heavy δ^{18}O values, which are assumed to correspond with periods of bank exposure. In isotope Stages 1-12, the phase relationship between aragonite content and δ^{18}O is very

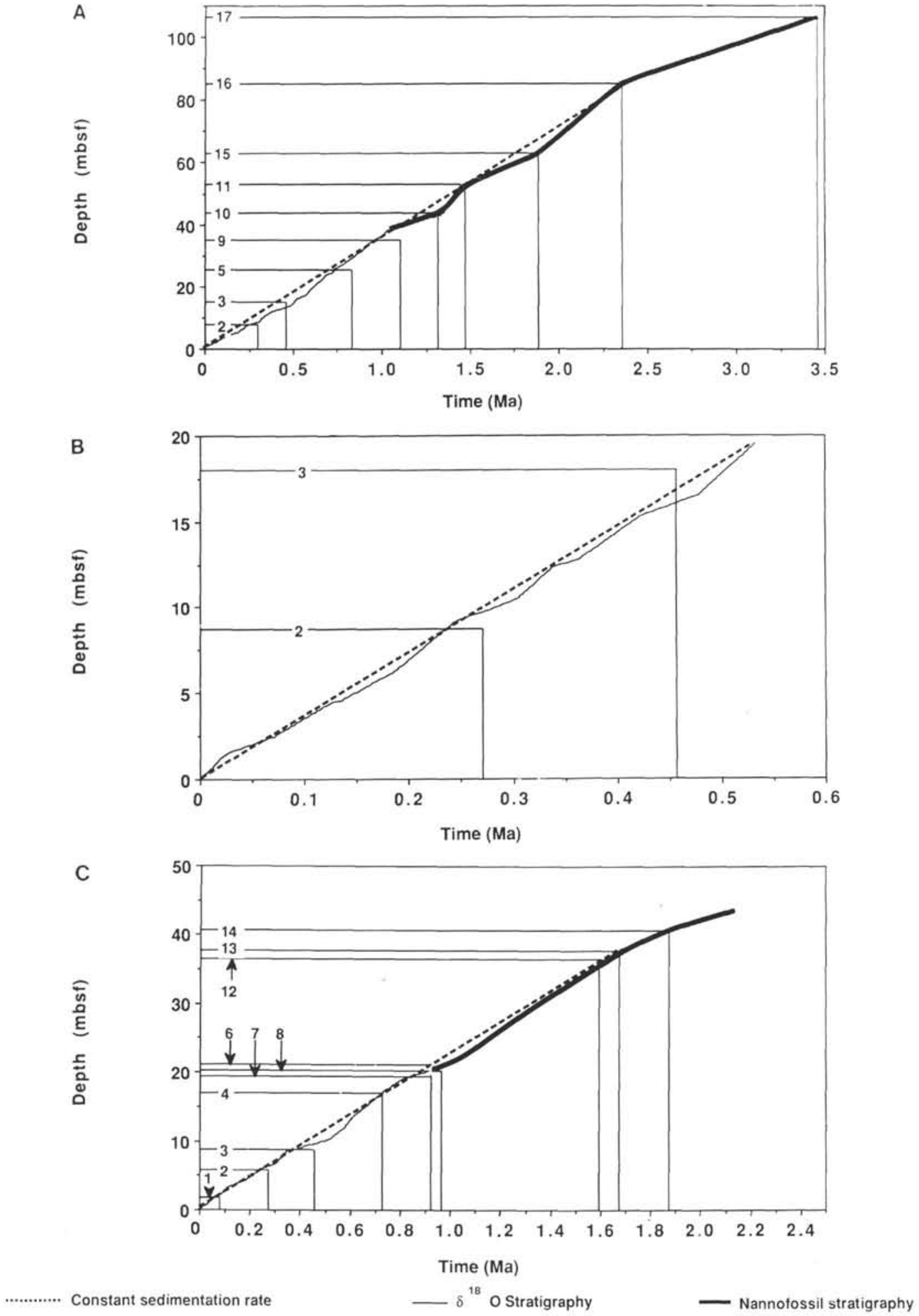

Figure 7. Age vs. depth curves for **(A)** the top 108 m of Hole 716B, **(B)** the top 19.5 m of Hole 714A, and **(C)** the top 43.5 m of Hole 633A. Age vs. depth models for the last 1.1 m.y. in Holes 716B and 633A and for the last 0.55 m.y. in Hole 714A (thin line) are based on oxygen isotope-stratigraphy, assuming constant sedimentation rates for each isotope stage. Available datum levels (plotted as numbers on the diagrams and identified in Table 2) are based on nannofossil stratigraphy (Holes 716B, 714A, and 633A) and magnetic stratigraphy (Hole 633A). Age vs. depth models for times earlier than 1.1 Ma in Holes 716B and 633A are based on established datum levels, nannofossil stratigraphy for Holes 716B and 633A, and magnetic stratigraphy for Hole 633A (thick line). Sedimentation rates are assumed constant between the different datum levels. Notice that the late Pliocene sedimentation rates are lower than the Pleistocene sedimentation rates by a almost a factor of 2. A change of sedimentation rates occurred at 2.5 Ma in Hole 716B and at 1.7 Ma in Hole 633A.

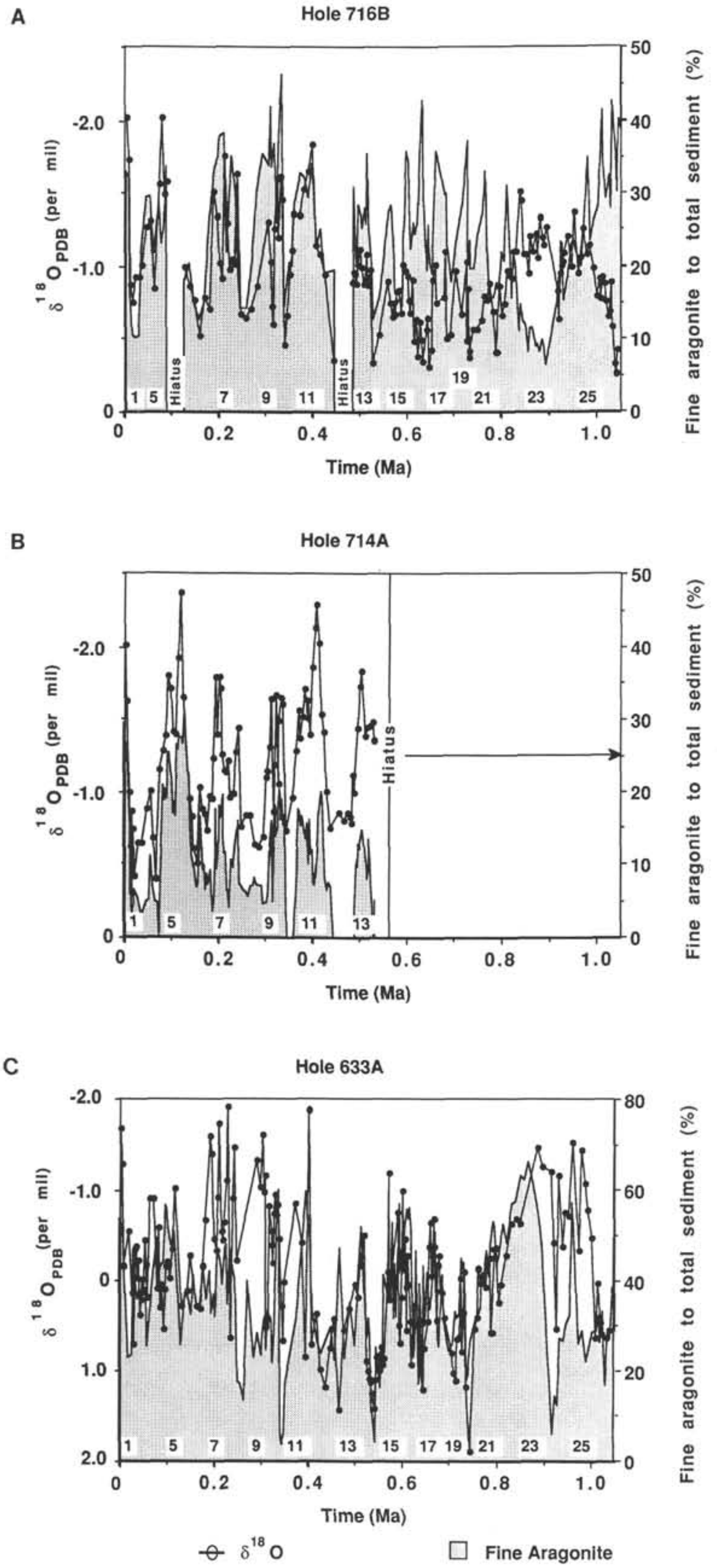

Figure 8. General comparison between planktonic $\delta^{18}O$ and aragonite (fine aragonite to total sediment) records for the past 1.05 m.y. in Holes 716B (**A**), 714A (**B**), and Hole 633A (**C**). The $\delta^{18}O$ and aragonite records are limited to the last 0.55 m.y. in Hole 714A because of a 7.5-Ma-long hiatus at 19.5 mbsf. Oxygen isotope interglacial stages are identified by odd numbers from 1 to 25. (Figures 9, 10, and 11 are blow ups of these three records).

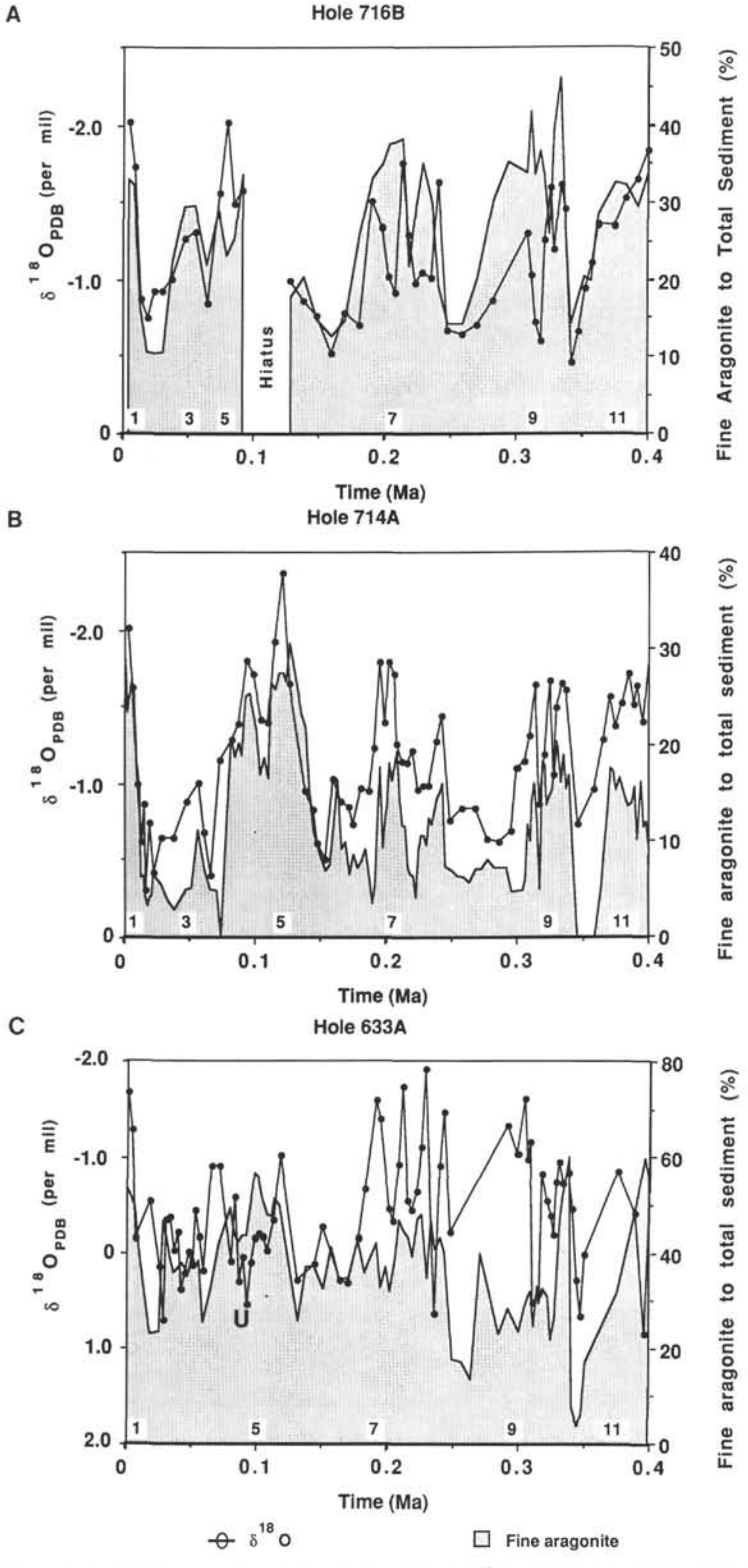

Figure 9. Detailed comparison between planktonic $\delta^{18}O$ and aragonite records for the last 0.4 m.y. for Holes 716B (**A**), 714A (**B**), and 633A (**C**). Oxygen isotope interglacial stages are identified by odd numbers from 1 to 11. Note the in-phase correlation between the $\delta^{18}O$ and aragonite records. Hole 716B displays the best match between the two records. Note in Hole 714A and 633A the general aragonite decrease with time. Conversely, in Hole 716B, average aragonite values have a tendency to increase with time. In Hole 714A, the aragonite minima usually occur at the very end of each interglacial stage instead of during each glacial stages, as in Holes 716B and 633A.

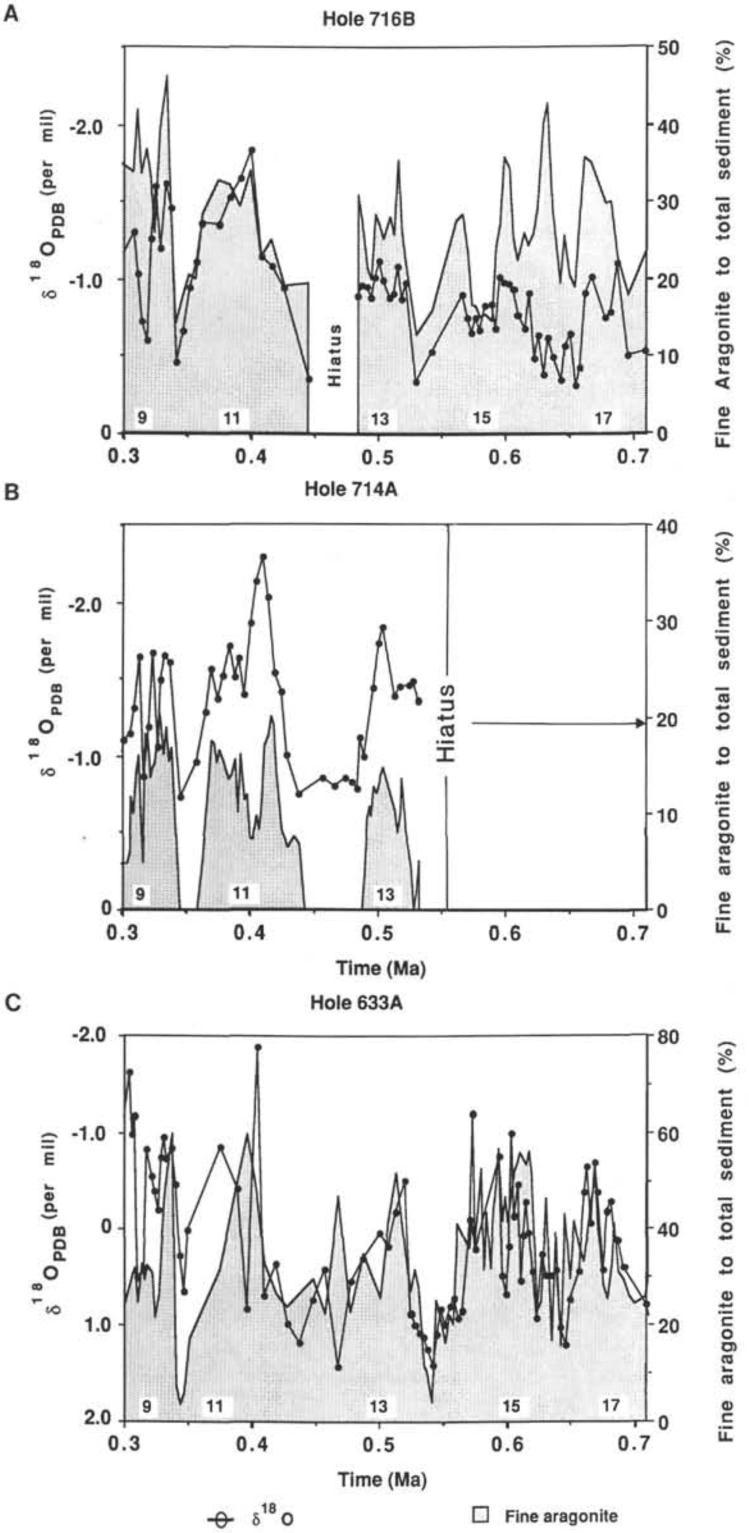

Figure 10. Detailed comparison between planktonic $\delta^{18}O$ and aragonite records between 0.3 and 0.7 Ma in Holes 716B (**A**), 714A (**B**), and 633A (**C**). Oxygen isotope interglacial stages are identified by odd numbers from 9 to 17. Note the in-phase correlation between $\delta^{18}O$ and aragonite records down to Stage 14. In Stages 15 and 16 of Hole 716B, $\delta^{18}O$ and aragonite records are totally out of phase. A major aragonite peak occurs during the second half of glacial Stage 16 and an aragonite minimum is located in the middle of Stage 15. In Hole 633A, an aragonite maximum occurs just at the end of glacial Stage 16.

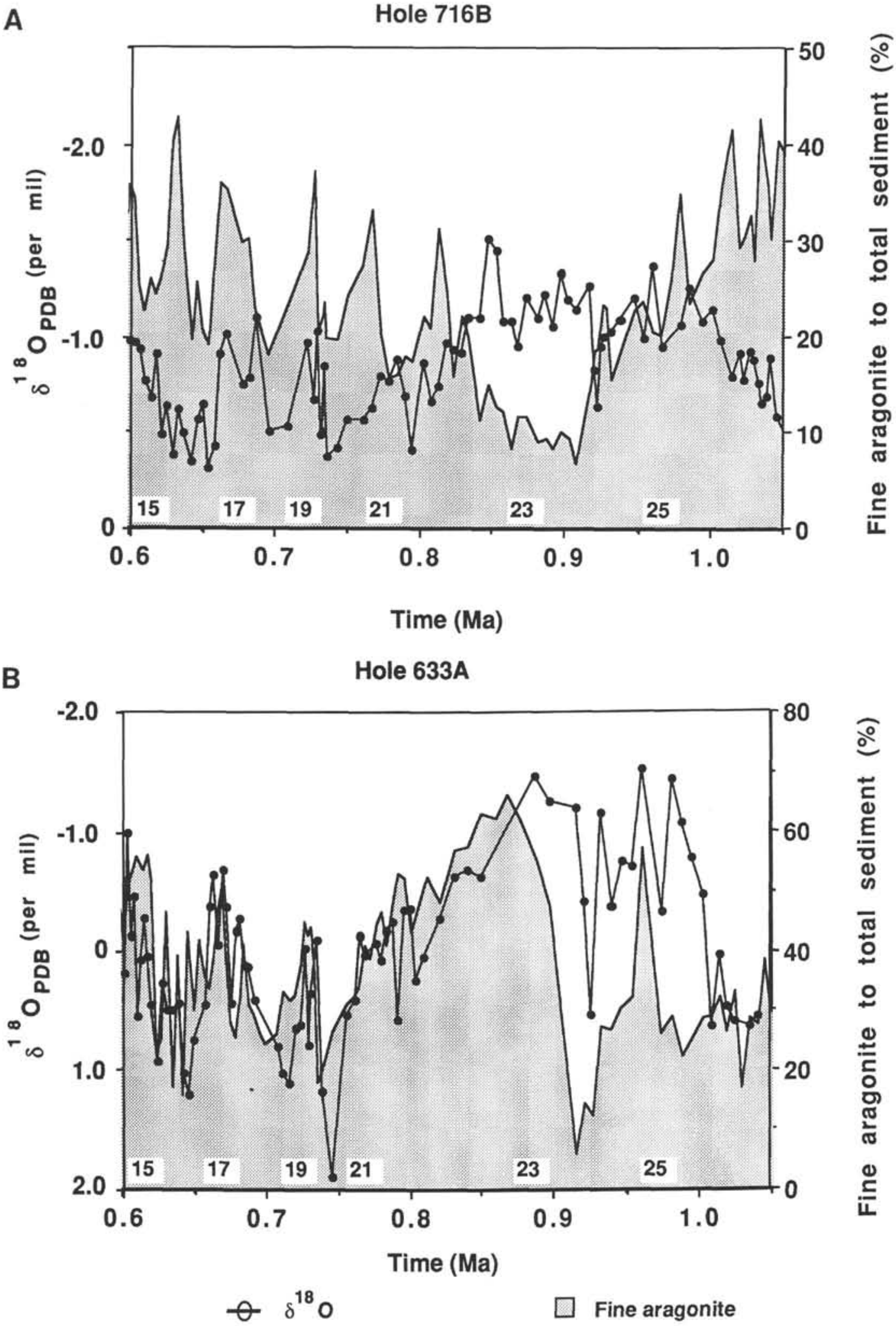

Figure 11. Detailed visual comparison between planktonic $\delta^{18}O$ and aragonite records between 0.6 and 1.1 Ma in Holes 716B (**A**) and 633A (**B**). Oxygen isotope interglacial stages are identified by odd numbers from 15 to 25. Note the out-of-phase relationship between the $\delta^{18}O$ and aragonite records in Stages 21–26 and particularly during interglacial Stage 23 in both holes. The strongest aragonite minimum of the last 1 m.y. occurred in both holes at the beginning of interglacial Stage 23 (0.9 Ma), corresponding to light $\delta^{18}O$ values. Hole 716B displays an out-of-phase relationship between $\delta^{18}O$ and aragonite records during the entire Stage 23, whereas the sharp aragonite increase in Hole 633A clearly lags behind the $\delta^{18}O$ depletion by at least 10 k.y.

clear in Hole 716B (Figs. 8A, 9A, and 10A). This phase relationship is also observed in Hole 714A (Figs. 8B, 9B, and 10B), with the exceptions of a few subtle lags at the interglacial to glacial boundaries, in which $\delta^{18}O$ enrichment lags behind the aragonite decrease (i.e., the $\delta^{18}O$ maximum occurs after the aragonite minimum). The aragonite/$\delta^{18}O$ relationship is not as clear for Hole 633A as it is in the Maldives holes (Figs. 8C, 9C, and 10C). We are quite confident, however, that the few correlative problems encountered in Hole 633A might be more analytical than primary in origin and possibly related to the occurrence of small hiatuses, since good correlations have been observed in the Bahamas at least down to Stages 10 (Droxler et al., 1983) and 12 (Boardman et al., 1986).

Further back in time (Stages 13–26), the "in-phase correlations" between both aragonite and $\delta^{18}O$ records disappear at certain levels. In Holes 716B and 633A (Figs. 8A and 8C, 10A and 10C, and 11A and 11B), Stages 15 and 16 and the interval including Stages 21, 23, 25, 26, and 27 are the most obvious cases in which aragonite and $\delta^{18}O$ records are either out of phase or display major lag times. In Hole 716B, Stages 15 and 16 are clear examples in which both signals are out of phase (Fig. 10A). For instance, an aragonite peak occurs during the second part of Stage 16, well before the glacial-to-interglacial Stage 16/15 transition. An aragonite minimum also occurs in the middle of interglacial Stage 15. In Hole 633A, at the same glacial/interglacial stage boundary, aragonite reaches a maximum well before the lightest $\delta^{18}O$ value of Stage 15 (Fig. 10C). The other interval, during which aragonite and $\delta^{18}O$ records are not in phase in Holes 633A and 716B, is in the general transition from early to middle Pleistocene Stages 27–21, but especially during Stage 23 (Figs. 8A, 8C, 11A, and 11B).

In Stage 23 of Hole 716B, aragonite and $\delta^{18}O$ are completely out of phase (Fig. 11A). The $\delta^{18}O$ depletion at the glacial/interglacial Stage 24/23 boundary corresponds to a decrease of aragonite, whereas some of the lightest $\delta^{18}O$ values at the very beginning of Stage 23 (0.9 Ma) correspond to the lowest aragonite values (<10%) observed during the entire Pleistocene. In addition, the gradual enrichment of $\delta^{18}O$ values toward the end of Stage 23 surprisingly corresponds to a gradual aragonite increase. Similar out-of-phase relationships can be observed in Stages 22/21 and 26/25. An aragonite minimum occurs at the beginning of Stage 21 defined with light values of $\delta^{18}O$, an aragonite maximum at the transition between Stages 22/21 and glacial Stage 26 corresponds to a general interval characterized by high aragonite values marked with two aragonite maxima.

The clearest case of aragonite increase lagging behind $\delta^{18}O$ depletion occurs at the beginning of interglacial Stage 23 in Hole 633A (Fig. 11B). Therefore, the aragonite minimum at the very beginning of Stage 23 (0.9 Ma), which corresponds to the lowest $\delta^{18}O$ values, coincides with the aragonite minimum observed in Hole 716B (Figs. 8A, 8C, 11A, and 11B). Stages 22/21 cannot be well distinguished in Hole 633A and trying to observe phase changes or lags between aragonite and $\delta^{18}O$ would be questionable. Aragonite reaches high values only during the second half of Stage 25. The coincidental occurrence of the most pronounced aragonite minimum during the beginning of Stage 23 in Holes 633A (Bahamas) and 716B (Maldives) cannot be as accidental as one would first think. This period of time (Stages 23/22) is also marked in Holes 633A and 716B by the last short downcore appearance of magnesian calcite (Fig. 12). The penultimate downcore occurrence of magnesian calcite appears synchronously again in Holes 633A and 716B centered within Stage 15, another interval in which aragonite and $\delta^{18}O$ are also out of phase or lag behind one another as in Stage 23 (Figs. 10A and 10C). The comparison between the aragonite records from the Bahamas and the Maldives, with the deep carbonate record in the equatorial Pacific Ocean, will help in the interpretation of these peculiar Pleistocene intervals (see "Results" section below).

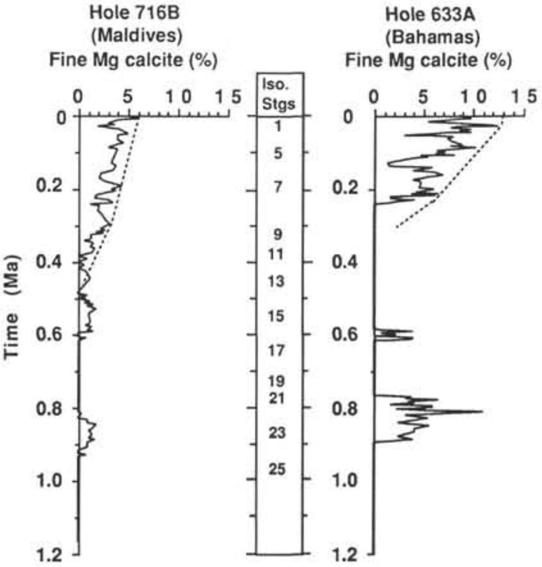

Figure 12. Time variations of magnesian calcite in Hole 716B and Hole 714A for the past 1.2 m.y. Note in Hole 716B the gradual decrease of magnesian calcite from the surface sediment to 0.4 Ma, its reappearance between 0.5 and 0.6 Ma (Stage 15), as well as its final reappearance between 0.8 and 0.9 Ma (Stage 23). An identical pattern is observed in Holes 633A (this figure) and 632A (see Reymer et al., 1988, fig. 3).

Below Stage 26, the aragonite record in Hole 716B is completed down to 108 mbsf, corresponding to the early Pleistocene and late Pliocene (1.0–3.5 Ma) (Fig. 13). As in the late and middle Pleistocene, aragonite cycles are well developed. Aragonite, ubiquitous in Hole 716B, decreases downcore mostly through one clear step between 1.8 and 2.0 Ma, separating two segments characterized by a distinct average aragonite content (Fig. 13). In the first segment (between 1.0 and 1.8 Ma), aragonite content roughly averages 30% and reaches the highest values for the entire 3.5-m.y. record. Aragonite content averages 15% in the second segment (between 2.0 and 3.5 Ma); this average value is the lowest for the past 3.5 m.y. (Fig. 13). The comparison between $\delta^{18}O$ and aragonite records for the early Pleistocene and the late Pliocene is not possible since we have yet to produce a $\delta^{18}O$ curve for Hole 716B below 1.1 Ma.

In Hole 633A from the Bahamas, existing aragonite and $\delta^{18}O$ records (Droxler et al., 1988b) can be compared during the early Pleistocene and late Pliocene, equivalent to the period between 1.0 and 2.1 Ma (Figs. 14, 15A, 15B, and 15C). Identification of $\delta^{18}O$ stages during the early Pleistocene and part of the late Pliocene (up to 1.7 or 1.9 Ma) have been attempted by several authors (Van Donk, 1976; Ruddiman et al., 1986, 1987; and Williams et al., 1988). Each study came up with a different number of stages for the past 1.7 m.y. At the top of the normal polarity Olduvai Subchron (1.67 Ma), Stage 37 was identified in V16-205 by Van Donk (1976), Stage 47 or 49 in V28-239 by Shackleton and Opdyke (1976), Stage 65 in Site 607 by Ruddiman et al. (1987), and finally Stage 59 in the composite record of Williams et al. (1988). In Hole 633A, the top of the Olduvai Subchron (1.67 Ma) corresponds to Stage 49 (Fig. 15B), a similar number of stages to those in V28-239 following Shackleton and Opdyke's stage selection. We use our stage numbers in this study for the early Pleistocene and late Pliocene in Hole 633A only to

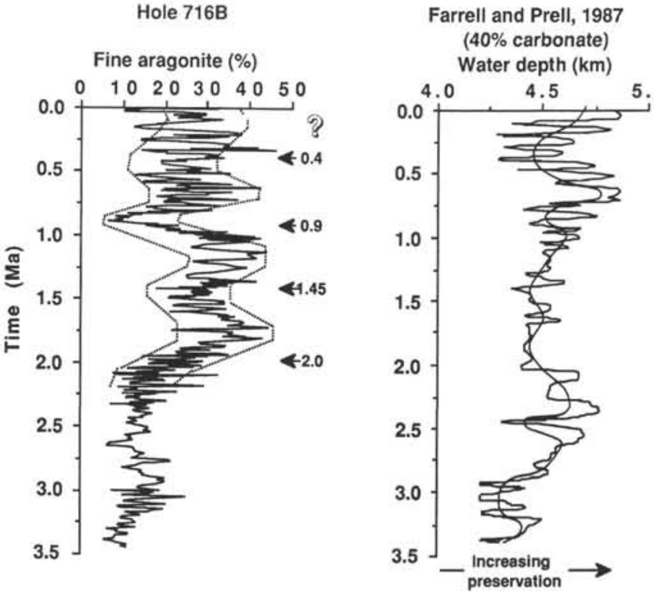

Figure 13. Time variations of aragonite in Hole 716B for the past 3.5 m.y. Note the aragonite supercycles (roughly with a 0.5-m.y.-long period) superposed on the aragonite cycles (visually estimated as 100- and 40-k.y.-long cycles). Note also the obvious, but unexplained, deviation of the aragonite record from the supercycles during the past 0.4 m.y. The aragonite record is compared with the bathymetric time variations of the 40% carbonate contour in the equatorial Pacific Ocean (Farrell and Prell, 1987). Note the rather unimpressive comparison between the timing of the aragonite supercycles and the general carbonate record of Farrell and Prell (1987). This observation contrasts, however, in Figure 19 with the good agreement for the past 2.0 m.y. between the timing of the aragonite supercycles and the carbonate record of Core RC11-209 from the equatorial Pacific Ocean (Hays et al., 1969; Moore et al., 1982).

be able to refer to specific cycles without claiming to introduce here a new stage numbering system.

In Hole 633A, asymmetric aragonite cycles are well defined during the early Pleistocene. Though the aragonite cycles are present during the late Pliocene, they are not as clear, however, as during the Pleistocene and aragonite is not detected during half of the time between 1.65 and 2.1 Ma. The early Pleistocene aragonite cycles are not always in phase with $\delta^{18}O$. The in-phase relationship seems to be the case only for interglacial Stages 33, 39, 41, 45(?), and 47 (Fig. 15A and 15B). Most of the time (Stages 29, 31, 35, 37, and 49), as in interglacial Stage 23, the aragonite minimum occurs at the very beginning of the interglacial stage and the sharp aragonite increase lags roughly 10 k.y. behind the rapid $\delta^{18}O$ depletion at each glacial-to-interglacial transition. It is only in a few cases (for instance in Stage 27) that aragonite peaks occur during the second part of a glacial stage or at the glacial-to-interglacial transition.

In summary, during the late Pleistocene, aragonite and $\delta^{18}O$ are usually in phase (i.e., in the Bahamas in several of the piston cores studied [Droxler et al., 1983, 1989; Boardman et al., 1986] and Hole 633A [Droxler et al., 1988b, and this chapter]). They are also in phase in piston cores from the Nicaragua Rise and the Maldives (Droxler et al., 1989) and in Holes 714A and 716B in the Maldives (this chapter), with the exception of piston cores on the Queensland Plateau (southwest Pacific Ocean), where aragonite and $\delta^{18}O$ are out of phase during the past 100 k.y. (Droxler et al. 1989)]. Further back in time (middle/early Pleistocene and late Pleistocene), however, and during certain intervals, aragonite and $\delta^{18}O$ records become out of phase or display detectable lags between one another. Intervals during which aragonite and $\delta^{18}O$ do not appear in phase seem to be correlatable between the Maldives and Bahamas records. As mentioned above, these intervals, during the last 1.1 m.y., are Stages 15 and 16 and Stages 21–26 (an interval centered on Stage 23), located at the early to middle Pleistocene transition. In addition, magnesian calcite, as a secondary component, reappears unexpectedly during these two particular intervals (Stages 15 and 23). The observation that aragonite cycles are not always in phase with $\delta^{18}O$ is important to our argument that the aragonite cycles are not only a direct input function resulting from bank flooding and exposure, but that these cycles are also the result of seafloor dissolution of this aragonite input. This is analogous with the carbonate sea floor dissolution of the planktonic calcitic input. We are aware that the $\delta^{18}O$ record is only a proxy indicator of sea level and that sea-level high stands during certain interglacial stages can be short of flooding a flat top bank or can also overflow a bank and result in drowning it.

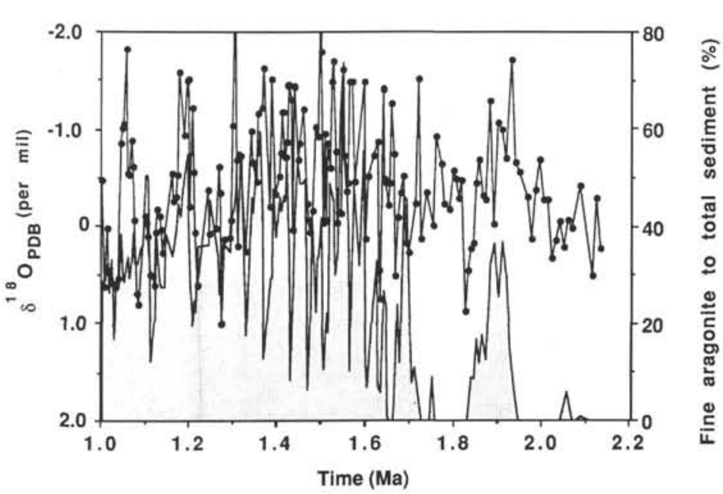

Figure 14. General comparison between planktonic $\delta^{18}O$ and aragonite records from 1.0 to 2.1 Ma in Hole 633A (see Fig. 15 for more detailed comparisons).

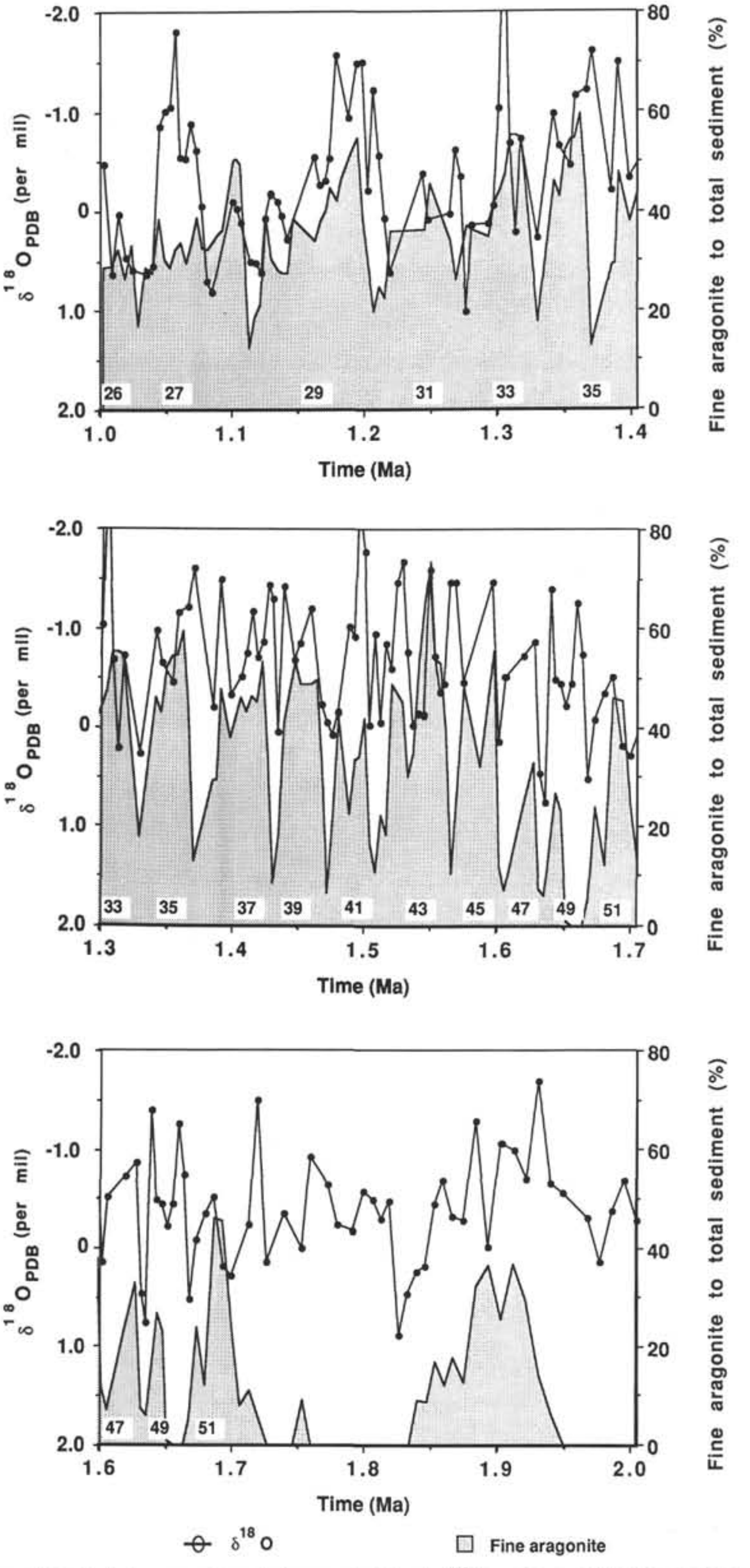

Figure 15. Detailed comparison between planktonic $\delta^{18}O$ and aragonite records from 1.0 to 2.1 Ma in Hole 633A. Oxygen isotope interglacial stages are identified by odd numbers from 27 to 51 between 1.0 and 1.7 Ma (top of Olduvai Subchron). Aragonite cycles are either in phase with the $\delta^{18}O$ cycles or the sharp aragonite increases lag behind the glacial-to-interglacial stage boundaries by 10 k.y. or more, as is clearly the case in Stage 23 (Fig. 11). Note that the irregular low values of aragonite, or intervals characterized by the absence of aragonite, show no clear relationship with the $\delta^{18}O$ record during the late Pliocene (1.6–2.1 Ma).

Comparison between Fine Aragonite and Carbonate Preservation Records

The Last 0.7 m.y. in Holes 714A and 716B

Peterson and Prell (1985) demonstrated in a set of piston cores from the Ninetyeast Ridge (eastern equatorial Indian Ocean) that carbonate preservation, based on a composite dissolution index (CDI), varies periodically through time with dominant 100- and 40-k.y. cyclicity. In their data set, the carbonate preservation pattern appears to be offset from the $\delta^{18}O$ glacial/interglacial records. Preservation maxima occur at glacial-to-interglacial transitions, whereas dissolution maxima occur at interglacial to glacial transitions. This particular pattern has been suggested to be global in several studies (e.g., Crowley, 1983, 1985). The data set of Peterson and Prell (1985) also shows evidence of the existence of a longer supercycle, illustrated by generally poor carbonate preservation between 0.3 and 0.6 Ma. This supercycle is also well developed in the carbonate records of the equatorial Pacific Ocean, where a poor carbonate interval occurred between 0.2 and 0.5 Ma (Adelseck, 1977; Hays et al., 1969; Moore et al., 1982; Vincent, 1985; Farrell and Prell, 1987, 1989), and in the North Atlantic Ocean, where the 0.2–0.45-Ma interval in the mid-Brunhes is known for its poor preservation interval (Crowley, 1985).

Our interpretation of the aragonite cycles, since Droxler et al. (1983), says that these cycles not only record an input function of bank-derived aragonite, produced by alternate flooding and exposure of the nearby banks, but also a preservation of that input tied to climate-induced variable seafloor dissolution. To test our interpretation, we compared (Fig. 16) Peterson and Prell's CDI record with the carbonate preservation record based on the pteropod ratio of Hole 716B and the aragonite 0.6-m.y. record of Holes 714A and 716B. Peterson and Prell's age/depth model is based on oxygen isotope stratigraphy, as is our model with ages of stage boundaries defined by Imbrie et al. (1984). The pteropod ratio is defined as (# whole pteropods)/(# whole pteropods + # pteropod fragments). Decreasing values of the pteropod ratio, therefore, correspond to decreasing preservation. The similarities between the aragonite record of Hole 714A (water depth, 2100 mbsl) and Peterson and Prell's preservation curve are quite impressive. The clear general aragonite decrease with time corresponds to the general decrease of preservation with age noticed by Peterson and Prell as part of the "Brunhes dissolution cycle," with the poorest preservation intervals located between 0.3 and 0.6 Ma. Peaks of dissolution in Peterson and Prell's curve correspond to well-defined aragonite minima in Hole 714A, which occur at the end of each interglacial stage, and peaks of preservation correspond to sharp aragonite increases at each glacial-to-interglacial transition (Fig. 16). As expected, the comparison between the aragonite record in Hole 716B (a rather shallow site with a water depth of 540 mbsl) and the Peterson and Prell's CDI record is not as convincing as it is with the aragonite record in the deepest site (Hole 714A). The aragonite record does not display a systematic decrease with time. Also, although sharp aragonite increases generally coincide with the preservation peaks in Peterson and Prell's CDI Record, the dissolution maxima on the CDI curve correspond to high aragonite values at about 0.3 and 0.4 Ma or to aragonite decreases on the last two interglacial to glacial (7/6 and 5/4) transitions.

In Figure 16, the CDI carbonate preservation curve of Peterson and Prell (1985) is also juxtaposed with the variations with time of the pteropod ratio for Hole 716B during the past 0.6 m.y. The two curves (CDI and pteropod ratio) are again overlain on top of each other in Figure 17. The excellent match between the two curves, mostly between 0 and 0.35 Ma, illustrates that fragmentation of pteropod tests amply records the mid-Brunhes dissolution interval in Hole 716B (540 m of water depth). This

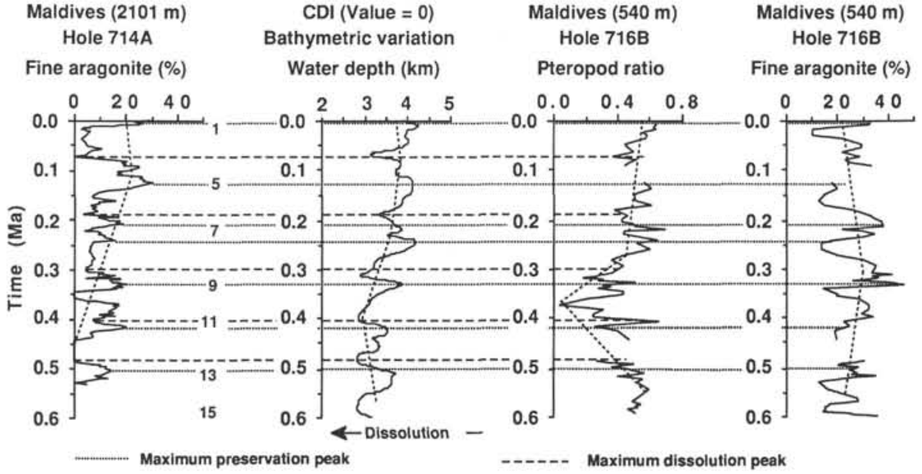

Figure 16. The 0.6-m.y.-long aragonite records for Holes 716B and 714A compared with the carbonate preservation record (CDI) of Peterson and Prell (1985) from the eastern equatorial Indian Ocean, and the Hole 716B pteropod ratio (whole tests/whole tests + fragments). The CDI and pteropod ratio curves are superposed on top of each other in Figure 17 to show the excellent correlation between the two. Note the general agreement between the Hole 714A aragonite record, the CDI from Peterson and Prell (1985), and the Hole 716B pteropod ratio for evidence of a mid-Brunhes poor preservation interval. Also, note the detailed correlations between the CDI record and the Hole 714A aragonite record: maximum preservation peaks correspond to aragonite maxima, and maximum dissolution peaks correspond to aragonite minima, or to an interval during which aragonite was not detected. Correlation between the Hole 714A aragonite record and the Hole 716B pteropod ratio curve shows some similarities, but not as good as with the CDI record. Correlation between the aragonite record and the pteropod ratio curve for the same samples in Hole 716B surprisingly shows no systematic similarities.

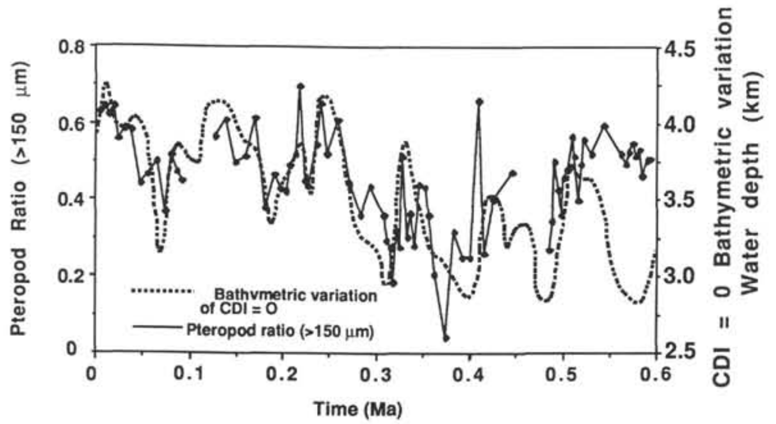

Figure 17. Variations with time of the Hole 716B pteropod ratio are superposed on the CDI bathymetric variations from the eastern equatorial Indian Ocean (Peterson and Prell, 1985) for the past 0.6 m.y. to show the good correlation between the two records. Note the particularly excellent correlation for the past 0.35 m.y. Also, note the clear mid-Brunhes poor preservation interval between 0.3 and 0.5 Ma in both records.

interval was clearly established in deeper waters (below the calcite lysocline) with the CDI of Peterson and Prell (1985). It is puzzling, however, that during the past 0.6 m.y., well in phase with the $\delta^{18}O$ record, the aragonite record in Hole 716B (see above) seems to be solely an input signal, even though variations in pteropod-ratio values clearly show the influence of the mid-Brunhes carbonate dissolution. This is an unsolved riddle, especially since the long 3.5-m.y. aragonite record in Hole 716B clearly displays aragonite 0.5-m.y. supercycles between 0.5 and 2.0 Ma, which correlate with the well-established carbonate preservation supercycles of the deep equatorial Pacific Ocean (Hays et al., 1969) (see below).

The Last 0.4 m.y. in Hole 633A

According to Crowley (1985), the Atlantic pattern of carbonate preservation for the past 0.4 m.y. (i.e., interglacial carbonate preservation and glacial carbonate dissolution) is too simplistic and is not so distinct from the Pacific preservation pattern. Though carbonate dissolution is consistently at a minimum at the very beginning of each interglacial, when the lightest values of $\delta^{18}O$ indicate minimum ice volume, dissolution intensity appears to increase with increasing ice volume in a nonlinear fashion (Fig. 18). For example, dissolution can be low during some glacial intervals, such as is the case for part of glacial

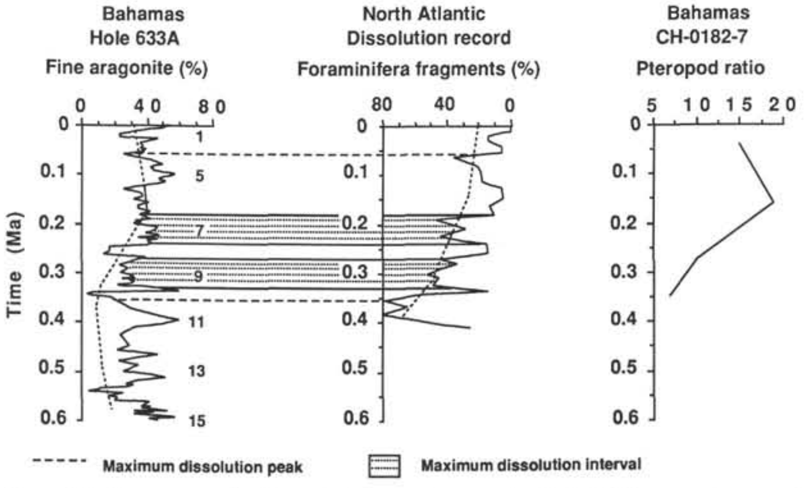

Figure 18. Comparison for the past 0.4 m.y. between the Hole 633A aragonite record, the eastern North Atlantic carbonate preservation record based on a foraminifer fragmentation curve (Crowley, 1985), and a carbonate preservation curve based on the pteropod ratio (= whole pteropods/[whole pteropods + fragments]; Haddad, 1986). Note the aragonite decrease with time in Hole 633A that parallels the decrease with time of carbonate preservation in foraminifer and pteropod curves, and clearly displays the second part of the mid-Brunhes poor preservation interval. Also, note the rather low aragonite values for interglacial Stages 7 and 9 that correspond to two well-defined strong dissolution intervals in the foraminifer carbonate preservation curve. Finally, note the similarities of the carbonate preservation records for the last 0.6 m.y. between the Indian (Figs. 16 and 17) and the North Atlantic oceans (Fig. 18).

Stages 6 and 8, which are characterized by two distinct dissolution minima. On the other hand, dissolution in the second part of interglacial Stages 9 and 11 is particularly intense. These dissolution and preservation features, out of phase with the simple glacial/interglacial stage couplet, are part of the increased mid-Brunhes dissolution interval centered between 0.3 and 0.4 Ma. The mid-Brunhes change corresponds to the most recent dissolution maximum of the long-term 0.5-m.y. carbonate preservation supercycles observed in the Pacific, Atlantic, and Indian oceans, indicating a long-term cyclic excursion of the oceanic carbonate reservoir on a global scale.

The good correlation between Crowley's (1985) 0.4-m.y. fragmentation curve for the northeast Atlantic Ocean (latitude 20°N) and the aragonite 0.4-m.y. aragonite record of Hole 633A is a priori unexpected. The general trend of increasing foraminifer fragmentation with time is consistent with the general decrease of average aragonite value for each glacial stage. In addition, high fragmentation intervals within interglacial Stages 7 and 9 correspond to unusually low aragonite values for the interglacial stages. The well-defined, sharp aragonite peak at the very beginning of Stage 9 correlates with the brief carbonate preservation event of Stage 9, and the lowest average aragonite value of glacial Stage 10 corresponds to a maximum in foraminifer fragmentation (Fig. 18).

The mid-Brunhes interval of low carbonate preservation, based on high numbers of foraminifer fragments in the deep Atlantic Ocean (Crowley, 1985) and low aragonite content in the Bahamas, is also recorded by low values of the pteropod ratio in a rather shallow (680 m water depth) periplatform core from the northwest Providence Channel (Haddad, 1986) (Fig. 18). Therefore, the mid-Brunhes trend of poor preservation is clear and common in the periplatform ooze of the Maldives and the Bahamas.

The Last 2.0 m.y. in Holes 633A and 716B and Core RC11-209 from the Equatorial Pacific Ocean

Next to the high-frequency (visually estimated as 100 and 40 k.y.) cycles, the 2.0-m.y.-long aragonite record in Hole 716B displays long aragonite cycles in the general envelope of data that are characterized by a periodicity close to 0.5 m.y. when estimated by eye. When one connects aragonite minima in the Pleistocene aragonite curve in Hole 633A from the Bahamas, similar low-frequency (0.4–0.5 m.y.) aragonite supercycles appear superimposed on the high-frequency aragonite cycles (Droxler et al., 1988b). Figure 19 shows the 2.0-m.y. aragonite records of Holes 633A and 716B side by side with the carbonate record of Core RC11-209 from the equatorial Pacific Ocean (Hays et al., 1969; Moore et al., 1982; Vincent, 1985). The age/depth model for RC11-209 is based on the published magnetostratigraphy (Hays et al., 1969), assuming constant sedimentation rates within each chron and subchron. Ages of upper and lower chron and subchron boundaries are from Harland et al. (1982). The timing of the aragonite supercycles in Holes 633A and 716B matches very well with the timing of the "carbonate preservation supercycles" in Core RC11-209, as well as in several deep carbonate (planktonic calcite) records in the Pacific (Hays et al., 1969; Saito et al., 1975; Adelseck, 1977; Moore et al., 1982; Vincent, 1985; Farrell and Prell, 1987), Indian (Oba, 1969; Peterson and Prell, 1985), and Atlantic oceans (Johnson et al., 1977; Crowley, 1985).

A priori, it is rather unexpected to observe such a correspondence between the two aragonite supercycles in Holes 633A and 716B, and more particularly with the Pacific long-term carbonate preservation cycles. The timing of the carbonate and aragonite supercycles is common to the three long records. Major intervals characterized by low carbonate values and low aragonite values occur between 0.4 and 0.5 Ma, 0.8 and 0.9 Ma, and 1.4 and 1.5 Ma. Most of the major carbonate dissolution events of Hays et al. (1969) and Vincent (1985), such as B3, B7, ..., M1, M3, ... M11, M13, ..., can be correlated in both aragonite supercycles. The major carbonate dissolution event M3 at 0.9 Ma, in every long carbonate record, is also the most obvious event in both aragonite records. The M3 event separates the early Pleistocene from the late/middle Pleistocene and seems to have influenced carbonate sedimentation throughout the entire water column worldwide. The aragonite supercycles seem to have vanished during the late Pliocene interval between 1.6 and 2.0 Ma in Hole 633A, where two distinct aragonite peaks at 1.7 and 1.9 Ma are separated by intervals during which no aragonite was detected in the carbonate fine fraction. During the same period of time in Hole 716B, the aragonite supercycles clearly appear and seem to correlate well with the carbonate record of the equatorial Pacific Ocean (Fig. 19).

The Last 3.5 m.y. in Hole 716B and the Equatorial Pacific Ocean Carbonate Preservation Record

The most detailed Pliocene-Pleistocene carbonate records have been collected from the equatorial Pacific Ocean. Farrell and Prell (1987) displayed them as bathymetric variations in carbonate preservation (expressed as carbonate content in %) vs. time. The carbonate record in the equatorial Pacific of Farrell and Prell (1987) displays clear carbonate preservation supercycles only during the last 1.0 m.y., with low carbonate values centered on 0.4 and 0.9 Ma. Farrell and Prell's carbonate record before 1.0 Ma does not display clear carbonate supercycles, as is the case in the carbonate record of Core RC11-209 between 1.0 and 2.0 Ma (Hays et al., 1969; Moore et al., 1982; Vincent, 1985).

Figure 13 displays side-by-side the 3.5-m.y. aragonite record for Hole 716B and the 40% contour of carbonate bathymetric variations for the past 3.5 m.y. (Farrell and Prell, 1987). The aragonite 0.5-m.y. supercycles clearly occur during the past 2.0 m.y. Intervals of generally low aragonite are spaced roughly every 0.5 m.y., at 0.4, 0.9, 1.45, and 2.0 Ma, and intervals with generally high aragonite at 0.65, 1.25, and 1.75 Ma. The aragonite supercycles disappear between 2.0 and 3.5 Ma. The aragonite values that average 15% after 2.0 Ma are the lowest of the entire 3.5-m.y. aragonite record. During the same time interval, however, carbonate preservation in the equatorial Pacific Ocean appears to be better than during the early Pleistocene (Farrell and Prell, 1987). The correspondence between the equatorial Pacific Ocean carbonate preservation record (Farrell and Prell, 1987) and the aragonite record in the Maldives is not as clear as with the carbonate preservation record based on the single Core RC11-209 (Hays et al., 1969; Fig. 19). Further back than 2.0 Ma (or 70 mbsf), the primary aragonite record might be significantly altered by burial diagenesis (Malone et al., this volume), which may explain the poor agreement between the aragonite record in the Maldives and the carbonate (calcite) record in the equatorial Pacific Ocean.

DISCUSSION

Global Occurrence of the Aragonite Supercycles

The rationale of this paper is based on two separate approaches: (1) comparison between $\delta^{18}O$ and aragonite records and (2) comparison between aragonite records and the carbonate (calcite) preservation records of the equatorial Pacific, Indian, and Atlantic oceans. The results that emerge from these two approaches point toward the same conclusion. The aragonite cycles in periplatform sediments have recorded not only an input function related to alternate flooding and exposure of the nearby shallow carbonate banks, but are also related to variations in the carbonate chemistry of intermediate-water masses through the dissolution or preservation of bank-derived aragonite at the seafloor.

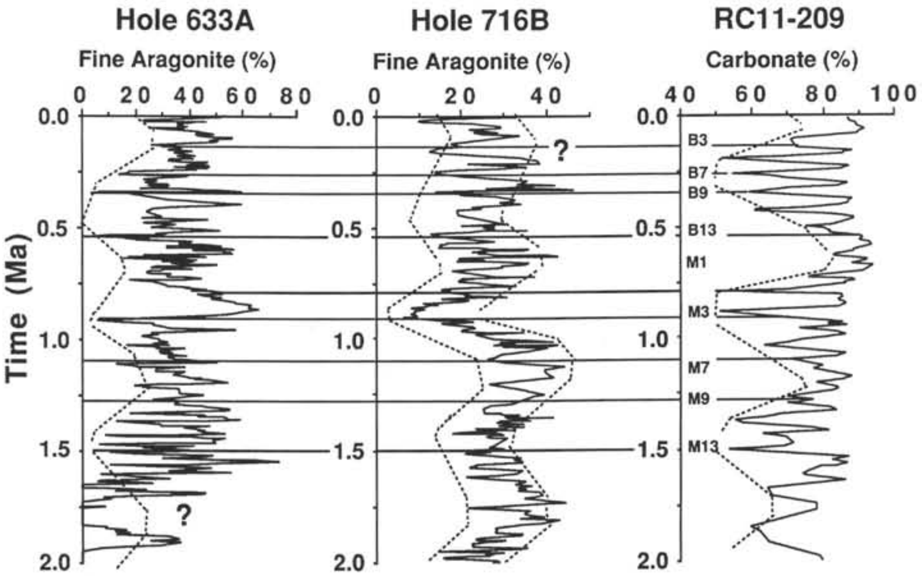

Figure 19. Comparison for the past 2.0 m.y. between the 0.5-m.y. aragonite supercycles in Holes 633A and 716B, and the 0.5-m.y. carbonate (calcite) supercycles well illustrated in Core RC11-209 (Hays et al., 1969) from the equatorial Pacific Ocean. Timing of the supercycles is almost identical for the three areas. The major dissolution event (M3) of Hays et al. (1969) at 0.9 Ma (early/middle Pleistocene boundary) corresponds to an interval of strong aragonite minima in both Holes 633A and 716B, and is centered at the beginning of interglacial oxygen isotope Stage 23 (see Fig. 11 for more details). The Hole 633A aragonite record deviated from the supercycle trend during the late Pliocene, whereas the Hole 716B aragonite record has been off the supercycle beat in the past 0.3 m.y.

The best evidence for this conclusion is contained in the deep periplatform sites: Hole 633A in the Bahamas and Hole 714A in the Maldives. The good correlation in Hole 714A between the 0.6-Ma aragonite record and the carbonate preservation record from the Ninetyeast Ridge (Fig. 16), and in Hole 633A between the 0.4-Ma aragonite record and the carbonate preservation record from the tropical eastern North Atlantic Ocean (Fig. 18) show quite clearly that the influence of dissolution increases in each of these aragonite records during the mid-Brunhes. This trend of decreasing aragonite content within the past four or five glacial stages was also observed in three other cores in the Bahamas, where aragonite values are at a minimum during Stage 10 and at a maximum during isotope Stage 6 (Droxler et al., 1988b, fig. 11). In a fourth core, the same trend is strengthened by using pteropod tests and fragments as a dissolution index (Haddad, 1986); stage 10 shows maximum pteropod dissolution, corresponding to the lowest aragonite minimum values, whereas Stage 6 shows minimum dissolution, corresponding to the highest values of the aragonite minimum. This trend corresponds well with the last half of the mid-Brunhes aragonite supercycle (Fig. 18).

Although the trend from late to mid-Brunhes toward more dissolution does not seem to appear during the past 0.4-m.y. aragonite record in shallow Hole 716B (Figs. 13, 16, and 19), it is a priori unexpected that (1) the mid-Brunhes dissolution increase is well illustrated in the pteropod ratio of Hole 716B (Figs. 16 and 17), and (2) the 2.0-Ma aragonite record in Hole 716B displays distinct 0.5-m.y. aragonite supercycles earlier than the mid-Brunhes (Figs. 13 and 19). The timing of these aragonite supercycles in Hole 716B is compatible with the timing of the carbonate preservation supercycles well established in the three major oceans, especially in Core RC11-209 from the equatorial Pacific Ocean (Hays et al., 1969; Moore et al., 1982), as well as with the aragonite supercycles in deep Hole 633A, where the dissolution-increasing trend from the late to the mid-Brunhes is clear. On the other hand, in Hole 633A, the aragonite supercycles, which are well established during the entire Pleistocene, become less distinct during the late Pliocene (1.6–2.0 Ma) period, during which the aragonite supercycles in Hole 716B are very distinct and regular.

The minima of the aragonite supercycles that correspond to the carbonate dissolution maxima in Hays et al. (1969) occurred approximately every 0.5 m.y.: at 0.40 Ma in Holes 633A, 714A, and 716B; at 0.90 and 1.45 Ma in Holes 633A and 716B; and at 2.00 Ma in Hole 716B. The maxima of the aragonite supercycles occurred at 0.15 Ma in Hole 633A; at 0.65 and 1.20 Ma in Holes 633A and 716B; and at 1.75 Ma in Hole 716B. We concluded that the mid-Brunhes dissolution event, well established as a carbonate low in the pelagic sediments (Farrell and Prell, 1989; Peterson and Prell, 1985; Crowley, 1985), or as an aragonite minimum in the periplatform sediment, is the youngest dissolution interval of the carbonate preservation supercycles. This interval, at least in the aragonite records, is clearly part of a cyclic change and not a steplike phenomenon, in the carbonate (calcite) records, as several authors have mentioned recently (Jansen et al., 1986; Chuey et al., 1987; Pisias and Rea, 1988). In addition, we stress that, because of the occurrence of aragonite supercycles at intermediate water depths in the periplatform environments of the Maldives and the Bahamas regions and the carbonate supercycles in deep waters of the Pacific, Indian, and Atlantic oceans at least during the Brunhes Epoch, we believe that these supercycles have affected the entire water column in low latitudes on a global scale.

Time lags and phase changes between $\delta^{18}O$ and aragonite records in the Maldives and the Bahamas also provide good evidence that alternate flooding and emergence cannot be the only cause of the aragonite cycles. The synchronous occurrence of these lags and phase changes in aragonite periplatform records of the Maldives and the Bahamas and the relationship of lags and phase changes with the carbonate and aragonite supercycles show that they are part of a global phenomenon. In the late and middle Pleistocene, the time during which the aragonite records in Holes 633A and 716B become out of phase with the $\delta^{18}O$ record corresponds to two distinct intervals within the carbonate preservation supercycles, as follows:

1. Stages 15 and 16 are recognized to be a time of rather good preservation. Farrell and Prell (1989) recognized a strong preservation event at 0.61–0.65 Ma. This is the time in Hole 716B at which an aragonite peak (45%) occurs. In the $\delta^{18}O$ record, this peak appears during the second half of glacial Stage 16. The same trend is also observed in Hole 633A, in which an aragonite peak (58%) occurs at the very end of glacial Stage 16. In Holes 633A and 716B, the aragonite and $\delta^{18}O$ records are in phase during Stages 17, 18, 19, and 20. This is a period of generally good preservation within the carbonate supercycles (i.e., see Farrell and Prell, 1989).
2. The second interval during which aragonite and $\delta^{18}O$ records become either totally or partially out of phase in Holes 633A and 716B is during Stages 21–26. This interval includes the very end of the Matuyama Chron and the Jaramillo Subchron and is centered on Stage 23. It is synchronous with a major carbonate dissolution event at 0.9 Ma, the M3 event of Hays et al. (1969) that corresponds to the major excursion in the carbonate preservation curve of Farrell and Prell (1987). In Hole 716B, Stage 23 is marked by one of the most extreme aragonite minima even though, based on the $\delta^{18}O$ record, it corresponds to an interglacial stage. In Hole 633A, this M3 dissolution event is not as clearly defined as in Hole 716B, but it still corresponds to the most-developed Pleistocene mismatch between aragonite and $\delta^{18}O$. The "M3/0.9 Ma" aragonite minimum occurs at the beginning of interglacial Stage 23. The sudden aragonite increase, from <10% to >65%, lags behind the $\delta^{18}O$ depletion, defining the Stage 24/23 glacial-to-interglacial transition by more than 10 k.y. The occurrence of magnesian calcite during Stage 23 in Holes 633A and 716B is also quite significant. Magnesian calcite could have precipitated as cement as a result of the partial seafloor dissolution of aragonite. This interpretation remains hypothetical and will need to be tested by detailed petrographic and geochemical analyses.

Implications

Several implications are tied to the established occurrence of the global aragonite supercycles in periplatform sediments and their correlation with the carbonate (calcite) preservation supercycles in open-ocean pelagic sediments. The aragonite cycles and supercycles can no longer be treated simply as the response of the nearby shallow carbonate banks to sea-level fluctuations.

We think that modifications in the aragonite input, through partial or full dissolution at the sea floor of bank-derived aragonite, have recorded cyclic variations in carbonate chemistry of the overlying waters, though this interpretation seems better established in deep periplatform sites (Holes 633A and 714A) than in shallow sites (i.e., Hole 716B). Therefore, the aragonite cycles and supercycles become unique tools to understand how the carbonate chemistry of the water column at intermediate-water depths and low latitudes responded to Quaternary climatic changes. Carbonate chemistry variations at intermediate water-depths are practically unknown, since calcitic planktonic material is too stable to record subtle variations in the carbonate chemistry above the calcite lysocline. Based on the carbonate (calcite) records in the equatorial Pacific Ocean, Farrell and Prell (1989) were able to show that the top of the calcite lysocline (thought to correspond to the calcite saturation level in the water column) deepened by a minimum of 400 to 800 m during the last nine glacial stages corresponding to the past 0.8 m.y. Farrell and Prell related this deepening to an increase of the deep-water carbonate ion concentration, resulting in a more carbonate saturated-water mass. Climate-induced calcite lysocline excursions of similar magnitude have been reported by other authors. Berger (1977) suggested as much as a 1000-m lysocline excursion in the Pacific Ocean. In the Atlantic, Gardner (1975) reported a 200–700 m change, Berger (1968) and Crowley (1983) suggested that an excursion of 300 m may have occurred, and Balsam (1983) saw evidence for a change on the order of 1000–2000 m in the glacial-to-interglacial lysocline depth. Climate-induced shallowing and deepening of the water-column carbonate saturation levels over the orbital frequencies (10th–100th k.y.), as positive or negative feedbacks, are directly related to the cycling of deep-sea carbonate sediment, as well as oceanic and atmospheric carbon reservoirs.

Shoaling of the aragonite lysocline (aragonite saturation level) in intermediate-water masses, in parallel with the excursion of the calcite lysocline in deeper waters, is not too difficult to conceive. The records of the carbonate chemistry variations of intermediate water masses in periplatform ooze, though more subtle than in deep-water masses because of their quicker turnover rates and their more direct connection to the atmosphere are essential to our quest for a better understanding of the role of the atmosphere, the ocean, and carbonate sediments in the carbon-cycling processes.

Aragonite supercycles are well developed during the late Pliocene-Pleistocene, mainly between 0.3 and 2.0 Ma in the shallow Maldives site, Hole 716B. This would imply that the aragonite saturation level would have reached water depths shallow enough to be located within the oxygen minimum. Such a shallow aragonite saturation level is not unreasonable, given the shallow (300–400 m) aragonite saturation level in the central Pacific today at latitude 18°N (Berner, 1977). Another example from the Nicaragua Rise (Caribbean Sea) also shows waters within the oxygen minimum, between 700 and 1000 m, just at or below the aragonite saturation level today. Deeper waters become saturated again between 1000 and 1900 m and finally become undersaturated at or below 1900 m (Droxler et al., 1988c). Aragonite records from the Maldives and the Bahamas, partially interpreted as carbonate preservation records, would therefore illustrate some major excursions through time of the aragonite saturation level, indicating that the carbonate chemistry of the entire water column, and not only of the deep-ocean basins, has varied within the beat of the climate-induced fluctuations.

Similarities between the different aragonite and carbonate records during some time intervals point out that the entire water column has responded as a whole to certain climatic modulators, whereas differences between the aragonite records themselves, or between the intermediate aragonite and the deep carbonate (calcite) records may be related to basin-to-basin or intermediate-to-deep-water carbonate fractions. A possible example of basin-to-basin fractionation is illustrated in the aragonite records during the late Pliocene (1.6–2.0 Ma). In the Maldives (Hole 716B) during that period of time, aragonite supercycles are well defined and can be correlated well with the carbonate (calcite) preservation record. On the other hand, aragonite supercycles in the Bahamas (Hole 633A) during the same period of time were not observed, perhaps because aragonite was not even detected during half of this time. This discrepancy, between the Bahamas and the Maldives, is possibly related to the onset of the major glaciations in the North Atlantic Ocean at 2.4 Ma (i.e., Shackleton et al., 1984). This event could have had a 1.0-Ma-long "local" influence on the formation of corrosive intermediate water masses in the North Atlantic Ocean.

The other mismatch between the two aragonite supercycles occurs during the past 0.3 m.y. In the shallow Maldives site (Hole 716B), the Brunhes aragonite supercycle, clearly in sediment older than 0.3 Ma, displays a regular aragonite decrease since 0.3 Ma, instead of a general aragonite increase as expected during the period of time following the last mid-Brunhes carbonate preservation minimum (Figs. 13, 16, and 19). This mismatch is rather unexpected and not understood at this point because the mid-Brunhes dissolution interval based on the pteropod ratio is so clear in Hole 716B (Figs. 16 and 17). On the contrary, the last aragonite supercycle during the Brunhes Chron is well developed in the deep sites, in the Bahamas (Hole 633A) and in the Maldives (Hole 714A), following the trend of the deep carbonate (calcite) preservation record in the deep equatorial Pacific and Indian oceans, as well as in the deep tropical North Atlantic Ocean. Therefore, the paleoceanographic implications in relation to the establishment of the global aragonite supercycles in periplatform sediments become multifold.

Finally, mineralogical variations, observed downcore cannot be simply explained any more only by shallow burial diagenesis. First, the primary input of bank-derived metastable aragonite and magnesian calcite has changed through time. Then, chemical reactions occurring at the seafloor through interaction between surface sediments and overlying waters have also modified this primary input by removing, at specific time intervals, the primary input of bank-derived material. For instance, the general decrease of aragonite with time in the past 0.4 m.y. in Holes 633A and 714A, linked with the youngest mid-Brunhes interval of poor preservation and part of the global carbonate preservation supercycles, could easily be misinterpreted as early burial diagenesis (Mullins et al., 1985; Dix and Mullins, 1988). Good examples are (1) the reoccurrence of magnesian calcite in the Maldives and the Bahamas during Stages 15 and 23 and (2) the aragonite extreme minima during Stage 23 in both areas, correlated to the deep-water calcite dissolution event M3 of Hays et al. (1969). In Droxler et al. (1988a), we also demonstrated that major reversals of aragonite content occur within a longer time interval in Hole 633A. In this hole, aragonite is only partially detected during the late Pliocene (1.7–2.1 Ma), whereas during the early Pliocene (4.0–4.5 Ma) values of aragonite content (70%) are equal to or higher than the aragonite values observed during the interglacial late Pleistocene stages. The establishment of the carbonate (aragonite) preservation supercycles in periplatform sediments shows the importance of chemical processes that occur at the seafloor during discrete climatic intervals.

CONCLUSIONS

Long-term (roughly 0.5 m.y.) aragonite supercycles have been recorded in the periplatform environments of the Maldives and the Bahamas at least for the past 2.0 m.y. The aragonite supercycles generally correlate quite well not only between these two regions, but also with the carbonate (calcite) preservation records from the deep equatorial Pacific, Indian, and tropical North Atlantic oceans. By analogy, we interpret the aragonite supercycles in the periplatform environments as preservation cycles at intermediate-water depths.

Aragonite and planktonic $\delta^{18}O$ records are not always in phase, as is usually the case during the late Pleistocene. These mismatches between aragonite and $\delta^{18}O$ are good evidence that the aragonite cycles in periplatform sediments can no longer be explained solely by variations of aragonite input from the nearby shallow carbonate banks in response to their alternate flooding and exposure through cyclic sea-level fluctuations. Two major mismatches between the aragonite and $\delta^{18}O$ records synchronously occur in the Maldives and Bahamas regions during the past 1.1 m.y. During these two distinct time intervals (Stages 15 and 16 and Stages 21–27), aragonite and $\delta^{18}O$ are either totally out of phase or the aragonite record lags behind the $\delta^{18}O$ by several tens of thousands of years. The major mismatch event, which is located at the beginning of Stage 23 (0.9 Ma) and corresponds to the early to middle Pleistocene boundary, is illustrated by one of the most extreme aragonite minima during the entire Pleistocene in the Maldives and the Bahamas. This 0.9-m.y. event corresponds to the M3 major dissolution event in the carbonate preservation records of the equatorial Pacific Ocean.

The mid-Brunhes interval of poor carbonate preservation, well established in carbonate dissolution curves of the equatorial Pacific, Indian, and tropical Atlantic oceans, is clearly defined by aragonite lows in deep (1500–2000 m) periplatform sites of the Maldives and the Bahamas, as well as by increases in pteropod fragmentation in the shallow sites (500–700 m).

Paleoceanographic and paleoclimatologic implications linked to the occurrence of the aragonite cycles and supercycles in periplatform sediments at intermediate water depths are multifold. Their occurrence shows that the carbonate chemistry of the entire water column was influenced by long-term (0.5 m.y.) climate-induced and cyclic variations during the past 2.0 m.y. It also shows that the aragonite saturation levels were perhaps as shallow as 500 m at different time intervals in the equatorial Indian and tropical North Atlantic oceans, as is the case today in the central equatorial Pacific Ocean. Major changes of the water column carbonate chemistry, recorded in periplatform aragonite cycles and supercycles, are part of the climate-induced carbon cycling among the different atmospheric, oceanic, and sedimentary reservoirs.

The establishment of aragonite preservation supercycles in periplatform ooze shows the importance of the chemical processes that occur at the seafloor between surface sediments and the overlying waters, and that these processes are modulated by late Pliocene/Pleistocene climatic changes. Downcore decreases of aragonite and magnesian calcite, therefore, are not necessarily related to early burial diagenesis occurring within the top 10-20 m of sediment. The mid-Brunhes climate-induced poor carbonate preservation interval (around 0.4 Ma) is a clear example, during which aragonite values reach a minimum and then increase further down the core. This trend is even more clear in the Bahamas where the aragonite, which disappears during the late Pliocene, reaches values that are as high during the early Pliocene as during the late Pleistocene.

ACKNOWLEDGMENTS

This research was supported by several grants from USSAC-JOI to A. W. Droxler (Leg 115), J. L. Cullen (Leg 115), and A. W. Droxler and W. Schlager (Leg 101), as well as partially by NSF Grant No. OCE-8796273 to A. W. Droxler. We thank the personnel of the ODP Core Depository of Texas A&M in College Station, particularly C. Mato, for helping during the core sampling, and S. Walker, L. Baker, S. Staples, and D. Greene at Rice University for help during sample processing and analyses. We are particularly grateful to R. B. Dunbar, who made his Stable Isotope Laboratory at Rice University available to us for oxygen isotope analyses. J. W. Farrell and an anonymous person thoroughly reviewed the first manuscript.

REFERENCES

Adelseck, C. G., Jr., 1977. Recent and late Pleistocene sediments from the eastern equatorial Pacific Ocean: sedimentation and dissolution [Ph.D. dissert.]. Univ. California, San Diego.

Arrhenius, G., 1952. Sediment cores from the east Pacific. *Rep. Swed. Deep-Sea Exped.*, 5:1–227.

Austin, J. A., Schlager, W., et al., 1986. *Proc. ODP, Init. Repts.*, 101: College Station, TX (Ocean Drilling Program).

Backman, J., Duncan, R. A., et al., 1988. *Proc. ODP, Init. Repts.*, 115: College Station, TX (Ocean Drilling Program).

Balsam, W. B., 1983. Carbonate dissolution on the Muir Seamount (western North Atlantic): interglacial/glacial changes. *J. Sediment. Petrol.*, 53:719–731.

Berger, W. H., 1968. Planktonic foraminifera selective solution and paleoclimatic interpretation. *Deep-Sea Res.*, 15:31–43.

———, 1973. Deep-sea carbonates: Pleistocene dissolution cycles. *J. Foraminiferal Res.*, 3:187–195.

———, 1977. Deep-sea carbonate and deglaciation preservation spike in pteropods and foraminifera. *Nature,* 269:301–304.

———, 1978. Deep-sea carbonate: pteropod distribution and the aragonite compensation depth. *Deep-Sea Res.*, 25:447–452.

Berner, R. A., 1977. Sedimentation and dissolution of pteropods in the ocean. *In* Andersen, N. R., and Malahoff, A. (Eds.), *The Fate of Fossil Fuel CO_2 in the Oceans:* New York (Plenum Press), 243–260.

———, 1981. Pelagic sedimentation of aragonite: its geochemical significance. *Science,* 211:940–942.

Berner, R. A., Berner, E. K., and Keir, R. S., 1976. Aragonite dissolution on the Bermuda Pedestal, its depth and geochemical significances. *Earth Planet. Sci. Lett.*, 30: 169–178.

Birch, G. F., 1979. In-progress reports of the year 1978. Cape Town, Univ. Dept. Geol., Mar. Geol. Program, Tech. Rep., 11:122–126.

Boardman, M. R. 1978. Holocene deposition in northwest Providence Channel, Bahamas: a geochemical approach [Ph.D. dissert.]. Univ. North Carolina, Chapel Hill.

Boardman, M. R., and Neumann, A. C., 1984. Sources of periplatform carbonate: northwest Providence Channel, Bahamas. *J. Sediment. Petrol.*, 54:1110–1112.

———, 1985. Sources of periplatform carbonates: northwest Providence Channel, Bahamas—reply. *J. Sediment. Petrol.*, 55:929–931.

———, 1986. Reply on "Bank-top responses to Quaternary fluctuations in sea level recorded in periplatform sediments." *Geology,* 14: 1040–1041.

Boardman, M. R., Neumann, A. C., Baker, P. A., Dulin, L. A., Kenter, R. J., Hunter, G. E., and Kiefer, K. B., 1986. Bank-top responses to Quaternary fluctuations in sea level recorded in periplatform sediments. *Geology,* 14:28–31.

Burns, S. J., 1983. The sedimentary process of a deep-water carbonate slope: southern Little Bahama Bank, Bahamas [M.S. thesis]. Univ. North Carolina, Chapel Hill.

Burns, S. J., and Neumann, A. C., 1987. Pelagic sedimentation on an inactive gullied slope, northwest Providence Channel, Bahamas. *Mar. Geol.*, 77:277–286.

Chen, C., 1964. Pteropod ooze from Bermuda Pedestal. *Science,* 144: 60–62.

———, 1968. Pleistocene pteropods in pelagic sediments. *Nature,* 219:1145–1149.

Chuey, J. M., Rea, D. K, and Pisias, N. G., 1987. Late Pleistocene paleoclimatology of central equatorial Pacific, a quantitative record of eolian and carbonate deposition. *Quat. Res.*, 28:323–339.

Crowley, T. J., 1983. Calcium carbonate preservation patterns in the central North Atlantic during the last 150,000 years. *Mar. Geol.*, 51: 1–41.

———, 1985. Late Quaternary carbonate changes in the North Atlantic and Atlantic/Pacific comparisons. *In* Sundquist, E. T., and Broecker, W. S. (Eds.), *The Carbon Cycle and Atmospheric CO_2: Natural Variations Archean to Present.* Am. Geophys. Union Monogr., 32:271–284.

Diester-Haas, L., 1985. Late Quaternary sedimentation on the eastern Walvis Ridge, southeast Atlantic (HPC 532 and four piston cores). *Mar. Geol.*, 65:145–189.

Dix, G. R., and Mullins, H. T., 1988. A regional perspective of shallow-burial diagenesis of deep water periplatform carbonates from the Northern Bahamas. *In* Austin, J. A., Jr., Schlager, W., et al., *Proc. ODP, Sci. Results,* 101: Washington (Ocean Drilling Program), 279–302.

Droxler, A. W., 1984. Late Quaternary glacial cycles in the Bahamian Deep Basins and in the adjacent ocean [Ph.D. dissert.]. Univ. Miami, Coral Gables, FL.

———, 1985. Last deglaciation in the Bahamas: a dissolution record from variations of aragonite content? *In* Sundquist, E. T., and Broecker, W. S. (Eds.), *The Carbon Cycle and Atmospheric CO_2: Natural Variations Archean to Present.* Am. Geophys. Union Monogr., 32:195–207.

———, 1986. Comment on "Bank-top responses to Quaternary fluctuations in sea level recorded in periplatform sediments. *Geology,* 14:1039–40.

Droxler, A. W., Bruce, C. H., Sager, W. W., and Watkins, D. H., 1988b. Pliocene-Pleistocene variations in aragonite content and planktonic oxygen-isotope record in Bahamian periplatform ooze, Hole 633A. *In* Austin, J. A., Jr., Schlager, W., et al., *Proc. ODP, Sci. Results,* 101: College Station, TX (Ocean Drilling Program), 221–244.

Droxler, A. W., Glaser, K. S., Morse, J. W., and Baker, P. A., 1988c. Good agreement between carbonate mineralogical depth variations of surficial periplatform ooze and carbonate saturation levels of overlying intermediate water. New data from the Nicaragua Rise. *Eos,* 69:1048. (Abstract)

Droxler, A. W., Haddad, G. A., and Mucciarone, D. A., 1989. Influence of the "Brunhes Carbonate Cycle" on the periplatform 1-m.y.-long aragonite record in the Bahamas and the Maldives. *3rd Int. Conf. Paleoceanogr., Terra Abstr.*, 1:16–17.

Droxler, A. W., Morse, J. W., and Kornicker, W. A., 1988a. Controls on carbonate mineral accumulation in Bahamian basins and adjacent Atlantic Ocean sediments. *J. Sediment. Petrol.*, 58:120–130.

Droxler, A. W., and Schlager, W., 1985a. Glacial/interglacial sedimentation rates and turbidite frequency in the Bahamas. *Geology,* 13: 799–802.

———, 1985b. Sources of periplatform carbonates: northwest Providence Channel, Bahamas—discussion. *J. Sediment. Petrol.*, 55:928–929.

Droxler, A. W., Schlager, W., and Whallon, C. C., 1983. Quaternary aragonite cycles and oxygen-isotope records in Bahamian carbonate ooze. *Geology,* 11:235–239.

Farrell, J. W., and Prell, W. L.,1987. Climate forcing of calcium carbonate sedimentation: a 4.0 m.y. record from the central equatorial Pacific Ocean. *Eos,* 68:333.

———, 1989. Climatic change and $CaCO_3$ preservation: an 800,000 year bathymetric reconstruction from the central equatorial Pacific Ocean. *Paleoceanography,* 4:447–466.

Gardner, J. V., 1975. Late Pleistocene carbonate dissolution cycles in the eastern equatorial Atlantic. *In* Sliter, W. V., Bé, A.W.H., and Berger, W. H. (Eds.), *Dissolution of Deep-Sea Carbonates.* Spec. Publ., Cushman Found. Foraminiferal Res., 13:129–141.

Haddad, G. A., 1986. A study of carbonate dissolution, stable isotope chemistry, and minor element composition of pteropods and forams deposited in the Northwest Providence Channel, Bahamas, during the past 500,000 years [M.S. thesis]. Duke Univ., Durham, NC.

Hanna, J. C., and Moore, C. H., 1979. Quaternary temporal framework of reef to basin sedimentation, Grand Cayman, B.W.I. *Geol. Soc. Am., Abstr. Programs,* 11:438.

Harland, W. B., Cox, A. V., Llewellyn, P. G., Pickton, C.A.G., Smith, A. G., and Walters, R., 1982. *A Geologic Time Scale:* Cambridge (Cambridge Univ. Press).

Hays, J. D., Saito, T., Opdyke, N. D., and Burckle, L. H., 1969. Pliocene-Pleistocene sediments of the equatorial Pacific: their paleomagnetic biostratigraphic and climatic record. *Geol. Soc. Am. Bull.*, 80:1481–1514.

Herman, Y., 1971. Vertical and horizontal distribution of pteropods in Quaternary sequences. *In* Funnel, B. M., and Riedel, W. R. (Eds.), *The Micropaleontology of the Oceans:* Cambridge (Cambridge Univ. Press), 463–486.

Hine, A. C., Wilber, R. J., and Neumann, C., 1981. Carbonate sand bodies along contrasting shallow bank margins facing open seaways in northern Bahamas. *AAPG Bull.*, 65:261–290.

Imbrie, J., Hays, J. D., Martinson, D. G., McIntyre, A., Mix, A. C., Mortley, J. J., Pisias, N. G., Prell, W. S., and Shackleton, N. J., 1984. The orbital theory of Pleistocene climate: support from a revised chronology of the marine $\delta^{18}O$ record. *In* Berger, A., Imbrie, J., Hays, J., Kukla, G., and Saltzman, B. (Eds.), *Milankovitch and Climate* (Pt. 1): Hingham, MA (D. Reidel), 69–305.

Jansen, J.H.F., Kuijpers, A., and Troelstra, S. R., 1986. A mid-Brunhes climatic event: long-term changes in global atmospheric and ocean circulation. *Science,* 232:619–622.

Johnson, D. A., Ledbetter, M., and Burckle, L. H., 1977. Vema Channel paleoceanography: Pleistocene dissolution cycles and episodic bottom water flow. *Mar. Geol.*, 23:1–33.

Kier, J. S., and Pilkey, O. H., 1971. The influence of sea level changes on sediment carbonate mineralogy, Tongue of the Ocean, Bahamas. *Mar. Geol.*, 11:189–200.

Lynts, G. W., Judd, J. B., and Stehman, C. F., 1973. Late Pleistocene history of Tongue of the Ocean, Bahama. *Geol. Soc. Am. Bull.*, 84: 2605–2684.

Milliman, J. D., 1974. *Marine Carbonates:* Berlin-Heidelberg-New York (Springer-Verlag).

Moore, T. C., Jr., Pisias, N. G., and Dunn, D. A., 1982. Carbonate time series of the Quaternary and late Miocene sediments in the Pacific Ocean: a spectral comparison. *Mar. Geol.,* 46:217–233.

Müller, G., and Gastner, M., 1971. The "Karbonat-Bombe," a simple device for the determination of the carbonate content in sediments, soils and other materials. *N. Jahrb. Mineral. Monatsh.,* 10:466–469.

Mullins, H. T., 1983. Comment on "Eustatic control of turbidites and winnowed turbidites." *Geology,* 11:57–58.

Mullins, H. T., Neumann, A. C., Wilber, R. J., Hine, A. C., and Chinsburg, S. J., 1980. Carbonate sediment drifts in northern Straits of Florida. *AAPG Bull.,* 64:1701–1717

Mullins, H. T., Sherwood, W. W., Gardulski, A. F., Hinchey, E. J., Masters, P. M., and Siegel, D. I., 1985. Shallow subsurface diagenesis of Pleistocene periplatform ooze: northern Bahamas. *Sedimentology,* 32:473–494.

Oba, T., 1969. Biostratigraphy and isotopic paleotemperatures of some deep-sea cores from the Indian Ocean. *Tohoku Univ. Sci. Rep., 2nd Ser. (Geol.),* 41:129–195.

Peterson, L. C., and Prell, W. L., 1985a. Carbonate dissolution in Recent sediments of the eastern equatorial Indian Ocean: preservation and carbonate loss above the lysocline. *Mar. Geol.,* 64:259–290.

________, 1985b. Carbonate preservation and rates of climatic change: an 800 kyr record from the Indian Ocean. *In* Sundquist, E. T., and Broecker, W. S. (Eds.), *The Carbon Cycle and Atmospheric Co*$_2$*: Natural Variations Archean to Present.* Am. Geophys. Union Monogr., 32:251–269.

Pisias, N. G., and Rea, D. K., 1988. Late Pleistocene paleoclimatology of the central equatorial Pacific: sea-surface temperature response to the southeast tradewinds. *Paleoceanography,* 3:21–37.

Pisias, N. G., Heath, R. G., and Moore, T. C., 1975. Lag times for oceanic responses to climatic change. *Nature,* 256:716–717.

Prell, W. L., 1982. Oxygen and carbon isotope stratigraphy for the Quaternary of Hole 502B: evidence for two modes of isotopic variability. *In* Prell, W. L., Gardner, J. F., et al., *Init.Repts. DSDP,* 68: Washington (U.S. Govt. Printing Office), 455–464.

Reymer, J.J.G., Schlager, W., and Droxler, A. W., 1988. ODP Site 632: Plio-Pleistocene sedimentation cycles in a Bahamian Basin. *In* Austin, J. A., Jr., Schlager, W., et al., *Proc. ODP, Sci. Results,* 101: College Station, TX (Ocean Drilling Program), 213–220.

Ruddiman, W. F., McIntyre, A., and Raymo, M., 1987. Paleo-environmental results from North Atlantic Sites 607 and 609. *In* Ruddiman, W. F., Kidd, R., Thomas, E., et al., *Init. Repts. DSDP,* 94, Pt. 2: Washington (U.S. Govt. Printing Office), 855–878.

Ruddiman, W. F., Raymo, M., and McIntyre, A., 1986. Matuyama 41,000-year cycles: North Atlantic Ocean and Northern Hemisphere ice sheets. *Earth Planet. Sci. Lett.,* 80:117–129.

Saito, T., Burckle, L. H., and Hays, J. D., 1975. Late Miocene to Pleistocene biostratigraphy of equatorial Pacific sediments. *In* Saito, T., and Burckle, L. H. (Eds.), *Late Neogene Epoch Boundaries:* New York (Micropaleontology Press), 226–244.

Schlager, W., and Chermark, A., 1979. Modern sediment facies of platform-basin transition, Tongue of the Ocean, Bahamas. *In* Doyle, L., and Pilkey, O. H. (Eds.), *Geological Continental Slopes.* Spec. Publ., Soc. Econ. Paleontol. Mineral., 27:193–208.

Schlager, W., and James, N. P., 1978. Low-magnesian calcite limestones forming at the deep-sea floor, Tongue of the Ocean, Bahamas. *Sedimentology,* 15:675–702.

Shackleton, N. J., 1986. The Plio-Pleistocene Ocean: stable isotope history. *In* Hsü, K. J. (Ed.), *Mesozoic and Cenozoic Oceans:* Washington (American Geophysical Union), Geodyn. Ser., 15:141–153.

Shackleton, N. J., and Opdyke, N. D., 1973. Oxygen isotope and palaeomagnetic stratigraphy of equatorial Pacific core V28-238: oxygen isotope temperatures and ice volumes on a 10^5 year and 10^6 year scale. *Quat. Res.,* 3:39–55.

________, 1976. Oxygen isotope and paleomagnetic stratigraphy of Pacific core V28-239, late Pliocene to latest Pleistocene. *In* Cline, R. M., and Hays, J. D. (Eds.), *Investigations of Late Quaternary Paleoceanography and Paleoclimatology.* Mem. Geol. Soc. Am., 145:449–464.

Shackleton, N. J., Backman, J., Zimmerman, H., Kent, D. V., Hall, M. A., Schnitker, D., Baldauf, J., Desprairies, A., Homrighausen, R., Huddlestun, P., Keene, J. B., Kaltenback, A. J., Krumsiek, K.A.O., Morton, A. C., Murray, J. W., and Westberg-Smith, J., 1984. Oxygen isotope calibration of the onset of ice-rafting in DSDP Site 552A: history of glaciation in the North Atlantic region. *Nature,* 307:620–623.

Slowey, N. C., Neumann, A. C., and Baldwin, K. C.,1989. Seismic expression of Quaternary climatic cycles in the periplatform carbonate ooze of the northern Bahamas. *Geol. Soc. Am. Bull.,* 101:1563–1573.

Supko, P. R., 1963. A quantitative X-ray diffraction method for the mineralogical analysis of carbonate sediments from Tongue of the Ocean [M.S. thesis]. Univ. of Miami, Coral Gables, FL.

Thierstein, H. R., Geitzenauer, K. R., Molfino, B., and Shackleton, N. J., 1977. Global synchroneity of late Quaternary coccolith datum levels: validation by oxygen isotopes. *Geology,* 5:400–405.

Thompson, P. R., and Saito, T., 1974. Pacific Pleistocene sediments: planktonic foraminifera dissolution cycles and geochronology. *Geology,* 2:333–335.

Van Donk, J., 1976. ^{18}O record of the Atlantic Ocean for the entire Pleistocene Epoch. *In* Cline, R. M., and Hays, J. D. (Eds.), *Investigations of Late Quaternary Paleoceanography and Paleoclimatology.* Mem. Geol. Soc. Am., 145:147–163.

Vincent, E., 1985. Distribution stratigraphique de la teneur en carbonate dans les sédiments néogènes et quaternaires de l'océan Pacifique. *Bull. Soc. Gol. Fr.,* 8:915–924.

Volat, J., Pastouret, L., and Vergnaud-Grazzini, C., 1980. Dissolution and carbonate fluctuations in Pleistocene deep-sea cores: a review. *Mar. Geol.,* 34:1–28.

Williams, D. F., Gribble, D., Healy-Williams, N., and Leschak, P., 1985. Dissolution and water-mass patterns in the southeast Indian Ocean, Part II: the Pleistocene record from Brunhes to Matuyama age sediments. *Geol. Soc. Am. Bull.,* 96:190–202.

Williams, D. F., Thunell, R. C., Tappa, E., Rio, D., and Raffi, I., 1988. Chronology of the Pleistocene oxygen-isotope record: 0–1.88 m.y. B.P. *Palaeogeogr., Palaeoclimatol., Palaeoecol.,* 64:221–240.

Wilson, J. L., 1975. *Carbonate Facies in Geologic History:* Berlin-Heidelberg-New York (Springer-Verlag).

Date of initial receipt: 28 June 1989
Date of acceptance: 11 January 1990
Ms 115B-179

APPENDIX A

Carbonate Mineralogy and Oxygen Isotope Data and Pteropod Ratios for Sediment Samples from Hole 716B.

					Carbonate mineralogy					
Core, section, interval (cm)	Depth (m)	Time (Ma)	Carbonate (%)	Fine fraction (%)	Aragonite (%)	Calcite (%)	Mg calcite (%)	$\delta^{18}O$ PDB *G. sacculifera* (‰)	Aragonite to total sediment (%)	Pteropod ratio
1H-1, 20–22	0.2	0.005	92	51	70	19	11	−2.02	33	0.63
1H-1, 40–42	0.4	0.010	93	49	71	16	13	−1.73	32	0.65
1H-1, 60–62	0.6	0.014	86	31	61	24	15	−0.88	16	0.62
1H-1, 80–82	0.8	0.019	82	25	52	33	15	−0.75	11	0.64
1H-1, 100–102	1.0	0.024	82	25	49	34	17	−0.93	10	0.56
1H-1, 120–122	1.2	0.031	83	26	49	42	9	−0.93	10	0.59
1H-1, 140–142	1.4	0.038	87	40	65	23	12	−1.01	22	0.58
1H-2, 20–22	1.7	0.049	92	49	65	24	11	−1.27	29	0.44
1H-2, 40–42	1.9	0.055	91	49	67	24	9	−1.32	30	0.47
1H-2, 60–62	2.1	0.065	91	43	56	34	10	−0.85	22	0.50
1H-2, 80–82	2.3	0.074	92	49	64	26	10	−1.57	29	0.37
1H-2, 100–102	2.5	0.080	92	40	64	26	11	−2.02	23	0.52
1H-2, 120–122	2.7	0.086	90	42	68	24	8	−1.49	25	0.47
1H-2, 140–142	2.9	0.092	90	54	69	23	8	−1.58	34	0.45
2H-1, 20–22	4.1	0.128	86	33	63	25	12	−0.99	18	0.57
2H-1, 40–42	4.3	0.139	87	36	65	23	12	−0.86	20	0.61
2H-1, 60–62	4.5	0.149	81	33	56	31	13	−0.77	15	0.50
2H-1, 80–82	4.7	0.160	80	28	56	34	10	−0.52	13	0.52
2H-1, 100–102	4.9	0.170	82	31	58	34	8	−0.79	15	0.61
2H-1, 120–122	5.1	0.181	85	46	66	27	7	−0.71	26	0.38
2H-1, 140–142	5.3	0.191	89	54	69	22	9	−1.51	33	0.47
2H-2, 20–22	5.6	0.198	91	51	75	18	7	−1.35	35	0.43
2H-2, 40–42	5.8	0.203	92	59	70	23	7	−1.03	38	0.42
2H-2, 60–62	6	0.208	91	59	71	23	6	−0.91	38	0.49
2H-2, 80–82	6.2	0.213	93	53	77	18	5	−1.76	38	0.512
2H-2, 100–102	6.4	0.218	91	33	72	22	6	−1.30	22	0.70
2H-2, 120–122	6.6	0.223	91	47	69	27	4	−0.98	30	0.45
2H-2, 140–142	6.8	0.229	90	56	70	24	6	−1.05	35	0.44
2H-3, 20–22	7.1	0.236	92	47	69	23	8	−1.01	30	0.54
2H-3, 40–42	7.3	0.241	92	26	79	16	5	−1.63	19	0.65
2H-3, 60–62	7.5	0.248	85	30	55	37	8	−0.67	14	0.52
2H-3, 80–82	7.7	0.259	85	27	60	32	8	−0.65	14	0.61
2H-3, 100–102	7.9	0.271	82	38	66	26	8	−0.71	20	0.44
2H-3, 120–122	8.1	0.283	85	53	68	26	6	−0.87	30	0.36
2H-3, 140–142	8.3	0.294	90	58	68	26	6		35	0.44
2H-4, 20–22	8.6	0.308	94	49	73	22	5	−1.31	34	0.36
2H-4, 40–42	8.8	0.312	90	60	77	18	5	−1.04	42	0.29
2H-4, 60–62	9	0.315	89	57	66	30	4	−0.73	34	0.27
2H-4, 80–82	9.2	0.318	92	66	61	36	3	−0.60	37	0.18
2H-4, 100–102	9.4	0.322	92	56	65	30	5	−1.26	34	0.32
2H-4, 120–122	9.6	0.325	92	38	74	22	4	−1.60	26	0.28
2H-4, 140–142	9.8	0.329	92	62	69	29	2	−1.20	39	0.51
2H-6, 20–22	10.1	0.334	94	69	71	27	2	−1.62	46	0.30
2H-6, 40–42	10.3	0.337	93	43	76	21	3	−1.46	30	0.36
2H-6, 60–62	10.5	0.342	84	26	64	33	3	−0.46	14	0.28
2H-6, 80–82	10.7	0.347	86	33	62	33	5	−0.66	18	0.44
2H-6, 100–102	10.9	0.352	87	35	66	29	5	−0.95	20	0.43
2H-6, 120–122	11.1	0.357	91	32	69	27	4	−1.12	20	0.36
2H-6, 140–142	11.3	0.362	92	46	67	29	4	−1.36	28	0.20
2H-6, 20–22	11.6	0.375	90	48	75	22	3	−1.35	33	0.04
2H-6, 40–42	11.8	0.383	89	52	70	30	0	−1.53	32	0.32
2H-6, 60–62	12	0.391	90	48	68	30	2	−1.65	29	0.25
2H-6, 80–82	12.2	0.400	93	45	82	18	0	−1.834	34	0.25
2H-6, 100–102	12.4	0.408	89	34	76	22	2	−1.15	23	0.66
2H-6, 120–122	12.6	0.417	87	42	68	32	0	−1.08	25	0.26
2H-6, 140–142	12.8	0.426	83	33	70	27	3	−0.94	19	0.40
2H-7, 20–22	13.1	0.446	84	35	66	30	4	−0.35	20	0.472
3H-1, 20–22	13.7	0.485	92	50	67	33	0	−0.89	31	0.27
3H-1, 40–42	13.9	0.488	94	43	68	32	0	−0.96	28	0.34
3H-1, 60–62	14.1	0.491	90	34	70	27	3	−0.95	22	0.50
3H-1, 80–82	14.3	0.495	88	34	68	31	1	−0.88	20	0.43
3H-1, 100–102	14.5	0.498	89	39	81	17	2	−1.02	28	0.36
3H-1, 120–122	14.7	0.501	93	38	76	24	0	−1.12	27	0.45
3H-1, 140–142	14.9	0.505	90	36	77	21	2	−1.00	25	0.48
3H-2, 20–22	15.2	0.509	89	43	73	24	3	−0.89	28	0.56
3H-2, 40–42	15.4	0.513	92	36	78	20	2	−0.92	26	0.51
3H-2, 60–62	15.6	0.516	93	56	68	29	3	−1.10	36	0.40
3H-2, 80–82	15.8	0.519	94	42	66	31	3	−0.90	26	0.49
3H-2, 100–102	16.0	0.522	92	35	69	28	3	−0.99	22	0.56
3H-2, 120–122	16.2	0.530	84	27	56	36	8	−0.34	13	0.52
3H-2, 140–142	16.4	0.543	87	30	61	35	4	−0.53	16	0.60
3H-3, 20–22	16.7	0.562	87	48	66	31	3	−0.90	28	0.52
3H-3, 40–42	16.9	0.568	91	45	69	28	3	−0.75	28	0.49

APPENDIX A (continued).

					Carbonate mineralogy					
Core, section, interval (cm)	Depth (m)	Time (Ma)	Carbonate (%)	Fine fraction (%)	Aragonite (%)	Calcite (%)	Mg calcite (%)	δ^{18}O PDB *G. sacculifera* (‰)	Aragonite to total sediment (%)	Pteropod ratio
3H-3, 60–62	17.1	0.571	91	38	67	30	3	−0.65	23	0.52
3H-3, 80–82	17.3	0.574	91	29	64	33	3	−0.75	17	0.55
3H-3, 100–102	17.5	0.578	87	30	63	32	5	−0.67	17	0.51
3H-3, 120–122	17.7	0.581	87	29	60	35	5	−0.83	15	0.53
3H-3, 140–142	17.9	0.584	90	28	62	33	5	−0.84	16	0.46
3H-4, 20–22	18.2	0.590	90	27	60	36	4	−0.68	15	0.50
3H-4, 40–42	18.4	0.593	90	42	64	32	4	−1.01	24	0.51
3H-4, 60–62	18.6	0.596	93	43	68	32	0	−0.98	27	
3H-4, 80–82	18.8	0.600	93	55	70	30	0	−0.97	36	
3H-4, 100–102	19.0	0.603	95	51	72	28	0	−0.94	34	
3H-4, 120–122	19.2	0.606	92	37	75	25	0	−0.77	25	
3H-4, 140–142	19.4	0.610	91	38	66	32	2	−0.68	23	
3H-5, 20–22	19.7	0.615	92	42	68	32	0	−0.91	26	
3H-5, 40–42	19.9	0.618	91	37	73	27	0	−0.48	24	
3H-5, 60–62	20.1	0.622	91	39	73	27	0	−0.63	26	
3H-5, 80–82	20.3	0.626	93	45	70	30	0	−0.38	29	
3H-5, 100–102	20.5	0.630	94	62	69	31	0	−0.61	40	
3H-5, 120–122	20.7	0.633	93	63	73	27	0	−0.49	43	
3H-5, 140–142	20.9	0.637	90	44	73	27	0	−0.34	29	
3H-6, 20–22	21.2	0.643	87	34	66	34	0	−0.56	20	
3H-6, 40–42	21.4	0.647	92	40	70	30	0	−0.64	26	
3H-6, 60–62	21.6	0.650	87	36	66	34	0	−0.31	21	
3H-6, 80–82	21.8	0.654	85	33	68	32	0	−0.42	19	
3H-6, 100–102	22.0	0.658	87	46	66	34	0	−0.91	27	
3H-6, 120–122	22.2	0.662	90	58	68	32	0	−1.01	36	
3H-6, 140–142	22.4	0.665	95	53	70	30	0	−0.75	35	
4H-1, 20–22	23.3	0.680	91	48	68	32	0	−0.78	30	
4H-1, 40–42	23.5	0.684	90	47	71	29	0	−1.11	30	
4H-1, 60–62	23.7	0.687	91	37	68	32	0	−0.50	23	
4H-1, 80–82	23.9	0.695	92	43	46	54	0	−0.53	18	
4H-1, 100–102	24.1	0.706	89	43	62	38	0	−0.97	23	
4H-1, 120–122	24.3	0.717	89	46	71	29	0	−0.67	29	
4H-1, 140–142	24.5	0.729	88	62	68	32	0	−1.03	37	
4H-2, 20–22	24.8	0.729	92	28	80	20	0	−0.48	20	
4H-2, 40–42	25.0	0.731	92	34	68	32	0	−0.50	21	
4H-2, 60–62	25.2	0.733	91	34	71	29	0	−0.85	22	
4H-2, 80–82	25.4	0.734	90	36	72	28	0	−0.37	24	
4H-2, 100–102	25.6	0.736	84	35	68	32	0	−0.41	20	
4H-2, 120–122	25.8	0.743	86	34	67	33	0	−0.57	20	
4H-2, 140–142	26.0	0.750	86	38	75	25	0	−0.56	24	
4H-3, 20–22	26.3	0.761	92	42	71	29	0	−0.63	27	
4H-3, 40–42	26.5	0.767	94	44	80	20	0	−0.80	33	
4H-3, 60–62	26.7	0.773	94	31	72	28	0	−0.77	21	
4H-3, 80–82	26.9	0.779	91	25	69	31	0	−0.89	16	
4H-3, 100–102	27.1	0.784	92	28	63	27	0	−0.69	16	
4H-3, 120–122	27.3	0.790	91	27	71	29	0	−0.41	18	
4H-3, 140–142	27.5	0.795	91	27	69	31	0	−0.86	17	
4H-4, 20–22	27.8	0.803	91	35	68	32	0	−0.66	22	
4H-4, 40–42	28.0	0.808	92	32	71	29	0	−0.74	21	
4H-4, 60–62	28.2	0.813	95	46	71	29	0	−0.97	31	
4H-4, 80–82	28.4	0.818	93	35	77	22	1	−0.94	25	
4H-4, 100–102	28.6	0.822	92	25	69	31	0	−0.92	16	
4H-4, 120–122	28.8	0.827	93	34	69	31	0	−1.10	22	
4H-4, 140–142	29.0	0.831	94	30	71	26	3	−1.10	20	
4H-5, 20–22	29.3	0.838	95	18	67	28	5	−1.51	11	
4H-5, 40–42	29.5	0.843	95	23	67	25	8	−1.45	15	
4H-5, 60-62	29.7	0.847	95	22	61	32	7	−1.09	13	
4H-5, 80–82	29.9	0.852	97	18	68	24	8	−1.08	12	
4H-5, 100–102	30.1	0.856	96	14	60	32	8	−0.95	8	
4H-5, 120–122	30.3	0.861	97	20	60	34	6	−1.21	12	
4H-5, 140–142	30.5	0.866	95	20	62	31	7	−1.10	12	
4H-6, 20–22	30.8	0.872	97	14	66	26	8	−1.23	9	
4H-6, 40–42	31.0	0.878	95	15	65	23	12	−1.06	9	
4H-6, 60–62	31.2	0.882	96	14	60	31	9	−1.33	8	
4H-6, 80–82	31.4	0.886	93	17	63	31	6	−1.20	10	
4H-6, 100–102	31.6	0.891	94	16	62	32	6	−1.15	9	
4H-6, 120–122	31.8	0.895	95	12	58	34	8	−1.27	7	
5H-1, 20–22	33.0	0.920	92	25	66	34	0	−0.83	15	
5H-1, 40–42	33.2	0.922	85	34	64	36	0	−0.63	18	
5H-1, 60–62	33.4	0.924	85	35	63	37	0	−0.96	19	
5H-1, 80–82	33.6	0.927	89	40	66	34	0	−1.01	23	
5H-1, 100–102	33.8	0.929	91	38	67	31	2	−1.03	23	
5H-1, 120–122	34.0	0.933	91	26	66	34	0	−1.01	15	
5H-1, 140–142	34.2	0.939	91	31	65	35	0	−1.21	19	

APPENDIX A (continued).

					Carbonate mineralogy					
Core, section, interval (cm)	Depth (m)	Time (Ma)	Carbonate (%)	Fine fraction (%)	Aragonite (%)	Calcite (%)	Mg calcite (%)	$\delta^{18}O$ PDB *G. sacculifera* (‰)	Aragonite to total sediment (%)	Pteropod ratio
5H-2, 20–22	34.5	0.948	93	37	67	33	0	−1.00	23	
5H-2, 40–42	34.7	0.955	91	38	68	32	0	−1.37	24	
5H-2, 60–62	34.9	0.961	94	32	69	31	0	−0.95	21	
5H-2, 80–82	35.1	0.967	92	35	63	37	0	−1.07	20	
5H-2, 100–102	35.3	0.973	92	42	67	33	0	−1.26	26	
5H-2, 120–122	35.5	0.979	94	54	69	31	0	−1.09	35	
5H-2, 140–142	35.7	0.985	93	37	68	32	0	−1.15	24	
5H-3, 20–22	36.0	0.995	91	43	68	32	0	−0.99	27	
5H-3, 40–42	36.2	1.001	92	46	67	33	0	−0.79	28	
5H-3, 60–62	36.4	1.007	94	54	70	30	0	−0.92	36	
5H-3, 80–82	36.6	1.010	94	62	71	29	0	−0.78	41	
5H-3, 100–102	36.8	1.014	95	53	69	31	0	−0.93	34	
5H-3, 120–122	37.0	1.017	93	48	65	35	0	−0.88	29	
5H-3, 140–142	37.2	1.020	92	54	61	39	0	−0.76	30	
5H-4, 20–22	37.5	1.025	93	56	62	38	0	−0.66	33	
5H-4, 40–42	37.7	1.028	95	51	58	42	0	−0.69	28	
5H-4, 60–62	37.9	1.031	96	67	66	34	0	−0.89	43	
5H-4, 80–82	38.1	1.035	96	55	75	25	0	−0.58	40	
5H-4, 100–102	38.3	1.038	96	54	69	31	0	−0.33	36	
5H-4, 120–122	38.5	1.041	94	45	71	29	0	−0.26	30	
5H-4, 140–142	38.7	1.046	96	62	68	32	0	−0.45	40	
5H-5, 20–22	39.0	1.063	94	52	73	27	0	−0.36	36	
5H-5, 40–42	39.2	1.074	92	46	70	30	0	−0.05	30	
5H-5, 60–62	39.4	1.085	92	43	71	29	0	−0.29	28	
5H-5, 80–82	39.6	1.096	91	42	69	31	0	−0.34	26	
5H-5, 100–102	39.8	1.107	94	48	68	32	0	−0.37	30	
5H-5, 120–122	40.0	1.118	93	53	70	30	0	−0.61	35	
5H-5, 140–142	40.2	1.129	93	70	68	32	0	−0.60	44	
5H-6, 20–22	40.5	1.146	95	72	58	42	0	−0.83	39	
5H-6, 40–42	40.7	1.157	96	70	59	41	0	−0.65	40	
5H-6, 60–62	40.9	1.169	96	69	62	38	0	−0.26	41	
5H-6, 80–82	41.1	1.180	99	57	73	27	0		42	
5H-6, 100–102	41.3	1.191	99	48	72	28	0		34	
5H-6, 120–122	41.5	1.202	97	39	71	29	0		27	
5H-6, 140–142	41.7	1.213	98	42	70	30	0		29	
5H-7, 20–22	42.0	1.230	97	52	68	32	0		35	
5H-7, 40–42	42.2	1.241	99	51	71	29	0		36	
5H-7, 60–62	42.4	1.252	98	56	72	28	0		40	
5H-7, 80–82	42.6	1.264	98	50	75	25	0		37	
6H-1, 20–22	42.7	1.294	96	49	68	32	0		32	
6H-1, 40–42	42.9	1.305	97	42	67	33	0		27	
6H-1, 60–62	43.1	1.317	97	43	61	39	0		25	
6H-1, 80–82	43.3	1.336	96	40	66	34	0		26	
6H-1, 100–102	43.5	1.339	97	47	65	35	0		30	
6H-1, 120–122	43.7	1.342	97	45	66	34	0		29	
6H-1, 140–142	43.9	1.344	97	47	67	33	0		30	
6H-2, 20–22	44.2	1.348	98	51	67	33	0		33	
6H-2, 40–42	44.4	1.351	97	47	67	33	0		30	
6H-2, 60–62	44.6	1.353	95	62	52	48	0		31	
6H-2, 80–82	44.8	1.356	93	61	61	39	0		35	
6H-2, 100–102	45.0	1.359	94	69	64	36	0		42	
6H-2, 120–122	45.2	1.361	94	53	61	39	0		31	
6H-2, 140–142	45.4	1.364	95	62	60	40	0		35	
6H-3, 20–22	45.7	1.368	95	61	56	44	0		32	
6H-3, 40–42	45.9	1.371	94	69	56	44	0		36	
6H-3, 60–62	46.1	1.373	97	66	47	53	0		30	
6H-3, 80–82	46.3	1.376	95	54	57	43	0		29	
6H-3, 100–102	46.5	1.379	97	49	62	38	0		29	
6H-3, 120–122	46.7	1.381	97	51	58	42	0		29	
6H-3, 140–142	46.9	1.384	96	58	62	38	0		34	
6H-4, 20–22	47.2	1.388	96	66	55	45	0		35	
6H-4, 40–42	47.4	1.390	95	60	57	43	0		32	
6H-4, 60–62	47.6	1.393	96	55	55	45	0		29	
6H-4, 80–82	47.8	1.396	96	50	61	39	0		29	
6H-4, 100–102	48.0	1.398	96	56	62	38	0		33	
6H-4, 120–122	48.2	1.401	98	58	62	38	0		35	
6H-4, 140–142	48.4	1.402	96	54	60	40	0		32	
6H-5, 20–22	48.7	1.407	97	52	60	40	0		30	
6H-5, 40–42	48.9	1.410	96	53	46	54	0		23	
6H-5, 60–62	49.1	1.412	97	54	52	48	0		27	
6H-5, 80–82	49.3	1.415	98	61	55	45	0		32	
6H-5, 100–102	49.5	1.418	97	55	49	51	0		26	
6H-5, 120–122	49.7	1.421	97	55	54	46	0		28	
6H-5, 140–142	49,9	1.423	96	46	50	50	0		22	

APPENDIX A (continued).

					Carbonate mineralogy					
Core, section, interval (cm)	Depth (m)	Time (Ma)	Carbonate (%)	Fine fraction (%)	Aragonite (%)	Calcite (%)	Mg calcite (%)	$\delta^{18}O$ PDB *G. sacculifera* (‰)	Aragonite to total sediment (%)	Pteropod ratio
6H-6, 20–22	50.2	1.427	96	41	47	53	0		18	
6H-6, 40–42	50.4	1.430	97	57	53	47	0		30	
6H-6, 60–62	50.6	1.433	98	58	52	48	0		30	
6H-6, 80–82	50.8	1.435	95	61	52	48	0		30	
6H-6, 100–102	51.0	1.438	94	48	60	40	0		27	
6H-6, 120–122	51.2	1.441	94	51	56	44	0		27	
6H-6, 140–142	51.4	1.443	95	48	57	43	0		26	
6H-7, 20–22	51.7	1.447	96	51	58	42	0		28	
6H-7, 40–42	51.9	1.450	95	52	56	44	0		27	
6H-7, 60–62	52.1	1.452	95	55	60	40	0		31	
6H-7, 80–82	52.3	1.455	96	52	61	39	0		31	
7H-1, 20–22	51.31	1.455	94	60	50	50	0		28	
7H-1, 40–42	52.5	1.463	95	60	47	53	0		27	
7H-1, 60–62	52.7	1.471	92	65	51	49	0		31	
7H-1, 80–82	52.9	1.480	94	53	43	57	0		21	
7H-1, 100–102	53.1	1.488	95	52	55	45	0		27	
7H-1, 120–122	53.3	1.496	95	54	41	59	0		21	
7H-1, 140–142	53.5	1.504		16						
7H-2, 20–22	53.8	1.516	93	63	58	42	0		34	
7H-2, 40–42	54.0	1.524	94	66	52	48	0		32	
7H-2, 60–62	54.2	1.533	93	67	55	45	0		34	
7H-2, 80–82	54.4	1.541	92	68	55	45	0		34	
7H-2, 100–102	54.6	1.549	93	48	54	46	0		24	
7H-2, 120–122	54.8	1.557	94	45	52	48	0		22	
7H-2, 140–142	55.0	1.565		77						
7H-3, 20–22	55.3	1.578	95	70	52	48	0		35	
7H-3, 40–42	55.5	1.586	95	61	57	43	0		33	
7H-3, 60–62	55.7	1.594	93	55	58	42	0		30	
7H-3, 80–82	55.9	1.602	94	53	43	57	0		21	
7H-3, 100–102	56.1	1.610	94	49	55	45	0		25	
7H-3, 120–122	56.3	1.618	93	47	70	30	0		31	
7H-3, 140–142	56.5	1.627	92	54	71	29	0		35	
7H-4, 20–22	56.8	1.639	94	52	67	33	0		33	
7H-4, 40–42	57.0	1.647	94	55	71	29	0		37	
7H-4, 60–62	57.2	1.655	94	52	68	32	0		33	
7H-4, 80–82	57.4	1.663	94	58	65	35	0		35	
7H-4, 100–102	57.6	1.671	94	57	62	38	0		33	
7H-4, 120–122	57.8	1.680	94	66	61	39	0		38	
7H-4, 140–142	58.0	1.688	94	71	58	42	0		39	
7H-5, 20–22	58.3	1.700	94	65	61	39	0		37	
7H-5, 40–42	58.5	1.708	92	74	51	49	0		35	
7H-5, 60–62	58.7	1.716	92	73	56	44	0		38	
7H-5, 80–82	58.9	1.725	92	79	61	39	0		45	
7H-5, 100–102	59.1	1.733	89	77	52	48	0		36	
7H-5, 120–122	59.3	1.741	92	71	46	54	0		30	
7H-5, 140–142	59.5	1.749	94	50	46	54	0		22	
7H-6, 20–22	59.8	1.761	95	61	63	37	0		36	
7H-6, 40–42	60.0	1.769	93	67	56	44	0		35	
7H-6, 60–62	60.2	1.778	97	72	50	50	0		35	
7H-6, 80–82	60.4	1.786	93	68	57	43	0		36	
7H-6, 100–102	60.6	1.794	92	65	66	34	0		39	
7H-6, 120–122	60.8	1.802	94	55	66	34	0		34	
7H-6, 140–142	61.0	1.810	91	69	69	31	0		43	
7H-7, 20–22	61.3	1.823	93	75	57	43	0		39	
7H-7, 40–42	61.5	1.831	93	72	51	49	0		34	
8H-1, 20–22	61.9	1.847	91	70	44	56	0		28	
8H-1, 40–42	62.1	1.855	93	67	46	54	0		29	
8H-1, 60–62	62.3	1.863	93	70	43	57	0		28	
8H-1, 80–82	62.5	1.872	93	72	51	49	0		34	
8H-1, 100–102	62.7	1.880	92	73	50	50	0		34	
8H-1, 120–122	62.9	1.888	93	75	39	61	0		27	
8H-1, 140–142	63.1	1.893	94	68	37	63	0		24	
8H-2, 20–22	63.4	1.899	93	66	39	61	0		24	
8H-2, 40–42	63.6	1.903	94	64	51	49	0		31	
8H-2, 60–62	63.8	1.908	96	54	54	46	0		28	
8H-2, 80–82	64.0	1.912	96	56	49	51	0		26	
8H-2, 100–102	64.2	1.916	95	60	40	60	0		23	
8H-2, 120–122	64.4	1.920	95	62	39	61	0		23	
8H-2, 140–142	64.6	1.924	94	58	43	57	0		23	
3H-3, 20–22	64.9	1.930	94	51	48	52	0		23	
3H-3, 40–42	65.1	1.934	93	58	60	40	0		33	
3H-3, 60–62	65.3	1.939	93	71	54	46	0		35	
3H-3, 80–82	65.5	1.943	94	64	53	47	0		32	
3H-3, 100–102	65.7	1.947	93	62	52	48	0		30	
3H-3, 120–122	65.9	1.951	94	32	50	50	0		15	
3H-3, 140–142	66.1	1.955	93	74	44	56	0		30	

APPENDIX A (continued).

					Carbonate mineralogy					
Core, section, interval (cm)	Depth (m)	Time (Ma)	Carbonate (%)	Fine fraction (%)	Aragonite (%)	Calcite (%)	Mg calcite (%)	$\delta^{18}O$ PDB *G. sacculifera* (‰)	Aragonite to total sediment (%)	Pteropod ratio
3H-4, 20–22	66.4	1.961	93	60	46	54	0		26	
3H-4, 40–42	66.6	1.965	92	69	43	57	0		27	
3H-4, 60–62	66.8	1.969	92	58	51	49	0		27	
3H-4, 80–82	67.0	1.974	95	47	50	50	0		22	
3H-4, 100–102	67.2	1.978	94	44	39	61	0		16	
3H-4, 120–122	67.4	1.982	95	47	37	63	0		17	
3H-4, 140–142	67.6	1.986	94	57	39	61	0		21	
3H-5, 20–22	67.9	1.992	95	58	51	49	0		28	
3H-5, 40–42	68.1	1.996	93	58	54	46	0		29	
3H-5, 60–62	68.3	2.000	94	60	49	51	0		28	
3H-5, 80–82	68.5	2.004	94	56	40	60	0		21	
3H-5, 100–102	68.7	2.009	94	48	39	61	0		18	
3H-5, 120–122	68.9	2.013	94	40	43	57	0		16	
3H-5, 140–142	69.1	2.017	94	52	48	52	0		24	
3H-6, 20–22	69.4	2.023	94	51	60	40	0		29	
3H-6, 40–42	69.6	2.027	93	45	54	46	0		22	
3H-6, 60–62	69.8	2.031	93	42	53	47	0		21	
3H-6, 80–82	70.0	2.035	91	57	52	48	0		28	
3H-6, 100–102	70.2	2.040	92	58	50	50	0		27	
3H-6, 120–122	70.4	2.044	92	56	30	70	0		16	
3H-6, 140–142	71.6	2.048	92	48	25	75	0		11	
3H-7, 20–22	70.9	2.054	94	53	42	48	0		21	
3H-7, 40–42	71.1	2.058	93	42	51	49	0		20	
9H-1, 20–22	71.6	2.068	91	57	44	53	0		23	
9H-1, 40–42	71.8	2.073	93	49	29	69	0		13	
9H-1, 60–62	72.0	2.077	95	45	33	66	0		14	
9H-1, 80–82	72.2	2.081	94	48	40	59	0		18	
9H-1, 100–102	72.4	2.085	92	52	39	61	0		19	
9H-1, 120–122	72.6	2.089	92	46	43	57	0		18	
9H-1, 140–142	72.8	2.093	94	36	24	76	0		8	
9H-2, 20–22	73.1	2.099	95	34	29	71	0		9	
9H-2, 40–42	73.3	2.103	93	60	59	41	0		31	
9H-2, 60–62	73.5	2.108	90	46	48	49	3		20	
9H-2, 80–82	73.7	2.112	90	51	40	56	0		18	
9H-2, 100–102	73.9	2.116	91	46	47	52	0		20	
9H-2, 120–122	74.1	2.120	95	36	37	63	0		13	
9H-2, 140–142	74.3	2.124	91	44	46	50	0		18	
9H-3, 20–22	74.6	2.130	94	37	29	69	0		10	
9H-3, 40–42	74.8	2.134	94	43	31	69	0		13	
9H-3, 60–62	75.0	2.139	91	55	39	58	0		19	
9H-3, 80–82	75.2	2.143	91	58	38	61	0		20	
9H-3, 100–102	75.4	2.147	92	53	33	67	0		16	
9H-3, 120–122	75.6	2.151	91	47	39	61	0		17	
9H-3, 140–142	75.8	2.155	93	34	37	63	0		12	
9H-4, 20–22	76.1	2.161	92	31	47	53	0		13	
9H-4, 40–42	76.3	2.165	92	31	44	55	0		12	
9H-4, 60–62	76.5	2.169	94	31	41	59	0		12	
9H-4, 80–82	76.7	2.174	92	36	42	58	0		14	
9H-4, 100–102	76.9	2.178	92	31	50	49	0		14	
9H-4, 120–122	77.1	2.182	90	52	59	40	0		28	
9H-4, 140–142	77.3	2.186	92	58	56	42	0		30	
9H-5, 20–22	77.6	2.192	94	37	39	61	0		14	
9H-5, 40–42	77.8	2.193	96	32	29	71	0		9	
9H-5, 60–62	78.0	2.200	95	36	35	65	0		12	
9H-5, 80–82	78.2	2.205	94	37	38	62	0		13	
9H-5, 100–102	78.4	2.208	94	35	40	60	0		13	
9H-5, 120–122	78.6	2.213	94	31	47	53	0		14	
9H-5, 140–142	78.8	2.217	95	29	41	59	0		11	
9H-6, 20–22	79.1	2.223	96	29	38	62	0		10	
9H-6, 40–42	79.3	2.227	93	38	56	44	0		20	
9H-6, 60–62	79.5	2.231	92	52	48	52	0		23	
9H-6, 80–82	79.7	2.235	92	49	50	48	0		22	
9H-6, 100–102	79.9	2.240	93	37	44	56	0		15	
9H-6, 120–122	80.1	2.244	94	31	36	64	0		10	
9H-6, 140–142	80.3	2.248	93	42	47	53	0		18	
9H-7, 20–22	80.6	2.254	93	34	51	49	0		16	
9H-7, 40–42	80.8	2.258	93	33	42	55	0		13	
10H-1, 20–22	81.3	2.268	92	37	42	57	1		14	
10H-1, 40–42	81.5	2.273	92	37	34	65	1		11	
10H-1, 60–62	81.7	2.277	92	29	40	60	0		11	
10H-1, 80–82	81.9	2.281	92	33	39	61	0		12	
10H-1, 100–102	82.1	2.285	94	32	46	54	0		14	
10H-1, 120–122	82.3	2.289	93.5	33	42	58	0		13	
10H-1, 140–142	82.5	2.293	94	31	49	51	0		14	
10H-2, 20–22	82.8	2.299	93	42	52	48	0		20	
10H-2, 40–42	83.0	2.304	93	46	36	61	3		15	

APPENDIX A (continued).

					Carbonate mineralogy					
Core, section, interval (cm)	Depth (m)	Time (Ma)	Carbonate (%)	Fine fraction (%)	Aragonite (%)	Calcite (%)	Mg calcite (%)	$\delta^{18}O$ PDB *G. sacculifera* (‰)	Aragonite to total sediment (%)	Pteropod ratio
10H-2, 60–62	83.2	2.308	94	44	39	60	1		16	
10H-2, 80–82	83.4	2.312	95	34	36	64	0		12	
10H-2, 100–102	83.6	2.316	95	39	32	68	0		12	
10H-2, 120–122	83.8	2.320	94	37	50	50	0		18	
10H-2, 140–142	84.0	2.324	93	33	49	51	0		15	
10H-3, 20–22	84.3	2.330	93	31	25	73	2		7	
10H-3, 40–42	84.5	2.335	95	36	31	69	0		11	
10H-3, 60–62	84.7	2.339	95	34	39	61	0		13	
10H-3, 80–82	84.9	2.343	93	41	42	58	0		16	
10H-3, 100–102	85.1	2.347	94	36	43	56	1		14	
10H-3, 120–122	85.3	2.353	95	33	41	54	5		13	
10H-3, 140–142	85.5	2.363	94	39	46	54	0		17	
10H-4, 20–22	85.8	2.379	94	31	43	57	0		13	
10H-4, 40–42	86.0	2.390	95	32	45	55	0		14	
10H-4, 60–62	86.2	2.400	94	33	45	0			17	
10H-4, 80–82	86.4	2.411	93	30	56	44	0		16	
10H-4, 100–102	86.6	2.422	95	28	55	43	2		14	
10H-4, 120–122	86.8	2.432	94	30	53	45	2		15	
10H-4, 140–142	87.0	2.443	94	25	49	51	0		11	
10H-5, 20–22	87.3	2.459	94	31	48	51	1		14	
10H-5, 40–42	87.5	2.469	93	30	41	56	3		11	
10H-5, 60–62	87.7	2.480	94	30	39	60	1		11	
10H-5, 80–82	87.9	2.490	93	30	46	54	0		13	
10H-5, 100–102	88.1	2.501	93	29	54	46	0		14	
10H-5, 120–122	88.3	2.510	95	29	58	42	0		16	
10H-5, 140–142	88.5	2.520	94	27	64	36	0		16	
10H-6, 20–22	88.8	2.538	93	30	55	45	0		15	
10H-6, 40–42	89.0	2.549	93	29	61	39	0		17	
10H-6, 60–62	89.2	2.559	93	32	47	52	1		14	
10H-6, 80–82	89.4	2.570	93	33	35	65	0		11	
10H-6, 100–102	89.6	2.580	94	32	41	59	0		12	
10H-6, 120–122	89.8	2.594	94	29	42	58	0		12	
10H-6, 140–142	90.0	2.602	92	35	39	61	0		13	
10H-7, 20–22	90.3	2.618	92	30	39	61	0		11	
10H-7, 40–42	90.5	2.628	95	26	29	71	0		7	
11H-1, 20–22	90.9	2.649	95	29	24	76	0		7	
11H-1, 40–42	91.1	2.660	94	46	21	79	0		9	
11H-1, 60–62	91.3	2.671	95	45	30	70	0		13	
11H-1, 80–82	91.5	2.681	96	41	33	67	0		13	
11H-1, 100–102	91.7	2.692	93	36	39	61	0		13	
11H-1, 120–122	91.9	2.703	93	36	41	59	0		14	
11H-1, 140–142	92.1	2.713	93	39	42	58	0		15	
11H-2, 20–22	92.4	2.729	93	40	38	62	0		14	
11H-2, 40–42	92.6	2.740	92	42	36	64	0		14	
11H-2, 60–62	92.8	2.750	93	44	30	70	0		12	
11H-2, 80–82	93.0	2.761	93	51	44	56	0		21	
11H-2, 100–102	93.2	2.771	94	51	45	55	0		22	
11H-2, 120–122	93.4	2.782	94	40	46	54	0		18	
11H-2, 140–142	93.6	2.793	95	39	41	59	0		15	
11H-3, 20–22	93.9	2.809	94	38	36	64	0		13	
11H-3, 40–42	94.1	2.819	95	35	31	69	0		10	
11H-3, 60–62	94.3	2.830	95	35	30	70	0		10	
11H-3, 80–82	94.5	2.840	94	36	36	64	0		12	
11H-3, 100–102	94.7	2.851	95	39	40	60	0		15	
11H-3, 120–122	94.9	2.862	95	37	40	60	0		14	
11H-3, 140–142	95.1	2.872	96	39	40	60	0		15	
11H-4, 20–22	95.4	2.888	96	36	43	57	0		15	
11H-4, 40–42	95.6	2.899	94	40	45	55	0		17	
11H-4, 60–62	95.8	2.909	94	45	48	52	0		20	
11H-4, 80–82	96.0	2.920	94	35	56	44	0		19	
11H-4, 100–102	96.2	2.930	95	38	56	44	0		20	
11H-4, 120–122	96.4	2.941	95	38	54	46	0		19	
11H-4, 140–142	96.6	2.952	93	38	50	50	0		17	
11H-5, 20–22	96.9	2.967	91	40	40	60	0		14	
11H-5, 40–42	97.1	2.978	93	39	38	62	0		14	
11H-5, 60–62	97.3	2.989	94	44	37	63	0		15	
11H-5, 80–82	97.5	2.999	93	57	36	64	0		19	
11H-5, 100–102	97.7	3.010	95	31	25	75	0		7	
11H-5, 120–122	97.9	3.020	92	52	37	63	0		18	
11H-5, 140–142	98.1	3.031	93	44	40	60	0		16	
11H-6, 20–22	98.4	3.047	94	39	28	72	0		10	
11H-6, 40–42	98.6	3.058	91	53	52	48	0		25	
11H-6, 60–62	98.8	3.068	94	45	46	54	0		19	
11H-6, 80–82	99.0	3.079	96	30	42	58	0		12	
11H-6, 100–102	99.2	3.089	95	33	33	67	0		10	

APPENDIX A (continued).

					Carbonate mineralogy					
Core, section, interval (cm)	Depth (m)	Time (Ma)	Carbonate (%)	Fine fraction (%)	Aragonite (%)	Calcite (%)	Mg calcite (%)	δ^{18}O PDB *G. sacculifera* (‰)	Aragonite to total sediment (%)	Pteropod ratio
11H-6, 120–122	99.4	3.100	93	45	36	64	0		15	
11H-6, 140–142	99.6	3.111	94	59	37	63	0		20	
11H-7, 20–22	99.9	3.127	95	32	30	70	0		9	
11H-7, 40–42	100.1	3.137	95	41	25	75	0		10	
11H-7, 60–62	100.3	3.148	93	59	36	64	0		20	
12H-1, 20–22	100.5	3.158	92	54	34	66	0		17	
12H-1, 40–42	100.7	3.169	95	45	37	63	0		16	
12H-1, 60–62	100.9	3.180	95	38	30	70	0		11	
12H-1, 80–82	101.1	3.190	94	45	29	71	0		12	
12H-1, 100–102	101.3	3.201	95	40	38	62	0		14	
12H-1, 120–122	101.5	3.211	94	36	29	71	0		10	
12H-1, 140–142	101.7	3.222	93	45	23	77	0		10	
12H-2, 20–22	102.0	3.238	93	37	36	64	0		12	
12H-2, 40–42	102.2	3.249	92	39	35	65	0		13	
12H-2, 60–62	102.4	3.259	94	38	38	62	0		13	
12H-2, 80–82	102.6	3.270	95	43	22	78	0		9	
12H-2, 100–102	102.8	3.280	95	41	25	75	0		10	
12H-2, 120–122	103.0	3.291	93	51	28	72	0		13	
12H-2, 140–142	103.2	3.302	93	36	20	80	0		7	
12H-3, 20–22	103.5	3.318	93	40	24	76	0		9	
12H-3, 40–42	103.7	3.328	93	40	23	77	0		8	
12H-3, 60–62	103.9	3.339	91	39	32	68	0		11	
12H-3, 80–82	104.1	3.349	94	49	24	76	0		11	
12H-3, 100–102	104.3	3.360	93	47	20	80	0		9	
12H-3, 120–122	104.5	3.370	94	38	23	77	0		8	
12H-3, 140–142	104.7	3.381	94	45	20	80	0		8	
12H-4, 20–22	105.0	3.397	95	39	16	84	0		6	
12H-4, 40–42	105.2	3.408	95	39	21	79	0		8	
12H-4, 60–62	105.4	3.418	96	37	25	75	0		9	
12H-4, 80–82	105.6	3.429	94	42	28	72	0		11	
12H-4, 100–102	105.8	3.439	95	45	23	77	0		10	
12H-4, 120–122	106.0	3.450	95	42	28	72	0		11	
12H-4, 140–142	106.2	3.460	95	49	22	78	0		10	
12H-5, 20–22	106.5	3.471	93	42	29	71	0		11	
12H-5, 40–42	106.7	3.482	94	39	25	75	0		9	
12H-5, 60–62	106.9	3.491	94	40	23	77	0		9	
12H-5, 80–82	107.1	3.501	95	44	21	79	0		9	
12H-5, 100–102	107.3	3.511	94	50	15	85	0		7	
12H-5, 120–122	107.5	3.520	94	42	18	82	0		7	
12H-5, 140–142	107.7	3.531	95	53	20	80	0		10	
12H-6, 20–22	107.9	3.542	94	46	29	71	0		12	
12H-6, 40–42	108.2	3.551	92	44	20	80	0		8	
12H-6, 60–62	108.4	3.563	95	41	9	91	0		4	
12H-6, 80–82	108.6	3.572	94	49	19	81	0		9	
12H-6, 100–102	108.8	3.581	94	48	22	78	0		10	
12H-6, 120–122	109.0	3.593	93	58	29	71	0		16	
12H-6, 140–142	109.2	3.602	93	55	29	71	0		15	
12H-7, 20–22	109.5	3.613	94	41	24	76	0		9	
12H-7, 40–42	109.7	3.623	94	58	19	81	0		10	

APPENDIX B

Carbonate Mineralogy and Oxygen Isotope Data for Sediment Samples from Hole 714A.

					Carbonate mineralogy				
Core, section, interval (cm)	Depth (m)	Time (Ma)	Carbonate (%)	Fine fraction (%)	Aragonite (%)	Calcite (%)	Mg calcite (%)	δ^{18}O PDB *G. sacculifera* (‰)	Aragonite to total sediment (%)
1H-1, 5–7	0.05	0.001	77	65	41	59	0		30
1H-1, 15–17	0.15	0.003	78	50	40	60	0	−2.01	23
1H-1, 25–27	0.25	0.005	78	51	35	65	0		26
1H-1, 35–37	0.35	0.006	75	56	37	63	0	−1.63	27
1H-1, 45–47	0.45	0.008	75	53	37	63	0		25
1H-1, 55–57	0.55	0.010	70	53	51	49	0	−1.00	18
1H-1, 65–67	0.65	0.012	65	61	61	39	0		15
1H-1, 75–77	0.75	0.014	60	34	70	30	0	−0.62	6
1H-1, 85–87	0.85	0.015	60	44	76	24	0	−0.86	6
1H-1, 95–97	0.95	0.016	56	44	83	17	0	−0.30	4
1H-1, 105–107	1.05	0.018	53	50	88	12	0		3
1H-1, 115–117	1.15	0.020	55	55	87	13	0	−0.74	4
1H-1, 125–127	1.25	0.021	58	42	82	18	0		4
1H-1, 135–137	1.35	0.022	59	47	77	23	0	−0.42	6
1H-2, 5–7	1.55	0.029	59	44	79	21	0	−0.64	6
1H-2, 15–17	1.65	0.033	61	42	85	15	0		4
1H-2, 25–27	1.75	0.038	60	47	90	10	0	−0.65	3
1H-2, 35–37	1.85	0.043	60	46			0		
1H-2, 45–47	1.95	0.047	61	38	79	21	0	−0.88	5
1H-2, 55–57	2.05	0.052	58	44	80	20	0		5
1H-2, 65–67	2.15	0.057	57	56	65	35	0	−1.00	11
1H-2, 75–77	2.25	0.061	49	56	75	25	0	−0.68	7
1H-2, 85–87	2.35	0.066	50	50	80	20	0	−0.40	5
1H-2, 95–97	2.45	0.071	51	54	83	17	0		5
1H-2, 105–107	2.55	0.074	41	57	100	0	0	−1.16	0
2H-1, 5–7	2.85	0.082	75	66	58	42	0	−1.29	21
2H-1, 15–17	2.95	0.085	74	67	62	38	0		19
2H-1, 25–27	3.05	0.088	75	68	60	40	0	−1.39	20
2H-1, 35–37	3.15	0.090	74	67	62	38	0		19
2H-1, 45–47	3.25	0.093	76	63	47	53	0	−1.80	25
2H-1, 55–57	3.35	0.096	74	61	44	56	0		25
2H-1, 65–67	3.45	0.099	74	57			0	−1.71	
2H-1, 75–77	3.55	0.102	69	62	49	51	0		22
2H-1, 85–87	3.65	0.104	70	55	56	44	0	−1.41	17
2H-1, 95–97	3.75	0.107	74	65	61	39	0		19
2H-1, 105–107	3.85	0.110	76	62	65	35	0	−1.40	17
2H-1, 115–117	3.95	0.113	77	66	48	52	0		26
2H-1, 125–127	4.05	0.115	76	62	45	55	0	−1.93	26
2H-1, 135–137	4.15	0.118	74	65	43	57	0		27
2H-1, 145–147	4.25	0.121	73	59	36	64	0	−2.38	28
2H-2, 5–7	4.35	0.124	75	55	35	65	0		27
2H-2, 15–17	4.45	0.127	67	68	33	67	0	−1.65	31
2H-2, 25–27	4.55	0.136	65	57	38	62	0		23
2H-2, 35–37	4.65	0.139	65	69	51	49	0	−0.95	22
2H-2, 45–47	4.75	0.142	66	58	61	39	0		15
2H-2, 55–57	4.85	0.145	64	49	65	35	0	−0.83	11
2H-2, 65–67	4.95	0.148	64	49	70	30	0	−0.61	9
2H-2, 75–77	5.05	0.151	63	50	75	25	0		8
2H-2, 85–87	5.15	0.154	62	53	79	21	0	−0.50	7
2H-2, 95–97	5.25	0.157	60	57	78	22	0		7
2H-2, 105–107	5.35	0.160	58	54	63	37	0	−1.03	12
2H-2, 115–117	5.45	0.163	62	65	59	41	0		16
2H-2, 125–127	5.55	0.166	59	38	59	41	0	−0.88	9
2H-2, 135–137	5.65	0.169	55	35	49	51	0		10
2H-2, 145–147	5.75	0.172	48	38	64	36	0	−0.85	7
2H-3, 5–7	5.85	0.175	55	44	64	36	0	−0.73	9
2H-3, 15–17	5.95	0.178	57	43	71	29	0		7
2H-3, 25–27	6.05	0.181	56	44	68	32	0	−0.97	8
2H-3, 35–37	6.15	0.184	61	47	68	32	0		9
2H-3, 45–47	6.25	0.187	59	47	79	21	0	−0.95	6
2H-3, 55–57	6.35	0.189	52	42	84	16	0		4
2H-3, 65–67	6.45	0.191	63	50	83	17	0	−1.24	5
2H-3, 75–77	6.55	0.193	64	53	64	36	0		12
2H-3, 85–87	6.65	0.195	75	42	44	56	0	−1.79	18
2H-3, 95–97	6.75	0.197	79	31	62	38	0		9
2H-3, 105–107	6.85	0.199	78	30	47	53	0	−1.40	12
2H-3, 115–117	6.95	0.201	81	29	43	57	0		13
2H-3, 125–127	7.05	0.203	78	37	37	63	0	−1.79	18
2H-3, 135–137	7.15	0.205	80	33	38	62	0		16
2H-3, 145–147	7.25	0.207	79	35	36	64	0	−1.71	18
2H-4, 5–7	7.35	0.209	74	41	36	64	0	−1.26	19
2H-4, 15–17	7.45	0.211	70	37	45	55	0		14
2H-4, 25–27	7.55	0.213	65	38	53	47	0	−1.15	11

APPENDIX B (continued).

					Carbonate mineralogy				
Core, section, interval (cm)	Depth (m)	Time (Ma)	Carbonate (%)	Fine fraction (%)	Aragonite (%)	Calcite (%)	Mg calcite (%)	δ^{18}O PDB *G. sacculifera* (‰)	Aragonite to total sediment (%)
2H-4, 35–37	7.65	0.215	63	44	58	42	0		12
2H-4, 45–47	7.75	0.217	60	40	70	30	0	−1.14	7
2H-4, 55–57	7.85	0.219	58	39	71	29	0		6
2H-4, 65–67	7.95	0.221	62	46	78	22	0	−1.22	6
2H-4, 75–77	8.05	0.223	64	42	85	15	0		4
2H-4, 85–87	8.15	0.225	67	45	70	30	0	−0.96	9
2H-4, 95–97	8.25	0.227	68	52	70	30	0		11
2H-4, 105–107	8.35	0.229	71	38	61	39	0	−0.99	10
2H-4, 115–117	8.45	0.231	75	34	63	37	0		9
2H-4, 125–127	8.55	0.233	76	36	55	45	0	−0.99	12
2H-4, 135–137	8.65	0.235	80	30	51	49	0		12
2H-5, 5–7	8.85	0.239	80	35	49	51	0	−1.28	14
2H-5, 15–17	8.95	0.241	83	35	48	52	0		15
2H-5, 25–27	9.05	0.243	82	40	51	49	0	−1.44	16
2H-5, 35–37	9.15	0.245	69	49	78	22	0		7
2H-5, 45–47	9.25	0.250	72	45	79	21	0	−0.76	7
2H-5, 55–57	9.35	0.254	72	44	80	20	0		6
2H-5, 65–67	9.45	0.259	70	43	79	21	0	−0.84	6
2H-5, 75–77	9.55	0.264	65	44	80	20	0		6
2H-5, 85–87	9.65	0.268	65	39	72	28	0	−0.84	7
2H-5, 95–97	9.75	0.273	66	46	77	23	0		7
2H-5, 105–107	9.85	0.277	62	42	69	31	0	−0.64	8
2H-5, 115–117	9.95	0.282	63	36	68	32	0		7
2H-5, 125–127	10.05	0.287	58		69	31	0	−0.62	
2H-5, 135–137	10.15	0.291	59	41	71	29	0		7
2H-5, 145–147	10.25	0.296	56	43	81	19	0	−0.69	5
2H-6, 5–7	10.35	0.301	60	50	84	16	0	−1.10	5
2H-6, 15–17	10.45	0.304	63	42	82	18	0		5
2H-6, 25–27	10.55	0.306	69	35	75	25	0	−1.15	6
2H-6, 35–37	10.65	0.308	71	43	62	38	0		12
2H-6, 45–47	10.75	0.309	74	36	63	37	0	−1.32	10
2H-6, 55–57	10.85	0.311	78	40	55	45	0		14
2H-6, 65–67	10.95	0.313	78	40	49	51	0	−1.64	16
2H-6, 75–77	11.05	0.315	73	33	50	50	0		12
2H-6, 85–87	11.15	0.317	73	28	76	24	0	−0.87	5
2H-6, 95–97	11.25	0.319	83	73	70	30	0		18
2H-6, 105–107	11.35	0.321	77	62	63	37	0	−1.19	18
2H-6, 115–117	11.45	0.322	78	52	66	34	0		14
2H-6, 125–127	11.55	0.324	77	53	64	36	0	−1.67	15
2H-6, 135–137	11.65	0.326	76	51	61	39	0		15
2H-6, 145–147	11.75	0.328	84	64	68	32	0	−1.06	17
2H-7, 5–7	11.85	0.330	87	71	67	33	0	−1.49	20
2H-7, 15–17	11.95	0.332	88	68	68	32	0		19
2H-7, 25–27	12.05	0.333	85	61	69	31	0	−1.65	16
2H-7, 35–37	12.15	0.335	83	56	59	41	0		19
2H-7, 45–47	12.25	0.337	81	50	62	38	0	−1.61	15
2H-7, 55–57	12.35	0.339	74	46	51	49	0		17
3H-1, 5–7	12.45	0.346	58	57	100	0	0	−0.73	0
3H-1, 15–17	12.55	0.352	60	60	100	0	0		0
3H-1, 25–27	12.65	0.359	65	61	100	0	0	−0.96	0
3H-1, 35–37	12.75	0.363	65	60	87	13	0		5
3H-1, 45–47	12.85	0.366	66	55	76	24	0	−1.29	9
3H-1, 55–57	12.95	0.368	72	53	69	31	0		12
3H-1, 65–67	13.05	0.370	75	61	62	38	0	−1.56	18
3H-1, 75–77	13.15	0.373	71	68	64	36	0		17
3H-1, 85–87	13.25	0.375	73	68	69	31	0	−1.37	15
3H-1, 95–97	13.35	0.377	79	72	71	29	0		17
3H-1, 105–107	13.45	0.380	78	64	69	31	0	−1.52	15
3H-1, 115–117	13.55	0.382	77	60	69	31	0		14
3H-1, 125–127	13.65	0.384	76	57	69	31	0	−1.71	14
3H-1, 135–137	13.75	0.387	74	62	70	30	0		14
3H-1, 145–147	13.85	0.389	76	64	68	32	0	−1.51	16
3H-2, 5–7	13.95	0.391	72	61	77	23	0	−1.63	10
3H-2, 15–17	14.05	0.394	77	70	70	30	0		16
3H-2, 25–27	14.15	0.396	78	64	77	23	0	−1.40	11
3H-2, 35–37	14.25	0.398	79	72	79	21	0		12
3H-2, 45–47	14.35	0.401	78	69	86	14	0	−1.86	7
3H-2, 55–57	14.45	0.403	77	59	84	16	0		7
3H-2, 65–67	14.55	0.405	78	59	79	21	0	−2.14	10
3H-2, 75–77	14.65	0.408	75	53	79	21	0		8
3H-2, 85–87	14.75	0.410	73	52	71	29	0	−2.30	11
3H-2, 95–97	14.85	0.412	74	56	59	41	0		17
3H-2, 105-107	14.95	0.415	77	54	56	44	0	−2.03	18
3H-2, 115–117	15.05	0.417	78	54	52	48	0		20
3H-2, 125–127	15.15	0.419	74	58	55	45	0	−1.54	19
3H-2, 135–137	15.25	0.422	71	48	58	42	0		14

APPENDIX B (continued).

					Carbonate mineralogy				
Core, section, interval (cm)	Depth (m)	Time (Ma)	Carbonate (%)	Fine fraction (%)	Aragonite (%)	Calcite (%)	Mg calcite (%)	$\delta^{18}O$ PDB *G. sacculifera* (‰)	Aragonite to total sediment (%)
3H-2, 145–147	15.35	0.425	68	42	71	29	0	−1.41	8
3H-3, 5–7	15.45	0.430	68	47	80	20	0	−1.01	6
3H-3, 15–17	15.55	0.434	59	53	76	24	0		8
3H-3, 25–27	15.65	0.439	59	55	79	21	0	−0.75	7
3H-3, 35–37	15.75	0.444	58	54	100	0	0		0
3H-3, 45–47	15.85	0.448	62	56	100	0	0		0
3H-3, 55–57	15.95	0.453	58	56	100	0	0		0
3H-3, 65–67	16.05	0.457	61	38	100	0	0	−0.86	0
3H-3, 75–77	16.15	0.462	62	47	100	0	0		0
3H-3, 85–87	16.25	0.467	63		100	0	0	−0.80	
3H-3, 95–97	16.35	0.471	62	54	100	0	0		0
3H-3, 105–107	16.45	0.476	58	57	100	0	0	−0.86	0
3H-3, 115–117	16.55	0.479	57	58	100	0	0		0
3H-3, 125–127	16.65	0.481	62	54	100	0	0	−0.83	0
3H-3, 135–137	16.75	0.483	62	62	100	0	0		0
3H-3, 145–147	16.85	0.484	59	50	100	0	0	−0.79	0
3H-4, 5–7	16.95	0.486	63	50	100	0	0	−1.12	0
3H-4, 15–17	17.05	0.488	62	62	100	0	0		0
3H-4, 25–27	17.15	0.490	60	62	90	10	0	−1.00	4
3H-4, 35–37	17.25	0.492	72	66	80	20	0		9
3H-4, 45–47	17.35	0.494	71	65	77	23	0		11
3H-4, 55–57	17.45	0.495	76	67	81	19	0		10
3H-4, 65–67	17.55	0.497	80	66	76	24	0	−1.44	13
3H-4, 75–77	17.65	0.499	76	53	70	30	0		12
3H-4, 85–87	17.75	0.501	79	54	70	30	0	−1.73	13
3H-4, 95–97	17.85	0.503	79	53	67	33	0		14
3H-4, 102–104	17.92	0.504	79	55	66	34	0	−1.84	15
3H-5, 5–7	18.45	0.514	78	60	78	22	0	−1.39	10
3H-5, 15–17	18.55	0.516	77	62	83	17	0		8
3H-5, 25–27	18.65	0.518	78	55	77	23	0	−1.45	10
3H-5, 35–37	18.75	0.519	79	59	71	29	0		14
3H-5, 45–47	18.85	0.521	76	57	76	24	0		10
3H-5, 55–57	18.95	0.523	73	44	78	22	0		7
3H-5, 65–67	19.05	0.525	75	20			0	−1.46	
3H-5, 75–77	19.15	0.527	70	47	87	13	0		4
3H-5, 85–87	19.25	0.529	69	46	100	0	0	−1.48	0
3H-5, 95–97	19.35	0.530	70	44	94	6	0		2
3H-5, 108–110	19.48	0.533	74	49	86	14	0	−1.36	5